

The Anatomy of Z' and Z with Flavour Changing Neutral Currents in the Flavour Precision Era

Andrzej J. Buras^{a,b}, Fulvia De Fazio^c and Jennifer Girrbach^{a,b}

^aTUM Institute for Advanced Study, Lichtenbergstr. 2a, D-85747 Garching, Germany

^bPhysik Department, Technische Universität München, James-Franck-Straße,
D-85747 Garching, Germany

^cIstituto Nazionale di Fisica Nucleare, Sezione di Bari, Via Orabona 4, I-70126 Bari, Italy

Abstract

The simplest extension of the Standard Model (SM) that generally introduces new sources of flavour violation and CP violation as well as right-handed (RH) currents is the addition of a $U(1)$ gauge symmetry to the SM gauge group. If the corresponding heavy gauge boson (Z') mediates FCNC processes in the quark sector at tree-level, these new physics (NP) contributions imply a pattern of deviations from SM expectations for FCNC processes that depends only on the couplings of Z' to fermions and on its mass. This implies stringent correlations between $\Delta F = 2$ and $\Delta F = 1$ observables which govern the landscape of the allowed parameter space for Z' -models. Anticipating the Flavour Precision Era (FPE) ahead of us we illustrate this by searching for allowed oases in this landscape assuming significantly smaller uncertainties in CKM and hadronic parameters than presently available. To this end we analyze $\Delta F = 2$ observables in $K^0 - \bar{K}^0$ and $B_{s,d}^0 - \bar{B}_{s,d}^0$ systems and rare K and B decays including both left-handed and right-handed Z' -couplings to quarks in various combinations. We identify a number of correlations between various flavour observables that could test and distinguish these different Z' scenarios. The important role of $b \rightarrow s\ell^+\ell^-$ and $b \rightarrow s\nu\bar{\nu}$ transitions in these studies is emphasized. Imposing the existing flavour constraints, a rich pattern of deviations from the SM expectations in $B_{s,d}$ and K meson systems emerges provided $M_{Z'} \leq 3$ TeV. While for $M_{Z'} \geq 5$ TeV Z' effects in rare $B_{s,d}$ decays are found typically below 10% and hard to measure even in the FPE, $K \rightarrow \pi\nu\bar{\nu}$ and $K_L \rightarrow \pi^0\ell^+\ell^-$ decays provide an important portal to scales beyond those explored by the LHC. We apply our formalism to NP scenarios with induced flavour changing neutral Z -couplings to quarks. We find that in the case of B_d and K decays such Z -couplings still allow for sizable departures from the SM. On the other hand in the B_s system, constraints on $b \rightarrow s\ell^+\ell^-$ transitions basically eliminate NP effects from such couplings.

1 Introduction

Elementary particle physicists are eagerly waiting for clear signals of New Physics (NP) from the LHC. While the recent discovery of a scalar particle with a mass of 125 GeV and the unexpectedly high direct CP violation in the charm decays could already be such signals, presently in both cases the SM explanations of these events are possible. In the first case it should be possible with increased statistic to answer the question whether the new particle observed at the LHC is the SM Higgs boson or another one belonging to a particular NP scenario. In the second case the situation is less optimistic in view of hadronic uncertainties but the measurements of other flavour observables in charm decays may tell us in due time whether the events seen by the LHCb is NP or not.

After numerous proposals for the physics beyond the SM in the last 35 years it is really time that we know which one if any of these proposal is realized in nature. In particular, an exciting question is whether beyond the SM Higgs, the first new particle to be discovered will be a new heavy gauge boson, a new heavy fermion or a new heavy scalar. If this discovery is to be made directly in high energy collisions then the only collider in this decade that could achieve this goal is the LHC. But what if *nature* is not nice to us and the lightest new particle has a mass of 5 – 10 TeV and will just escape a convincing detection at the LHC. While this is fortunately only a nightmare at present and many new particles could still be discovered by the LHC in the coming months and years, we cannot presently exclude the possibility that we will have to search for new particles first indirectly. In such a case the high precision flavour dedicated experiments will be of paramount importance. However, this will require the measurements of very many observables and a significant reduction of hadronic uncertainties in several of them through improved treatment of QCD effects, in particular improved lattice calculations.

Now over the last decades significant efforts have been made by theorists to suppress flavour changing neutral current (FCNC) processes so that they are absent at tree-level. In addition to the GIM mechanism [1] that governs the flavour physics in the SM, the frameworks of constrained Minimal Flavour Violation (CMFV) [2–4] and Minimal Flavour Violation at large (MFV) [5] were very instrumental in suppressing new flavour and CP-violating phenomena below the present experimental bounds even in the presence of new particles with masses of a few hundreds GeV. Selected reviews with comprehensive list of references can be found in [6, 7].

However, if the scale of NP is shifted to 5 – 10 TeV or even higher energy scales this kind of suppression is less important as FCNC processes are then naturally suppressed by the large scales of heavy particles mediating these phenomena. In fact while loop diagrams, like penguin diagrams of various sorts and box diagrams dominated the physics of FCNC processes in the last thirty years both within the SM and several of its extensions, we should hope at first sight that in the case of new particles with masses above 10 TeV this role will be taken over by tree-level diagrams. The reason is simple. Internal particles with such large masses, if hidden in loop diagrams, will

quite generally imply very small effects in FCNC processes that will be very difficult to measure. On the other hand tree diagrams could still in principle provide a large window to these very short distance scales.

We will demonstrate in the present paper that in the simplest extensions of the SM which contain just a new heavy neutral gauge boson (Z') with flavour-changing quark couplings, the correlations between $\Delta F = 2$ and $\Delta F = 1$ observables in the quark sector, in the absence of new heavy fermions and scalars have a significant impact on this optimistic expectations. In fact we find that these correlations preclude NP effects above 10% in rare B decay branching ratios and CP-asymmetries if $M_{Z'} \geq 5$ TeV. Much larger effects are still possible in rare K decays.

The reason is simple. A tree-level Z' contribution to $\Delta F = 2$ observables depends quadratically on $\Delta_{L,R}^{i,j}(Z')/M_{Z'}$, where $\Delta_{L,R}^{i,j}(Z')$ are flavour-violating couplings with i, j denoting quark flavours. For any high value of $M_{Z'}$, even beyond the reach of the LHC, it is possible to find couplings $\Delta_{L,R}^{i,j}(Z')$ which are not only consistent with the existing data but can even remove certain tensions found within the SM. The larger $M_{Z'}$, the larger $\Delta_{L,R}^{i,j}(Z')$ are allowed: $\Delta_{L,R}^{i,j}(Z') \approx a_{ij} M_{Z'}$ with a_{ij} sufficiently small to agree with $\Delta F = 2$ data. Once $\Delta_{L,R}^{i,j}(Z')$ are fixed in this manner, they can be used to predict Z' effects in $\Delta F = 1$ observables. However here NP contributions to the amplitudes are proportional to $\Delta_{L,R}^{i,j}(Z')/M_{Z'}^2$, and with the couplings proportional to $M_{Z'}$, Z' contributions to $\Delta F = 1$ observables decrease with increasing $M_{Z'}$.

Our analysis demonstrates that for $1 \text{ TeV} \leq M_{Z'} \leq 3 \text{ TeV}$, still in the reach of the LHC, indirect Z' effects can be well tested by means of rare K and B decays. For such values of $M_{Z'}$ effects up to 50% at the level of the branching ratios and measurable effects in CP-asymmetries are possible for $B_{s,d}$ meson systems. However for $M_{Z'} \geq 5 \text{ TeV}$, this begins to be very difficult even in the FPE as NP effects in rare and CP-violating B decays turn out to be typically below 10%. Significantly larger effects are still allowed in rare K decays.

On the other hand it is evident from this discussion that flavour-violating Z -couplings, that arise in various extensions of the SM, could in the presence of much lower value of M_Z provide clear NP effects in rare K and B decays even if NP generating these couplings is outside the reach of the LHC. In this manner flavour-violating Z couplings, similarly to Z' couplings in rare K decays, could turn out to be an important portal to short distance scales which cannot be explored by the LHC. We will demonstrate that this is still the case for rare B_d and K decays but not any longer for B_s decays and related CP asymmetries.

In this spirit, we will first ask in the present paper the following question:

- What can be learned about NP from precise measurements of flavour observables to be performed in this decade if the lightest messenger of NP is a heavy Z' gauge boson with arbitrary couplings to quarks and arbitrary mass? In particular we will ask the question whether it is possible to determine all these couplings

entirely with the help of quark-flavour violating observables for $M_{Z'}$ in the reach of the LHC. To this end we will assume that the flavour diagonal couplings of Z' to leptons have been determined in pure leptonic processes.

While there is a very rich literature on FCNC processes mediated by a $Z'(Z)$ gauge boson and several extensive analyses have been presented on various occasions¹, to our knowledge this specific question has not been addressed so far. After having positively answered this question we will ask the second question:

- What are the correlations between various flavour observables in this simple framework and how do they compare with the stringent correlations implied by the simplest BSM frameworks on the market, the class of models with constrained Minimal Flavour Violation (CMFV) [2–4] and the models with $U(2)^3$ flavour symmetry [23–30]?

The simple model analyzed here can be considered as a part of a bigger theory as already analyzed in numerous papers in the literature. Moreover its simplicity provides an analytic insight into the departure from SM expectations in flavour physics and the role of right-handed (RH) currents. In fact certain lessons gained from the involved studies of the LHT model [31, 32] and RS scenario with custodial protection (RSc) [33] as summarized in [34] will be seen here in a much simpler setting. In particular our analysis in the K system, where we investigate the correlation between ε_K and the $K \rightarrow \pi\nu\bar{\nu}$ decays, can be considered as an explicit dynamical example for the findings of [34].

While the violation of stringent relations of CMFV is evident in this framework due to new sources of flavour and CP violation, it is of interest to impose $U(2)^3$ symmetry on Z' couplings and study its phenomenological implications. Such a study is more transparent than in more complicated models in which loop diagrams with heavy fermions and scalars accompanied by many free parameters dominate the NP contributions to FCNC processes.

The analysis of Z' flavour physics presented here can be considered as a generalization of our recent paper [35] in which we have analyzed in detail the pattern of flavour violating Z' tree-level contributions in a specific 331 model (the $\overline{331}$ model). The generalization in question is three-fold:

- First of all we consider general structure of Z' couplings to SM quarks so that at the fundamental level there are no correlations between flavour violation from NP in K , B_d and B_s meson systems. While certain correlations between them could be generated once the constraints from experimental data are imposed, significant NP effects in ε_K and in particular in rare K decays are now possible, while this was not the case in the $\overline{331}$ model.

¹It is not possible to refer to all these papers. Selected analyses can be found in [8–21]. See also the review in [22].

- Also a new important feature of NP contributions in the present paper is the presence of flavour-violating right-handed (RH) Z' couplings to SM quarks, which has profound implications for correlations between $\Delta F = 2$ and $\Delta F = 1$ observables identified in scenarios with only left-handed (LH) couplings. Also correlations between rare decays with $\nu\bar{\nu}$ and $\mu^+\mu^-$ in the final state can be modified in a profound manner.
- While in the $\overline{331}$ model the flavour diagonal couplings of Z' to neutrinos and muons were fixed and smaller than the corresponding ordinary Z couplings, in a general case considered here they could be larger than the latter, enhancing thereby the branching ratios for rare leptonic and semi-leptonic decays for fixed quark couplings.

As advertised above, our anatomy of Z' scenarios will lead us to the conclusion that the correlations between various flavour observables will test this type of NP in the FPE provided $M_{Z'} \leq 3$ TeV. For $M_{Z'} \geq 5$ TeV this will be very difficult, except for rare K decays and in the second part of our paper we will apply our formalism to the case of flavour-violating Z couplings. Here the effects in rare B_d decays and in particular K decays can be much larger than those allowed in the case of Z' for $M_{Z'} \geq 1$ TeV, but in the B_s system significant NP effects from flavour violating Z coupling are already ruled out by present constraints from $b \rightarrow s\mu^+\mu^-$ transitions. Similar conclusions have been reached in [36, 37] in a more general context.

For readers interested mainly in our results and less in the formalism presented in subsequent sections we have made an overview of all correlations and anticorrelations found by us and of the related figures in Tables 9 and 10. The comments in the last column of this table indicate the relevance of a given correlation or anticorrelation.

Our paper is organized as follows. In Section 2 we describe our strategy by listing processes to be considered. Our analysis will only involve processes which are theoretically clean and have simple structure. Here we will also introduce a number of different scenarios for the Z' couplings to quarks thereby reducing the number of free parameters. In Section 3 we will first present a compendium of formulae for master functions that govern FCNC processes with Z' contributions taken into account. Subsequently we present formulae for flavour observables in $\Delta F = 2$ transitions including for the first time NLO QCD corrections to tree-level Z' contributions. Finally formulae for rare K and B decays considered by us are collected. In Section 4 we calculate Z' contributions to the $B \rightarrow X_s\gamma$ decay improving on the calculation of QCD corrections present in the Z' -literature by using the general formulae of [38]. In Section 5 we present a general qualitative view on NP contributions to flavour observables in four scenarios for the Z' couplings. In Section 6 we present our strategy for the numerical analysis and in Section 7 we execute our strategy for the determination of Z' couplings and discuss several scenarios of its couplings in question, identifying stringent correlations between various observables. In Section 8 we investigate what the imposition of the $U(2)^3$ flavour symmetry on $\Delta_L^{i,j}(Z')$ couplings would imply. In Section 9 we apply our formalism to the

SM Z boson for which the mass M_Z and the diagonal lepton couplings are known. A summary of our main results and a brief outlook for the future are given in Section 10.

2 Strategy

Our paper is dominated by tree-level contributions to FCNC processes mediated by a heavy neutral gauge boson Z' . These contributions are governed by the couplings $\Delta_{L,R}^{ij}(Z')$ to quarks and the corresponding Feynman rule has been shown in Fig 1. Here (i, j) denote quark flavours. As we will see in addition to a general form of these couplings it will be instructive to consider the following four scenarios for them keeping the pair (i, j) fixed:

1. Left-handed Scenario (LHS) with complex $\Delta_L^{bq} \neq 0$ and $\Delta_R^{bq} = 0$,
2. Right-handed Scenario (RHS) with complex $\Delta_R^{bq} \neq 0$ and $\Delta_L^{bq} = 0$,
3. Left-Right symmetric Scenario (LRS) with complex $\Delta_L^{bq} = \Delta_R^{bq} \neq 0$,
4. Left-Right asymmetric Scenario (ALRS) with complex $\Delta_L^{bq} = -\Delta_R^{bq} \neq 0$,

with analogous scenarios for the pair (s, d) . We will see that these simple scenarios will give us a profound insight into the flavour structure of models in which NP is dominated by left-handed currents or right-handed currents or left-handed and right-handed currents of the same size. In particular the last two scenarios will exhibit a very clear distinction between $K \rightarrow \pi\nu\bar{\nu}$ decays and $B_{s,d} \rightarrow \mu^+\mu^-$ which are governed by V and A couplings, respectively. Moreover we will consider a scenario with underlying flavour $U(2)^3$ symmetry which will imply relations between Δ_L^{bd} and Δ_L^{bs} couplings and interesting phenomenological consequences.

The idea of looking at the first three NP scenarios is not new and has been in particular motivated by a detailed study of supersymmetric flavour models with NP dominated by LH currents, RH currents or equal amount of LH and RH currents [39]². Moreover, it has been found in several studies of non-supersymmetric frameworks like LHT model [31] or Randall-Sundrum scenario with custodial protection (RSc) [33] that models with the dominance of LH or RH currents exhibit quite different patterns of flavour violation. Our analysis will demonstrate it in a transparent manner.

Let us then outline our strategy for the determination of Z' couplings to quarks and for finding correlations between flavour observables in the context of the simple scenarios listed above. Our strategy will only be fully effective in the second half of this decade, when hadronic uncertainties will be reduced and the data on various observables significantly improved. It involves ten steps including a number of working assumptions:

²Similar scenarios have been considered subsequently in [36, 40]

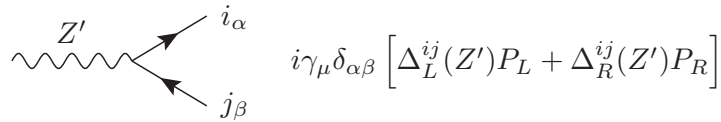


Figure 1: *Feynman rule for the coupling of a colourless neutral gauge boson Z' to quarks, where i, j denote different quark flavours and α, β the colours. $P_{L,R} = (1 \mp \gamma_5)/2$.*

Step 1:

Determination of CKM parameters by means of tree-level decays and of the necessary non-perturbative parameters by means of lattice calculations. This step will provide the results for all observables considered below within the SM as well as all non-perturbative parameters entering the NP contributions. As $|V_{ub}|$ is presently poorly known, it will be interesting in the spirit of our recent papers [30, 41] to investigate how the outcome of this step depends on the value of $|V_{ub}|$ with direct implications for the necessary size of NP contributions which will be different in different observables.

Step 2:

We will assume that the ratios

$$\frac{\Delta_A^{\mu\bar{\mu}}(Z')}{M_{Z'}}, \quad \frac{\Delta_L^{\nu\bar{\nu}}(Z')}{M_{Z'}} \quad (1)$$

have been determined in pure leptonic processes. We will further assume that these ratios are real but could have both signs. In principle these ratios can be determined up to the sign from quark flavour violating processes considered below but their knowledge increases predictive power of our analysis. In particular the knowledge of their signs allows to remove certain discrete ambiguities and is crucial for the distinction between LHS and RHS scenarios in $B_{s,d} \rightarrow \mu^+ \mu^-$ decays.

Step 3:

Here we will consider the B_s^0 system and the observables

$$\Delta M_s, \quad S_{\psi\phi}, \quad \mathcal{B}(B_s \rightarrow \mu^+ \mu^-), \quad S_{\mu^+ \mu^-}^s, \quad (2)$$

where $S_{\mu^+ \mu^-}^s$ measures CP violation in $B_s \rightarrow \mu^+ \mu^-$ decay [42, 43]. Explicit expressions for these observables in terms of the relevant couplings can be found in Section 3.

Concentrating in this step on the LHS scenario, NP contributions to these three observables are fully described by

$$\frac{\Delta_L^{bs}(Z')}{M_{Z'}} = -\frac{\tilde{s}_{23}}{M_{Z'}} e^{-i\delta_{23}}, \quad \frac{\Delta_A^{\mu\bar{\mu}}(Z')}{M_{Z'}}, \quad (3)$$

with the second ratio known from Step 2. Here $\tilde{s}_{23} \geq 0$ and it is found to be below unity but it does not represent any mixing parameter as in [35]. The minus sign is

introduced to cancel the minus sign in V_{ts} in the phenomenological formulae listed in the next section.

Thus we have four observables to our disposal and two parameters in the quark sector to determine. This allows to remove certain discrete ambiguities, determine all parameters uniquely and predict correlations between these four observables that are characteristic for this scenario.

Step 4:

Repeating this exercise in the B_d^0 system we have to our disposal

$$\Delta M_d, \quad S_{\psi K_S}, \quad \mathcal{B}(B_d \rightarrow \mu^+ \mu^-), \quad S_{\mu^+ \mu^-}^d \quad (4)$$

Explicit expressions for these observables in terms of the relevant couplings can be found in Section 3.

Now NP contributions to these three observables are fully described by

$$\frac{\Delta_L^{bd}(Z')}{M_{Z'}} = \frac{\tilde{s}_{13}}{M_{Z'}} e^{-i\delta_{13}}, \quad \frac{\Delta_A^{\mu\bar{\mu}}(Z')}{M_{Z'}}, \quad (5)$$

with the last one known from Step 2. Again we can determine all the couplings uniquely to be used in the steps below. Our notations and sign conventions are as in Step 3 with $\tilde{s}_{13} \geq 0$ but no minus sign as V_{td} has no such sign.

Step 5:

Moving to the K system we have to our disposal

$$\varepsilon_K, \quad K^+ \rightarrow \pi^+ \nu \bar{\nu}, \quad K_L \rightarrow \pi^0 \nu \bar{\nu}, \quad K_L \rightarrow \pi^0 \ell^+ \ell^-, \quad K_L \rightarrow \mu^+ \mu^-, \quad (6)$$

where in view of hadronic uncertainties the last decay on this list will only be used to make sure that the existing rough bound on its branching ratio is satisfied. In the present paper we do not study the ratio ε'/ε , which is rather accurately measured but subject to much larger hadronic uncertainties than observables listed in (6). Explicit expressions for the observables in the K system in terms of the relevant couplings can be found in Section 3.

Now NP contributions to these four observables are fully described by

$$\frac{\Delta_L^{sd}(Z')}{M_{Z'}} = -\frac{\tilde{s}_{12}}{M_{Z'}} e^{-i\delta_{12}}, \quad \frac{\Delta_L^{\nu\bar{\nu}}(Z')}{M_{Z'}}, \quad \frac{\Delta_A^{\mu\bar{\mu}}(Z')}{M_{Z'}} \quad (7)$$

where we assumed the couplings to neutrinos to be left-handed and real. The ratios involving leptonic couplings are known already from Step 2. Consequently, we can determine all couplings involved by using the data on the observables in (6). Moreover we identify certain correlations characteristic for LHS scenario. $\tilde{s}_{12} \geq 0$ and the minus sign is chosen to cancel the one of V_{ts} .

Step 6: As all parameters of LHS scenario has been fixed in the first five steps we are in the position to make predictions for the following processes

$$B \rightarrow X_s \ell^+ \ell^-, \quad B \rightarrow K \ell^+ \ell^-, \quad B \rightarrow K^* \ell^+ \ell^- \quad (8)$$

$$B \rightarrow K \nu \bar{\nu}, \quad B \rightarrow K^* \nu \bar{\nu}, \quad B \rightarrow X_s \nu \bar{\nu}, \quad (9)$$

$$B \rightarrow X_s \gamma, \quad B \rightarrow K^* \gamma \quad (10)$$

and test whether they provide additional constraints on the couplings.

Step 7:

We repeat Steps 3-6 for the case of RHS. We will see that in view of the change of the sign of NP contribution to $B_{s,d} \rightarrow \mu^+ \mu^-$ and $K_L \rightarrow \mu^+ \mu^-$ decays the structure of the correlations between various observables will distinguish this scenario from the LHS one. Yet, as we will find out, by going from LHS to RHS scenario we can keep results of Steps 3-5 unchanged by interchanging simultaneously two *big oases* in the parameter space that we encountered already in our study of the $\overline{33\overline{1}}$ model. This LH-RH invariance present in Steps 3-5 can be broken by the $b \rightarrow s \ell^+ \ell^-$ and $b \rightarrow s \nu \bar{\nu}$ transitions listed in (8) and (9), respectively. They will allow us very clearly to distinguish the physics of RH currents from LH ones. As only RH couplings are present in the NP contributions in this scenario we can use the parametrization of these couplings as in (3), (5) and (7) keeping in mind that now RH couplings are involved.

Step 8:

We repeat Steps 3-6 for the case of LRS. Here the new feature is the vanishing of NP contributions to $B_{s,d} \rightarrow \mu^+ \mu^-$ and $K_L \rightarrow \mu^+ \mu^-$ decays and rather sizable NP contributions to $\Delta F = 2$ observables due to the presence of LR operators. As the LH and RH couplings are equal we can again use the parametrization of these couplings as in (3), (5) and (7) but their values will change due to different constraints from $\Delta F = 2$ transitions. Also in this step the $b \rightarrow s \ell^+ \ell^-$ and $b \rightarrow s \nu \bar{\nu}$ transitions will play very important role.

Step 9:

We repeat Steps 3-6 for the case of ALRS. Here the new feature is the vanishing of NP contributions to $K^+ \rightarrow \pi^+ \nu \bar{\nu}$ and $K_L \rightarrow \pi^0 \nu \bar{\nu}$ decays, while $B_{s,d} \rightarrow \mu^+ \mu^-$, including $S_{\mu^+ \mu^-}^{d,s}$ CP asymmetries and again the $b \rightarrow s \ell^+ \ell^-$ and $b \rightarrow s \nu \bar{\nu}$ transitions will exhibit their strength in testing the theory in a different environment: rather sizable NP contributions to $\Delta F = 2$ observables due to the presence of LR operators. As the LH and RH couplings differ only by a sign we can again use the parametrization of these couplings as in (3), (5) and (7) but their values will change due to different constraints from $\Delta F = 2$ transitions.

Step 10:

One can consider next the case of simultaneous LH and RH couplings that are unrelated to each other. This step is more challenging as one has more free parameters and in

order to reach clear cut conclusions one would need a concrete model for Z' couplings or a very involved numerical analysis [36,40]. We will therefore leave out this step from our paper.

Once this analysis of Z' contributions is completed it will be straightforward to apply it to the case of the SM Z boson with flavour violating couplings.

We should remark that we have left from this analysis ε'/ε . This ratio is important for the tests of $Z'(Z)$ FCNC scenarios as it is very sensitive to any NP contribution [44–46]. However, due to significant hadronic uncertainties it is less suitable for the determination of the $Z'(Z)$ FCNC couplings than the decays used by us when the latter will be precisely measured. On the other hand having these couplings one can make predictions for ε'/ε and study correlations.

3 Compendium for the Z' Contributions

3.1 Parametrization

First it will be useful to introduce a useful parametrization of Z' contributions by generalizing the master functions known from CMFV models and the LHT model to include in addition to left-handed currents also right-handed currents. In the case of the RSc model this has already been done in [33] but our parametrization below is a bit different than the one in the latter paper. For our purposes it will be sufficient to consider the following functions:

- For $\Delta F = 2$ processes

$$S(K), \quad S(B_d), \quad S(B_s), \quad (11)$$

where we will include in the definitions of these functions the contributions of operators with LL , RR and LR Dirac structures.

- For decays with $\nu\bar{\nu}$ in the final state

$$X_{L,R}(K), \quad X_{L,R}(B_d), \quad X_{L,R}(B_s). \quad (12)$$

- For decays with $\mu\bar{\mu}$ in the final state

$$Y_A(K), \quad Y_A(B_d), \quad Y_A(B_s). \quad (13)$$

All these functions in contrast to the SM and more generally CMFV models depend on the meson considered and moreover are complex valued.

In the SM the corresponding *flavour universal real valued* functions are given as follows ($x_t = m_t^2/M_W^2$):

$$S_0(x_t) = \frac{4x_t - 11x_t^2 + x_t^3}{4(1-x_t)^2} - \frac{3x_t^2 \log x_t}{2(1-x_t)^3}, \quad (14)$$

$$X_0(x_t) = \frac{x_t}{8} \left[\frac{x_t + 2}{x_t - 1} + \frac{3x_t - 6}{(x_t - 1)^2} \ln x_t \right], \quad (15)$$

$$Y_0(x_t) = \frac{x_t}{8} \left(\frac{x_t - 4}{x_t - 1} + \frac{3x_t \log x_t}{(x_t - 1)^2} \right). \quad (16)$$

In other CMFV models they take different values still keeping flavour universality and being real valued. This implies very stringent relations between various observables in three meson system in question which have been reviewed in [3]. It is evident that in the presence of Z' tree-level contributions the breakdown of flavour universality and also the presence of new complex phases implies the violation of these relations. Generalizing the three SM functions to twelve functions listed in (11)–(13), allows to describe these new effects in a transparent manner. In what follows we will list explicit expressions for these functions. Subsequently we will show how they enter the branching ratios for various decays.

The derivation of the formulae listed below is so simple that we will not present it here. From the normalization of the corrections from Z' to the master functions in question and the formulae for observables given subsequently, it will be clear how these functions have been defined in the corresponding effective Hamiltonians. In any case, the compendium given below is self-contained as far as numerical analysis is concerned.

3.2 Master Functions Including Z' Contributions

Calculating the contributions of Z' to various decays it is straightforward to write down the expressions for the master functions in terms of the couplings defined in Fig. 1.

3.2.1 $\Delta F = 2$ Master Functions

We define the relevant CKM factors

$$\lambda_i^{(K)} = V_{is}^* V_{id}, \quad \lambda_t^{(d)} = V_{tb}^* V_{td}, \quad \lambda_t^{(s)} = V_{tb}^* V_{ts}, \quad (17)$$

and introduce

$$g_{\text{SM}}^2 = 4 \frac{G_F}{\sqrt{2}} \frac{\alpha}{2\pi \sin^2 \theta_W} = 1.78137 \times 10^{-7} \text{ GeV}^{-2}. \quad (18)$$

The $\Delta F = 2$ master functions for $M = K, B_q$ are given as follows

$$S(M) = S_0(x_t) + \Delta S(M) \equiv |S(M)|e^{i\theta_S^M} \quad (19)$$

with $\Delta S(M)$ receiving contributions from various operators so that it is useful to write

$$\Delta S(M) = [\Delta S(M)]_{\text{VLL}} + [\Delta S(M)]_{\text{VRR}} + [\Delta S(M)]_{\text{LR}}. \quad (20)$$

The contributing operators are defined for the K system as follows [47, 48]

$$Q_1^{\text{VLL}} = (\bar{s}\gamma_\mu P_L d) (\bar{s}\gamma^\mu P_L d), \quad (21a)$$

$$Q_1^{\text{VRR}} = (\bar{s}\gamma_\mu P_R d) (\bar{s}\gamma^\mu P_R d), \quad (21b)$$

$$Q_1^{\text{LR}} = (\bar{s}\gamma_\mu P_L d) (\bar{s}\gamma^\mu P_R d), \quad (21c)$$

$$Q_2^{\text{LR}} = (\bar{s}P_L d) (\bar{s}P_R d). \quad (21d)$$

with analogous expressions for $B_{s,d}$ systems. For instance in the B_s system $Q_1^{\text{VLL}} = (\bar{b}\gamma_\mu P_L s) (\bar{b}\gamma^\mu P_L s)$. Here we suppressed colour indices as they are summed up in each factor. For instance $\bar{s}\gamma_\mu P_L d$ stands for $\bar{s}_\alpha \gamma_\mu P_L d_\alpha$ and similarly for other factors.

$[\Delta S(M)]_{\text{VLL}}$ and $[\Delta S(M)]_{\text{VRR}}$ can be obtained directly from our previous paper [35]:

$$[\Delta S(B_q)]_{\text{VLL}} = \left[\frac{\Delta_L^{bq}(Z')}{\lambda_t^{(q)}} \right]^2 \frac{4\tilde{r}}{M_{Z'}^2 g_{\text{SM}}^2}, \quad [\Delta S(K)]_{\text{VLL}} = \left[\frac{\Delta_L^{sd}(Z')}{\lambda_t^{(K)}} \right]^2 \frac{4\tilde{r}}{M_{Z'}^2 g_{\text{SM}}^2}, \quad (22)$$

where $\tilde{r} = 0.985$ for $M_{Z'} = 1 \text{ TeV}$. $[\Delta S(M)]_{\text{VRR}}$ is then found from the formula above by simply replacing L by R. For the case of tree-level Z exchanges $\tilde{r} = 1.068$.

In order to calculate the LR contributions we introduce quantities familiar from SM expressions for mixing amplitudes

$$T(B_q) = \frac{G_F^2}{12\pi^2} F_{B_q}^2 \hat{B}_{B_q} m_{B_q} M_W^2 \left(\lambda_t^{(q)} \right)^2 \eta_B, \quad (23)$$

$$T(K) = \frac{G_F^2}{12\pi^2} F_K^2 \hat{B}_K m_K M_W^2 \left(\lambda_t^{(K)} \right)^2 \eta_2, \quad (24)$$

where η_i are QCD corrections and \hat{B}_i known SM non-perturbative factors.

Then

$$T(K)[\Delta S(K)]_{\text{LR}} = \frac{\Delta_L^{sd}(Z') \Delta_R^{sd}(Z')}{M_{Z'}^2} [C_1^{\text{LR}}(\mu_{Z'}) \langle Q_1^{\text{LR}}(\mu_{Z'}, K) \rangle + C_2^{\text{LR}}(\mu_{Z'}) \langle Q_2^{\text{LR}}(\mu_{Z'}, K) \rangle]. \quad (25)$$

Including NLO QCD corrections [48] the Wilson coefficients of LR operators are given by

$$C_1^{\text{LR}}(\mu_{Z'}) = 1 + \frac{\alpha_s}{4\pi} \left(-\log \frac{M_{Z'}^2}{\mu_{Z'}^2} - \frac{1}{6} \right), \quad (26)$$

$$C_2^{\text{LR}}(\mu_{Z'}) = \frac{\alpha_s}{4\pi} \left(-6 \log \frac{M_{Z'}^2}{\mu_{Z'}^2} - 1 \right). \quad (27)$$

Next

$$\langle Q_i^a(\mu_{Z'}, K) \rangle \equiv \frac{m_K F_K^2}{3} P_i^a(\mu_{Z'}, K) \quad (28)$$

are the matrix elements of operators evaluated at the matching scale $\mu_{Z'} = \mathcal{O}(M_{Z'})$ and P_i^a are the coefficients introduced in [47]. The $\mu_{Z'}$ dependence of $C_i^a(\mu_{Z'})$ cancels the one of $P_i^a(\mu_{Z'})$ so that $S(K)$ does not depend on $\mu_{Z'}$.

Similarly for B_q systems we have

$$T(B_q)[\Delta S(B_q)]_{\text{LR}} = \frac{\Delta_L^{bq}(Z') \Delta_R^{bq}(Z')}{M_{Z'}^2} [C_1^{\text{LR}}(\mu_{Z'}) \langle Q_1^{\text{LR}}(\mu_{Z'}, B_q) \rangle + C_2^{\text{LR}}(\mu_{Z'}) \langle Q_2^{\text{LR}}(\mu_{Z'}, B_q) \rangle], \quad (29)$$

where the Wilson coefficients $C_i^a(\mu_{Z'})$ are as in the K system and the matrix elements are given by

$$\langle Q_i^a(\mu_{Z'}, B_q) \rangle \equiv \frac{m_{B_q} F_{B_q}^2}{3} P_i^a(\mu_{Z'}, B_q). \quad (30)$$

Finally, we collect in Table 1 central values of $\langle Q_i^a(\mu_{Z'}) \rangle$. They are given in the $\overline{\text{MS}}$ -NDR scheme and are based on lattice calculations in [49, 50] for $K^0 - \bar{K}^0$ system and in [51] for $B_{d,s}^0 - \bar{B}_{d,s}^0$ systems. For the $K^0 - \bar{K}^0$ system we have just used the average of the results in [49, 50] that are consistent with each other. As the values of the relevant B_i parameters in these papers have been evaluated at $\mu = 3 \text{ GeV}$ and 4.2 GeV , respectively, we have used the formulae in [47] to obtain the values of the matrix elements in question at $\mu_{Z'}$. For simplicity we choose this scale to be $M_{Z'}$ but any scale of this order would give the same results for the physical quantities up to NNLO QCD corrections that are negligible at these high scales. The renormalization scheme dependence of the matrix elements is canceled by the one of the Wilson coefficients.

In the case of tree-level Z -exchanges we evaluate the matrix elements at $m_t(m_t)$ as the inclusion of NLO QCD corrections allows us to choose any scale of $\mathcal{O}(M_Z)$ without changing physical results. Then in the formulae above one should replace $M_{Z'}$ by M_Z and $\mu_{Z'}$ by $m_t(m_t)$. The values of hadronic matrix elements at $m_t(m_t)$ in the $\overline{\text{MS}}$ -NDR scheme are given in Table 1.³

³We thank Robert Ziegler for checking the results in this table.

	$\langle Q_1^{\text{LR}}(M_{Z'}) \rangle$	$\langle Q_2^{\text{LR}}(M_{Z'}) \rangle$	$\langle Q_1^{\text{LR}}(m_t) \rangle$	$\langle Q_2^{\text{LR}}(m_t) \rangle$
$K^0 - \bar{K}^0$	-0.14	0.22	-0.11	0.18
$B_d^0 - \bar{B}_d^0$	-0.25	0.34	-0.21	0.27
$B_s^0 - \bar{B}_s^0$	-0.37	0.51	-0.30	0.40

Table 1: Hadronic matrix elements $\langle Q_i^a \rangle$ in units of GeV^3 at $M_{Z'} = 1 \text{ TeV}$ and at $m_t(m_t)$

3.2.2 $\Delta F = 1$ Master Functions

We find

$$X_L(K) = \eta_X X_0(x_t) + \frac{\Delta_L^{\nu\bar{\nu}}(Z') \Delta_L^{sd}(Z')}{g_{\text{SM}}^2 M_{Z'}^2 V_{ts}^* V_{td}}, \quad (31)$$

$$X_R(K) = \frac{\Delta_L^{\nu\bar{\nu}}(Z') \Delta_R^{sd}(Z')}{g_{\text{SM}}^2 M_{Z'}^2 V_{ts}^* V_{td}}, \quad (32)$$

$$X_L(B_q) = \eta_X X_0(x_t) + \left[\frac{\Delta_L^{\nu\bar{\nu}}(Z')}{M_{Z'}^2 g_{\text{SM}}^2} \right] \frac{\Delta_L^{qb}(Z')}{V_{tq}^* V_{tb}}, \quad (33)$$

$$X_R(B_q) = \left[\frac{\Delta_L^{\nu\bar{\nu}}(Z')}{M_{Z'}^2 g_{\text{SM}}^2} \right] \frac{\Delta_R^{qb}(Z')}{V_{tq}^* V_{tb}}, \quad (34)$$

$$Y_A(K) = \eta_Y Y_0(x_t) + \frac{[\Delta_A^{\mu\bar{\mu}}(Z')]}{M_{Z'}^2 g_{\text{SM}}^2} \left[\frac{\Delta_L^{sd}(Z') - \Delta_R^{sd}(Z')}{V_{ts}^* V_{td}} \right] \equiv |Y_A(K)| e^{i\theta_Y^K}, \quad (35)$$

$$Y_A(B_q) = \eta_Y Y_0(x_t) + \frac{[\Delta_A^{\mu\bar{\mu}}(Z')]}{M_{Z'}^2 g_{\text{SM}}^2} \left[\frac{\Delta_L^{qb}(Z') - \Delta_R^{qb}(Z')}{V_{tq}^* V_{tb}} \right] \equiv |Y_A(B_q)| e^{i\theta_Y^{B_q}}. \quad (36)$$

Here $\eta_{X,Y}$ are QCD factors which for $m_t = m_t(m_t)$ are close to unity [52, 53].

$$\eta_X = 0.994, \quad \eta_Y = 1.012. \quad (37)$$

3.2.3 Effective Hamiltonian for $b \rightarrow s\ell^+\ell^-$

For our discussion of constraints from $b \rightarrow s\ell^+\ell^-$ transitions we will need the corresponding effective Hamiltonian which is a generalization of the SM one:

$$\mathcal{H}_{\text{eff}}(b \rightarrow s\ell\bar{\ell}) = \mathcal{H}_{\text{eff}}(b \rightarrow s\gamma) - \frac{4G_F}{\sqrt{2}} \frac{\alpha}{4\pi} V_{ts}^* V_{tb} \sum_{i=9,10} [C_i(\mu) Q_i(\mu) + C'_i(\mu) Q'_i(\mu)] \quad (38)$$

where

$$Q_9 = (\bar{s}\gamma_\mu P_L b)(\bar{\ell}\gamma^\mu \ell), \quad Q_{10} = (\bar{s}\gamma_\mu P_L b)(\bar{\ell}\gamma^\mu \gamma_5 \ell) \quad (39)$$

$$Q'_9 = (\bar{s}\gamma_\mu P_R b)(\bar{\ell}\gamma^\mu \ell), \quad Q'_{10} = (\bar{s}\gamma_\mu P_R b)(\bar{\ell}\gamma^\mu \gamma_5 \ell). \quad (40)$$

Here $\mathcal{H}_{\text{eff}}(b \rightarrow s\gamma)$ stands for the effective Hamiltonian for the $b \rightarrow s\gamma$ transition that involves the dipole operators. An explicit formula for the latter Hamiltonian will be presented in the next section. For the Wilson coefficients we find

$$\sin^2 \theta_W C_9 = [\eta_Y Y_0(x_t) - 4 \sin^2 \theta_W Z_0(x_t)] - \frac{1}{g_{\text{SM}}^2} \frac{1}{M_{Z'}^2} \frac{\Delta_L^{sb}(Z') \Delta_V^{\mu\bar{\mu}}(Z')}{V_{ts}^* V_{tb}}, \quad (41)$$

$$\sin^2 \theta_W C_{10} = -\eta_Y Y_0(x_t) - \frac{1}{g_{\text{SM}}^2} \frac{1}{M_{Z'}^2} \frac{\Delta_L^{sb}(Z') \Delta_A^{\mu\bar{\mu}}(Z')}{V_{ts}^* V_{tb}}, \quad (42)$$

$$\sin^2 \theta_W C'_9 = -\frac{1}{g_{\text{SM}}^2} \frac{1}{M_{Z'}^2} \frac{\Delta_R^{sb}(Z') \Delta_V^{\mu\bar{\mu}}(Z')}{V_{ts}^* V_{tb}}, \quad (43)$$

$$\sin^2 \theta_W C'_{10} = -\frac{1}{g_{\text{SM}}^2} \frac{1}{M_{Z'}^2} \frac{\Delta_R^{sb}(Z') \Delta_A^{\mu\bar{\mu}}(Z')}{V_{ts}^* V_{tb}}, \quad (44)$$

where we have defined

$$\begin{aligned} \Delta_V^{\mu\bar{\mu}}(Z') &= \Delta_R^{\mu\bar{\mu}}(Z') + \Delta_L^{\mu\bar{\mu}}(Z'), \\ \Delta_A^{\mu\bar{\mu}}(Z') &= \Delta_R^{\mu\bar{\mu}}(Z') - \Delta_L^{\mu\bar{\mu}}(Z'). \end{aligned} \quad (45)$$

Here $Z_0(x_t)$ is the SM one-loop function, analogous to $X_0(x_t)$ and $Y_0(x_t)$, that represents gauge invariant combination of Z - and photon penguin diagrams:

$$Z_0(x) = -\frac{1}{9} \log x + \frac{18x^4 - 163x^3 + 259x^2 - 108x}{144(x-1)^3} + \frac{32x^4 - 38x^3 - 15x^2 + 18x}{72(x-1)^4} \log x. \quad (46)$$

The presence of additional coupling $\Delta_R^{\mu\bar{\mu}}(Z')$ or $\Delta_L^{\mu\bar{\mu}}(Z')$, in addition to $\Delta_A^{\mu\bar{\mu}}(Z')$, introduces two new parameters and allows thereby to avoid present constraints on the coefficients C_9 and C'_9 . Therefore only the constraints on C_{10} and C'_{10} from $B \rightarrow K^* \ell^+ \ell^-$, $B \rightarrow K \ell^+ \ell^-$ and $B \rightarrow X_s \ell^+ \ell^-$ will be relevant in the case of Z' . In the case of FCNC processes mediated by Z , which will be discussed in Section 9, all leptonic couplings are known and also the constraints on the coefficients C_9 and C'_9 have to be taken into account.

The formulae above do not include QCD renormalization group effects which influence only C_9 and C'_9 . They will be taken into account in the model independent bounds on these coefficients in Section 9.

3.3 Basic Formulae for Observables

3.3.1 $\Delta F = 2$ Observables

The $\Delta B = 2$ mass differences are given as follows:

$$\Delta M_d = \frac{G_F^2}{6\pi^2} M_W^2 m_{B_d} |\lambda_t^{(d)}|^2 F_{B_d}^2 \hat{B}_{B_d} \eta_B |S(B_d)|, \quad (47)$$

$$\Delta M_s = \frac{G_F^2}{6\pi^2} M_W^2 m_{B_s} |\lambda_t^{(s)}|^2 F_{B_s}^2 \hat{B}_{B_s} \eta_B |S(B_s)|. \quad (48)$$

The corresponding mixing induced CP-asymmetries are then given by

$$S_{\psi K_S} = \sin(2\beta + 2\varphi_{B_d}), \quad S_{\psi\phi} = \sin(2|\beta_s| - 2\varphi_{B_s}), \quad (49)$$

where the phases β and β_s are defined by

$$V_{td} = |V_{td}| e^{-i\beta}, \quad V_{ts} = -|V_{ts}| e^{-i\beta_s}. \quad (50)$$

$\beta_s \simeq -1^\circ$. The new phases φ_{B_q} are directly related to the phases of the functions $S(B_q)$:

$$2\varphi_{B_q} = -\theta_S^{B_q}. \quad (51)$$

Our phase conventions are as in [35] and our previous papers quoted in this work.

For the CP-violating parameter ε_K and ΔM_K we have respectively

$$\varepsilon_K = \frac{\kappa_\varepsilon e^{i\varphi_\varepsilon}}{\sqrt{2}(\Delta M_K)_{\text{exp}}} [\Im(M_{12}^K)], \quad \Delta M_K = 2\Re(M_{12}^K), \quad (52)$$

where

$$(M_{12}^K)^* = \frac{G_F^2}{12\pi^2} F_K^2 \hat{B}_K m_K M_W^2 [\lambda_c^2 \eta_1 x_c + \lambda_t^2 \eta_2 S(K) + 2\lambda_c \lambda_t \eta_3 S_0(x_c, x_t)]. \quad (53)$$

Here, $S_0(x_c, x_t)$ is a *real valued* one-loop box function for which explicit expression is given e.g. in [54]. The factors η_i are QCD corrections evaluated at the NLO level in [55–59]. For η_1 and η_3 also NNLO corrections have been recently calculated [60, 61]. Next $\varphi_\varepsilon = (43.51 \pm 0.05)^\circ$ and $\kappa_\varepsilon = 0.94 \pm 0.02$ [62, 63] takes into account that $\varphi_\varepsilon \neq \frac{\pi}{4}$ and includes long distance effects in $\Im(\Gamma_{12})$ and $\Im(M_{12})$.

In the rest of the paper, unless otherwise stated, we will assume that all four parameters in the CKM matrix have been determined through tree-level decays without any NP pollution and pollution from QCD-penguin diagrams so that their values can be used universally in all NP models considered by us.

3.3.2 $B_{d,s} \rightarrow \mu^+ \mu^-$

With the assumption that the CKM parameters have been determined independently of NP and are universal we find

$$\frac{\mathcal{B}(B_q \rightarrow \mu^+ \mu^-)}{\mathcal{B}(B_q \rightarrow \mu^+ \mu^-)^{\text{SM}}} = \left| \frac{Y_A(B_q)}{\eta_Y Y_0(x_t)} \right|^2, \quad (54)$$

where $Y_A(B_q)$ is given in (36).

As stressed in [42, 43, 64]⁴, when comparing the theoretical branching ratio $\mathcal{B}(B_s \rightarrow \mu^+ \mu^-)$ with experimental data quoted by LHCb, ATLAS and CMS, a correction factor has to be included which takes care of $\Delta\Gamma_s$ effects that influence the extraction of this branching ratio from the data:

$$\mathcal{B}(B_s \rightarrow \mu^+ \mu^-)_{\text{th}} = r(y_s) \mathcal{B}(B_s \rightarrow \mu^+ \mu^-)_{\text{exp}}, \quad r(0) = 1. \quad (55)$$

Here

$$r(y_s) \equiv \frac{1 - y_s^2}{1 + \mathcal{A}_{\Delta\Gamma}^\lambda y_s} \approx 1 - \mathcal{A}_{\Delta\Gamma}^\lambda y_s \quad (56)$$

with

$$y_s \equiv \tau_{B_s} \frac{\Delta\Gamma_s}{2} = 0.088 \pm 0.014. \quad (57)$$

The quantity $\mathcal{A}_{\Delta\Gamma}^\lambda$ is discussed below.

It is a matter of choice whether the factor $r(y_s)$ is included in the experimental branching ratio or in the theoretical calculation, provided $r(y_s)$ is not significantly affected by NP. Once it is measured, its inclusion in the experimental value, as advocated in [42], should be favoured as it would have no impact on the theoretical calculations of branching ratios that do not depend on $\Delta\Gamma_s$. As in the SM and CMFV $\mathcal{A}_{\Delta\Gamma}^\lambda = 1$ [43] and the factor $r(y_s)$ is universal, it is also a good idea to include this factor in experimental branching ratio. In this manner various CMFV relations remain intact.

If a given model predicts $\mathcal{A}_{\Delta\Gamma}^\lambda$ significantly different from unity and the dependence of $r(y_s)$ on model parameters is large one may include this factor in the theoretical branching ratio:

$$\mathcal{B}(B_s \rightarrow \mu^+ \mu^-)_{\text{corr}} = \frac{\mathcal{B}(B_s \rightarrow \mu^+ \mu^-)_{\text{th}}}{r(y_s)}. \quad (58)$$

The branching ratios $\mathcal{B}(B_q \rightarrow \mu^+ \mu^-)$ are only sensitive to the absolute value of $Y_A(B_q)$. However, as pointed out in [42, 43] in the flavour precision era these decays could allow to get also some information on the phase of $Y_A(B_q)$ and we want to investigate whether in the models considered this effect is significant. The authors of [43, 65] provide general expressions for $\mathcal{A}_{\Delta\Gamma}^\lambda$ and $S_{\mu^+ \mu^-}^s$ as functions of Wilson coefficients involved. Using these

⁴We follow here presentation and notations of [42, 43].

formulae we find in Z' models very simple formulae that reflect the fact that Z' and not scalar operators dominate NP contributions:

$$\mathcal{A}_{\Delta\Gamma}^\lambda = \cos(2\theta_Y^{B_s} - 2\varphi_{B_s}), \quad S_{\mu^+\mu^-}^s = \sin(2\theta_Y^{B_s} - 2\varphi_{B_s}) \quad (59)$$

Both $\mathcal{A}_{\Delta\Gamma}^\lambda$ and $S_{\mu^+\mu^-}^s$ are theoretically clean observables.

In the formulae (59) and (61) we took into account new phases in the $B_q - \bar{B}_q$ mixings as we deal here with the mixing induced CP violation. While smaller than the phases of $Y_A(B_q)$ their inclusion could be relevant one day. The SM phases cancel in this asymmetry [43, 65]⁵.

In the SM and CMFV models

$$\mathcal{A}_{\Delta\Gamma}^\lambda = 1, \quad S_{\mu^+\mu^-}^s = 0, \quad r(y_s) = 0.912 \pm 0.014 \quad (60)$$

independently of NP parameters.

While $\Delta\Gamma_d$ is very small and y_d can be set to zero, in the case of $B_d \rightarrow \mu^+\mu^-$ one can still consider the CP asymmetry $S_{\mu^+\mu^-}^d$ [65], for which we simply find

$$S_{\mu^+\mu^-}^d = \sin(2\theta_Y^{B_d} - 2\varphi_{B_d}). \quad (61)$$

The most recent results from LHCb read [66, 67]

$$\mathcal{B}(B_s \rightarrow \mu^+\mu^-) = (3.2_{-1.2}^{+1.5}) \times 10^{-9}, \quad \mathcal{B}(B_s \rightarrow \mu^+\mu^-)^{\text{SM}} = (3.23 \pm 0.27) \times 10^{-9}, \quad (62)$$

$$\mathcal{B}(B_d \rightarrow \mu^+\mu^-) \leq 9.4 \times 10^{-10}, \quad \mathcal{B}(B_d \rightarrow \mu^+\mu^-)^{\text{SM}} = (1.07 \pm 0.10) \times 10^{-10}. \quad (63)$$

We have shown also SM predictions for these observables [68] that do not include the correction $r(y_s)$. If this factor is included one finds [42, 43]

$$\mathcal{B}(B_s \rightarrow \mu^+\mu^-)_{\text{corr}}^{\text{SM}} = (3.5 \pm 0.3) \cdot 10^{-9}. \quad (64)$$

It is this branching that should be compared in such a case with the results of LHCb given above. For the latest discussions of these issues see [42, 43, 65, 68].

As we will see below in the Z' models considered by us $0.5 \leq \mathcal{A}_{\Delta\Gamma}^\lambda \leq 1$ with the smallest values corresponding to the largest allowed values of $|S_{\psi\phi}|$. Thus the $\Delta\Gamma_s$ effect in question varies from 5% to 9%. In view of still large experimental error we will approximately include this effect in the experimental branching ratio using the values in (60). If this is done the experimental results in (62) is reduced by 9% and we find

$$\mathcal{B}(B_s \rightarrow \mu^+\mu^-)_{\text{corr}} = (2.9_{-1.1}^{+1.4}) \times 10^{-9}, \quad (65)$$

that should be compared with the SM result in (62). While the central theoretical value agrees very well with experiment, the large experimental error still allows for NP contributions. In our plots we will show the result in (65).

⁵We thank Robert Knegjens and Robert Fleischer for discussion of this point.

3.3.3 $K_L \rightarrow \mu^+ \mu^-$

Only the so-called short distance (SD) part to a dispersive contribution to $K_L \rightarrow \mu^+ \mu^-$ can be reliably calculated. Therefore in what follows this decay will be treated only as an additional constraint to be sure that the rough upper bound given below is not violated. We have then following [69] ($\lambda = 0.226$)

$$\mathcal{B}(K_L \rightarrow \mu^+ \mu^-)_{\text{SD}} = 2.08 \cdot 10^{-9} [\bar{P}_c(Y_K) + A^2 R_t |Y_A(K)| \cos \bar{\beta}_Y^K]^2, \quad (66)$$

where R_t is given in (125), $|V_{cb}| \equiv A\lambda^2$ and

$$\bar{\beta}_Y^K \equiv \beta - \beta_s - \theta_Y^K, \quad \bar{P}_c(Y_K) \equiv \left(1 - \frac{\lambda^2}{2}\right) P_c(Y_K), \quad (67)$$

with $P_c(Y_K) = 0.113 \pm 0.017$ [70]. Here β and β_s are the phases of V_{td} and V_{ts} defined in (50).

The extraction of the short distance part from the data is subject to considerable uncertainties. The most recent estimate gives [71]

$$\mathcal{B}(K_L \rightarrow \mu^+ \mu^-)_{\text{SD}} \leq 2.5 \cdot 10^{-9}, \quad (68)$$

to be compared with $(0.8 \pm 0.1) \cdot 10^{-9}$ in the SM [70].

3.3.4 $K^+ \rightarrow \pi^+ \nu \bar{\nu}$ and $K_L \rightarrow \pi^0 \nu \bar{\nu}$

These are the two theoretically cleanest rare decays in quark flavour physics. Reviews of these two decays can be found in [72–74]. The branching ratios for these two modes can be written generally as

$$\text{Br}(K^+ \rightarrow \pi^+ \nu \bar{\nu}) = \kappa_+ \left[\left(\frac{\text{Im} X_{\text{eff}}}{\lambda^5} \right)^2 + \left(\frac{\text{Re} X_{\text{eff}}}{\lambda^5} - P_c(X) \right)^2 \right], \quad (69)$$

$$\text{Br}(K_L \rightarrow \pi^0 \nu \bar{\nu}) = \kappa_L \left(\frac{\text{Im} X_{\text{eff}}}{\lambda^5} \right)^2, \quad (70)$$

where [75]

$$\kappa_+ = (5.36 \pm 0.026) \cdot 10^{-11}, \quad \kappa_L = (2.31 \pm 0.01) \cdot 10^{-10} \quad (71)$$

and [76–79].

$$P_c(X) = 0.42 \pm 0.03. \quad (72)$$

The short distance contributions are described by

$$X_{\text{eff}} = V_{ts}^* V_{td} (X_L(K) + X_R(K)) \quad (73)$$

where $X_{L,R}(K)$ are given in (31) and (32).

Experimentally we have [80]

$$\mathcal{B}(K^+ \rightarrow \pi^+ \nu \bar{\nu})_{\text{exp}} = (17.3_{-10.5}^{+11.5}) \cdot 10^{-11}, \quad (74)$$

and the 90% C.L. upper bound [81]

$$\mathcal{B}(K_L \rightarrow \pi^0 \nu \bar{\nu})_{\text{exp}} \leq 2.6 \cdot 10^{-8}. \quad (75)$$

In the SM one finds [78, 82]

$$\mathcal{B}(K^+ \rightarrow \pi^+ \nu \bar{\nu})_{\text{SM}} = (8.5 \pm 0.7) \cdot 10^{-11}, \quad (76)$$

$$\mathcal{B}(K_L \rightarrow \pi^0 \nu \bar{\nu})_{\text{SM}} = (2.6 \pm 0.4) \cdot 10^{-11}, \quad (77)$$

where the errors are dominated by CKM uncertainties. This should be compared with the experimental values given in (74) and (75). Clearly we have to wait for improved data.

3.3.5 $B \rightarrow \{X_s, K, K^*\} \nu \bar{\nu}$

Following the analysis of [83], the branching ratios of the $B \rightarrow \{X_s, K, K^*\} \nu \bar{\nu}$ modes in the presence of RH currents can be written as follows

$$\mathcal{B}(B \rightarrow K \nu \bar{\nu}) = \mathcal{B}(B \rightarrow K \nu \bar{\nu})_{\text{SM}} \times [1 - 2\eta] \epsilon^2, \quad (78)$$

$$\mathcal{B}(B \rightarrow K^* \nu \bar{\nu}) = \mathcal{B}(B \rightarrow K^* \nu \bar{\nu})_{\text{SM}} \times [1 + 1.31\eta] \epsilon^2, \quad (79)$$

$$\mathcal{B}(B \rightarrow X_s \nu \bar{\nu}) = \mathcal{B}(B \rightarrow X_s \nu \bar{\nu})_{\text{SM}} \times [1 + 0.09\eta] \epsilon^2, \quad (80)$$

where we have introduced the variables

$$\epsilon^2 = \frac{|X_L(B_s)|^2 + |X_R(B_s)|^2}{|\eta_X X_0(x_t)|^2}, \quad \eta = \frac{-\text{Re}(X_L(B_s) X_R^*(B_s))}{|X_L(B_s)|^2 + |X_R(B_s)|^2}, \quad (81)$$

with $X_{L,R}(B_s)$ defined in (33) and (34).

Moreover the average of the K^* longitudinal polarization fraction F_L also used in the studies of $B \rightarrow K^* \ell^+ \ell^-$ is a useful variable as it depends only on η :

$$\langle F_L \rangle = 0.54 \frac{(1 + 2\eta)}{(1 + 1.31\eta)}. \quad (82)$$

We should remark that the expressions in Eqs. (78)–(80), as well as the SM results in (83), refer only to the short-distance contributions to these decays. The latter are

obtained from the corresponding total rates subtracting the reducible long-distance effects pointed out in [84].

The predictions for the SM branching ratios are [83–85]

$$\begin{aligned}\mathcal{B}(B \rightarrow K\nu\bar{\nu})_{\text{SM}} &= (3.64 \pm 0.47) \times 10^{-6} , \\ \mathcal{B}(B \rightarrow K^*\nu\bar{\nu})_{\text{SM}} &= (7.2 \pm 1.1) \times 10^{-6} , \\ \mathcal{B}(B \rightarrow X_s\nu\bar{\nu})_{\text{SM}} &= (2.7 \pm 0.2) \times 10^{-5} ,\end{aligned}\tag{83}$$

to be compared with the experimental bounds [86–88]

$$\begin{aligned}\mathcal{B}(B \rightarrow K\nu\bar{\nu}) &< 1.4 \times 10^{-5} , \\ \mathcal{B}(B \rightarrow K^*\nu\bar{\nu}) &< 8.0 \times 10^{-5} , \\ \mathcal{B}(B \rightarrow X_s\nu\bar{\nu}) &< 6.4 \times 10^{-4} .\end{aligned}\tag{84}$$

As ϵ and η can be calculated in any model by means of (81) the expressions given above can be considered as fundamental formulae for any phenomenological analysis of these decays and a given model can be represented by a point in the $\epsilon - \eta$ plane. Measuring the three branching ratios allows uniquely to determine experimentally the point (ϵ, η) and to compare with any model result. We will illustrate this for Z' scenarios.

3.3.6 $K_L \rightarrow \pi^0 \ell^+ \ell^-$

The rare decays $K_L \rightarrow \pi^0 e^+ e^-$ and $K_L \rightarrow \pi^0 \mu^+ \mu^-$ are dominated by CP-violating contributions. The indirect CP-violating contributions are determined by the measured decays $K_S \rightarrow \pi^0 \ell^+ \ell^-$ and the parameter ε_K in a model independent manner. It is the dominant contribution within the SM where one finds [89]

$$\mathcal{B}(K_L \rightarrow \pi^0 e^+ e^-)_{\text{SM}} = 3.54_{-0.85}^{+0.98} (1.56_{-0.49}^{+0.62}) \cdot 10^{-11} ,\tag{85}$$

$$\mathcal{B}(K_L \rightarrow \pi^0 \mu^+ \mu^-)_{\text{SM}} = 1.41_{-0.26}^{+0.28} (0.95_{-0.21}^{+0.22}) \cdot 10^{-11} ,\tag{86}$$

with the values in parentheses corresponding to the destructive interference between directly and indirectly CP-violating contributions. The last discussion of the theoretical status of this interference sign can be found in [90] where the results of [91–93] are critically analysed. From this discussion, constructive interference seems to be favoured though more work is necessary. In view of significant uncertainties in the SM prediction we will mostly use these decays to test whether the correlations of them with $K_L \rightarrow \pi^0 \nu\bar{\nu}$ and $K^+ \rightarrow \pi^+ \nu\bar{\nu}$ decays can have an impact on the latter. To this end we will confine our analysis to the case of the constructive interference between the directly and indirectly CP-violating contributions.

The present experimental bounds

$$\mathcal{B}(K_L \rightarrow \pi^0 e^+ e^-)_{\text{exp}} < 28 \cdot 10^{-11} \quad [94], \quad \mathcal{B}(K_L \rightarrow \pi^0 \mu^+ \mu^-)_{\text{exp}} < 38 \cdot 10^{-11} \quad [95], \quad (87)$$

are still by one order of magnitude larger than the SM predictions, leaving thereby large room for NP contributions. In fact as our numerical analysis in Sections 7 and 9 demonstrates, these bounds have no impact on $K^+ \rightarrow \pi^+ \nu \bar{\nu}$ and $K_L \rightarrow \pi^0 \nu \bar{\nu}$ decays but the present data on $K^+ \rightarrow \pi^+ \nu \bar{\nu}$ do not allow to reach the above bounds in the $Z'(Z)$ scenarios considered.

In the LHT model the branching ratios for both decays can be enhanced at most by a factor of 1.5 [31, 96]. Slightly larger effects are still allowed in RSc [33].

In the LHT model, where only SM operators are present the effects of NP can be compactly summarised by generalisation of the real SM functions $Y_0(x_t)$ and $Z_0(x_t)$ to two complex functions Y_K and Z_K , respectively. As demonstrated in the context of the corresponding analysis within RSc [33], also in the presence of RH currents two complex functions Y_K and Z_K are sufficient to describe jointly the SM and NP contributions. Consequently the LHT formulae (8.1)–(8.8) of [31] with Y_K and Z_K given below can be used to study these decays in the context of tree-level Z' and Z exchanges. The original papers behind these formulae can be found in [89, 91, 92, 97, 98].

Using the formulae of [33] we find

$$Y_K = \eta_Y Y_0(x_t) + \left[\frac{\Delta_A^{\mu\bar{\mu}}(Z')}{M_{Z'}^2 g_{\text{SM}}^2} \right] \frac{\Delta_V^{sd}(Z')}{V_{ts}^* V_{td}}, \quad (88)$$

$$Z_K = Z_0(x_t) + \frac{1}{4 \sin^2 \theta_W} \left[\frac{2 \Delta_R^{\mu\bar{\mu}}(Z')}{M_{Z'}^2 g_{\text{SM}}^2} \right] \frac{\Delta_V^{sd}(Z')}{V_{ts}^* V_{td}}, \quad (89)$$

where Δ_V^{sd} is defined as in (45). These formulae with obvious changes can also be used for tree-level Z exchanges considered in Section 9.

The presence of additional coupling $\Delta_R^{\mu\bar{\mu}}(Z')$ in addition to $\Delta_A^{\mu\bar{\mu}}(Z')$, introduces as in $B \rightarrow K^* \ell^+ \ell^-$, $B \rightarrow K \ell^+ \ell^-$ and $B \rightarrow X_s \ell^+ \ell^-$ two new parameters and allows thereby to avoid present constraints if necessary. In our analysis we will set $\Delta_R^{\mu\bar{\mu}}(Z')$ to its SM value. In the case of FCNC processes mediated by Z , which will be discussed in Section 9, all leptonic couplings are known and the predictions for $K_L \rightarrow \pi^0 e^+ e^-$ and $K_L \rightarrow \pi^0 \mu^+ \mu^-$ are more specific. The numerical results are presented for Z' and Z contributions in Sections 7 and 9, respectively.

4 $B \rightarrow X_s \gamma$ Decay

4.1 Preliminaries

The $B \rightarrow X_s \gamma$ decay being the first loop induced B-decay determined experimentally has been extensively studied within the SM and its various extensions. For our cal-

calculation of Z' contributions to the relevant Wilson coefficients very useful turned out to be recent study of this decay within gauged flavour models in [38]. Indeed several formulae of this paper could be easily adapted to our analysis.

Let us recall that in the SM the LH structure of the W couplings to quarks requires the chirality flip, necessary for $b \rightarrow s\gamma$ transition to occur, only through the mass of the initial or the final state quark. Consequently the amplitude is proportional to m_b or m_s . In contrast in models like LR models RH couplings of W_R^\pm to quarks allow the chirality flip on the internal top quark line resulting in an enhancement factor m_t/m_b of NP contribution relative to the SM one at the level of the amplitude. However, in the present analysis Z' contributions to $B \rightarrow X_s \gamma$ involve only SM quarks with electric charge $-1/3$ and such an enhancement is absent. Therefore we do not expect large corrections to $B \rightarrow X_s \gamma$ from Z' exchanges, which is good as the SM agrees well with the data. Still it is of interest to check the size of these contributions. In doing this we include QCD corrections to Z' contributions at the LO using the general formulae of [38], while the SM contributions are included at the NNLO level.

Adopting the overall normalization of the SM effective Hamiltonian we have

$$\mathcal{H}_{\text{eff}}(b \rightarrow s\gamma) = -\frac{4G_F}{\sqrt{2}} V_{ts}^* V_{tb} [C_{7\gamma}(\mu_b) Q_{7\gamma} + C_{8G}(\mu_b) Q_{8G}] , \quad (90)$$

where $\mu_b = \mathcal{O}(m_b)$. The dipole operators are defined as

$$Q_{7\gamma} = \frac{e}{16\pi^2} m_b \bar{s}_\alpha \sigma^{\mu\nu} P_R b_\alpha F_{\mu\nu} , \quad Q_{8G} = \frac{g_s}{16\pi^2} m_b \bar{s}_\alpha \sigma^{\mu\nu} P_R T_{\alpha\beta}^a b_\beta G_{\mu\nu}^a . \quad (91)$$

In writing (90) we have dropped the primed operators that are obtained from (91) by replacing P_R by P_L . In the SM the primed operators (RL) are suppressed by m_s/m_b relative to the ones in (90). This is not the case for RL operators but as such contributions do not interfere with SM contributions that is dominant in any case we will neglect these contributions in the case of Z' as well. We have also suppressed current-current operators which are important for the QCD analysis. We will include these effects in the final formulae at the end of this section.

The coefficients $C_i(\mu_b)$ are calculated from their initial values at high energy scales by means of renormalization group methods. We distinguish between SM quark contributions with the matching scale $\mu_t = \mathcal{O}(m_t)$ and the Z' quark contributions with the matching scale $\mu_{Z'} = \mathcal{O}(M_{Z'})$. While in the LO approximation the results depend on the choice of the matching scale, the experience shows that taking as the matching scale the largest mass in the diagram appears to be a very good choice at LO. The choices made above follow this strategy.

We decompose next the Wilson coefficients at the scale $\mu_b = \mathcal{O}(m_b)$ as the sum of the SM contribution and the Z' contributions:

$$C_i(\mu_b) = C_i^{\text{SM}}(\mu_b) + \Delta C_i^{Z'}(\mu_b). \quad (92)$$

We recall that for the SM coefficients at $\mu_t = \mathcal{O}(m_t)$ we have ($x_t = m_t^2/M_W^2$) without QCD corrections

$$C_{7\gamma}^{\text{SM}}(\mu_t) = \frac{3x_t^3 - 2x_t^2}{4(x_t - 1)^4} \ln x_t + \frac{-8x_t^3 - 5x_t^2 + 7x_t}{24(x_t - 1)^3} \equiv C_{7\gamma}^{\text{SM}}(x_t), \quad (93)$$

$$C_{8G}^{\text{SM}}(\mu_t) = \frac{-3x_t^2}{4(x_t - 1)^4} \ln x_t + \frac{-x_t^3 + 5x_t^2 + 2x_t}{8(x_t - 1)^3} \equiv C_{8G}^{\text{SM}}(x_t). \quad (94)$$

In the next subsection, we summarize the results for Z' contributions to the Wilson coefficients of the dipole operators at the relevant matching scale $\mu_{Z'} = \mathcal{O}(M_{Z'})$. Subsequently we will present renormalization group QCD corrections to these coefficients. The final formula for the branching ratio for the $B \rightarrow X_s \gamma$ decay that includes SM and Z' contributions will be presented at the end of this section.

4.2 Z' contribution without QCD Corrections

A general analysis of neutral gauge boson contributions to $B \rightarrow X_s \gamma$ decay has been presented in [38]. In addition to SM-like LL contribution from Z' we have a new LR one, where L (R) stands for the P_L (P_R) projector in the basic penguin diagram involving the $s(b)$ -quark.

In what follows we present the results for a contribution of a fermion f carrying electric charge $-1/3$ and having the mass m_f . This will allow us to compute the contribution from SM down-quarks and in the future if necessary contributions involving new heavy quarks.

We first decompose the Wilson coefficients $\Delta C_i^{Z'}$ at the $\mu_{Z'}$ scale as the sum of the SM-like LL contribution and a new LR one:

$$\Delta C_{7\gamma}^{Z'}(\mu_{Z'}) = \Delta^{LL} C_{7\gamma}^{Z'}(\mu_{Z'}) + \Delta^{LR} C_{7\gamma}^{Z'}(\mu_{Z'}), \quad (95)$$

$$\Delta C_{8G}^{Z'}(\mu_{Z'}) = \Delta^{LL} C_{8G}^{Z'}(\mu_{Z'}) + \Delta^{LR} C_{8G}^{Z'}(\mu_{Z'}).$$

Adapting the formulae of [38] to our notation and denoting by f the down-quark exchanged in the diagram we find

$$\Delta^{LL} C_{7\gamma}^{Z'}(\mu_{Z'}) = -\frac{2}{3} \frac{1}{g_2^2} \frac{M_W^2}{M_{Z'}^2} \sum_f \frac{\Delta_L^{fs*}(Z') \Delta_L^{fb}(Z')}{V_{ts}^* V_{tb}} \left(C_{8G}^{\text{SM}}(x_f) + \frac{1}{3} \right), \quad (96)$$

$$\Delta^{LL} C_{8G}^{Z'}(\mu_{Z'}) = -3 \Delta^{LL} C_{7\gamma}^{Z'}(\mu_{Z'}),$$

with $x_f = m_f^2/M_{Z'}^2$, and summation is over the SM down-quarks.

For LR Wilson coefficients we find:

$$\Delta^{LR} C_{7\gamma}^{Z'}(\mu_{Z'}) = -\frac{2}{3} \frac{1}{g_2^2} \frac{M_W^2}{M_{Z'}^2} \sum_f \frac{m_f}{m_b} \frac{\Delta_L^{fs*}(Z') \Delta_R^{fb}(Z')}{V_{ts}^* V_{tb}} C_{8G}^{LR}(x_f), \quad (97)$$

$$\Delta^{LR} C_{8G}^{Z'}(\mu_{Z'}) = -3 \Delta^{LR} C_{7\gamma}^{Z'}(\mu_{Z'}),$$

with

$$C_{8G}^{LR}(x) = \frac{-3x}{2(1-x)^3} \ln x + \frac{3x(x-3)}{4(x-1)^2} - 1. \quad (98)$$

The summation is over SM down-quarks.

The following properties should be noted:

- 1) As opposed to the case of W^\pm contributions the factor m_f/m_b is either $\mathcal{O}(1)$ or smaller and LR contributions are not dominant.
- 2) $C_{8G}^{LR}(x)$ is a non-vanishing monotonic function of x and takes values in the range $[-1, -1/4]$ for x from 0 to ∞ .

4.3 Final Results including QCD corrections

In order to complete the analysis of $B \rightarrow X_s \gamma$ we have to include QCD corrections which play a very important role in this decay. In the SM these corrections are known at the NNLO level [99]. In the LR model a complete LO analysis has been done by Cho and Misiak [100] and after proper modification we can use their results in our model. In this context the recent analyses [38, 41] turned out to be very useful.

We find then

$$\Delta C_{7\gamma}^{Z'}(\mu_b) = \kappa_7(\mu_{Z'}) \Delta C_{7\gamma}^{Z'}(\mu_{Z'}) + \kappa_8(\mu_{Z'}) \Delta C_{8G}^{Z'}(\mu_{Z'}) + \Delta_{Z'}^{\text{current}}(\mu_b). \quad (99)$$

The last contribution in (99) results from the mixing of new neutral current-current operators generated from the Z' exchange that mix with the dipole operators. The renormalization group analysis of this contribution is very involved but fortunately the LO result is known from [38]. Therefore adapting the formulae (4.16), (4.17) and (5.6) of this paper to our notation we find

$$\Delta_{Z'}^{\text{current}}(\mu_b) = \sum_{\substack{A=L,R \\ f=u,c,t,d,s,b}} \kappa_{LA}^f \Delta^{LA} C_2^f(\mu_{Z'}) + \sum_{A=L,R} \hat{\kappa}_{LA}^d \Delta^{LA} \hat{C}_2^d(\mu_{Z'}), \quad (100)$$

where

$$\Delta^{AB} C_2^f(\mu_{Z'}) = -\frac{2}{g_2^2} \frac{M_W^2}{M_{Z'}^2} \frac{\Delta_A^{sb*}(Z') \tilde{\Delta}_B^{ff}(Z')}{V_{ts}^* V_{tb}}, \quad (101)$$

and

$$\Delta^{AB}\hat{C}_2^d(\mu_{Z'}) = -\frac{2}{g_2^2}\frac{M_W^2}{M_{Z'}^2}\frac{\Delta_A^{sd*}(Z')\Delta_B^{bd}(Z')}{V_{ts}^*V_{tb}}. \quad (102)$$

The diagonal couplings $\tilde{\Delta}_B^{ff}(Z')$ introduce additional parameters. For our numerical estimate we use their SM values.

Finally, κ 's are the NP magic numbers listed in Tab. 2 that is based on [38] which used $\alpha_s(M_Z = 91.1876 \text{ GeV}) = 0.118$. They have been obtained for $\mu_b = 2.5 \text{ GeV}$ as used in the SM calculations. We add that for $\mu_{Z'} = 2.5 \text{ TeV}$ we have $\kappa_7 = 0.427$ and $\kappa_8 = 0.128$.

μ_H	200 GeV	1 TeV	5 TeV	10 TeV	M_Z
κ_7	0.524	0.457	0.408	0.390	0.566
κ_8	0.118	0.125	0.129	0.130	0.111
$\kappa_{LL}^{u,c}$	0.039	0.057	0.076	0.084	0.030
κ_{LL}^t	-0.002	-0.003	-0.002	-0.001	–
κ_{LL}^d	-0.040	-0.057	-0.072	-0.079	-0.032
$\kappa_{LL}^{s,b}$	0.087	0.090	0.090	0.090	0.084
$\hat{\kappa}_{LL}^d$	0.128	0.147	0.163	0.168	0.116
$\kappa_{LR}^{u,c}$	0.085	0.128	0.173	0.193	0.065
κ_{LR}^t	0.004	0.012	0.023	0.028	–
κ_{LR}^d	-0.015	-0.025	-0.036	-0.041	-0.011
$\kappa_{LR}^{s,b}$	-0.078	-0.092	-0.106	-0.111	-0.070
$\hat{\kappa}_{LR}^d$	0.473	0.665	0.865	0.953	0.383

Table 2: The NP magic numbers relevant for QCD calculations [38]. For completeness, in the last column the case of a flavour-violating Z is included.

Using these formulae we find for $M_{Z'} = 1 \text{ TeV}$

$$\Delta C_{7\gamma}^{Z'}(\mu_b) = \mathcal{O}(10^{-4}). \quad (103)$$

While due to the presence of RH couplings, this contribution is by one order of magnitude larger than found in the $\overline{331}$ model [35], it is still negligible when compared with the SM value of -0.353 . Therefore we will not consider $B \rightarrow X_s \gamma$ decay further.

5 General Structure of New Physics Contributions

5.1 Preliminaries

We have seen in Section 2 that the small number of free parameters in each of LHS, RHS, LRS and ALRS scenarios allows to expect definite correlations between flavour

observables in each step of the strategy outlined there. These expectations will be confirmed through the numerical analysis below but it is instructive to develop first a qualitative general view on NP contributions in different scenarios before entering the details.

First, it should be realized that the confrontation of correlations in question with future precise data will not only depend on the size of theoretical, parametric and experimental uncertainties, but also in an important manner on the size of allowed deviations from SM expectations. The latter deviations are presently constrained dominantly by $\Delta F = 2$ observables and $B \rightarrow X_s \gamma$ decay. But as already demonstrated in [35, 36, 40] after the new data from the LHCb, ATLAS and CMS also the decays $B_{s,d} \rightarrow \mu^+ \mu^-$ and $b \rightarrow s \ell^+ \ell^-$ begin to play important roles in this context. We will see their impact on our analysis as well.

Now, in general NP scenarios in which there are many free parameters, it is possible with the help of some amount of fine-tuning to satisfy constraints from $\Delta F = 2$ processes without a large impact on the size of NP contributions to $\Delta F = 1$ processes. However, in the Z' scenarios considered here, in which NP in both $\Delta F = 2$ and $\Delta F = 1$ processes is governed by tree-diagrams, the situation is different. Indeed, due to the property of *factorization* of decay amplitudes into vertices and the propagator at the tree-level, the same quark flavour violating couplings and the same mass $M_{Z'}$ enter $\Delta F = 2$ and $\Delta F = 1$ processes undisturbed by the presence of fermions entering the usual box and penguin diagrams. Let us exhibit these correlations in explicit terms.

5.2 $\Delta F = 1$ vs. $\Delta F = 2$ Correlations

In order to obtain transparent expressions we introduce

$$r^{\text{VLL}} = r^{\text{VRR}} = \frac{8\tilde{r}}{g_{\text{SM}}^2} \quad (104)$$

which is the same for K and B_q systems. $\tilde{r} \approx 1$ is defined in (22). In the case of LR contributions to ΔS let us rewrite (25) and (29) as follows

$$[\Delta S(K)]_{\text{LR}} = \frac{r^{\text{LR}}(K)}{M_{Z'}^2} \frac{\Delta_L^{sd}(Z') \Delta_R^{sd}(Z')}{[\lambda_t^{(K)}]^2} \quad (105)$$

$$[\Delta S(B_q)]_{\text{LR}} = \frac{r^{\text{LR}}(B_q)}{M_{Z'}^2} \frac{\Delta_L^{bq}(Z') \Delta_R^{bq}(Z')}{[\lambda_t^{(q)}]^2} \quad (106)$$

where the quantities r^{LR} can be found by comparing these expressions with (25) and (29), respectively. They depend on low energy parameters, in particular on the meson system and logarithmically on $M_{Z'}$. The latter dependence can be neglected for all practical purposes as long as $M_{Z'}$ is in the range of a few TeV.

We can then derive the following relations between shifts in the basic functions in $\Delta F = 1$ and $\Delta F = 2$ processes which are independent of any parameters like \tilde{s}_{ij} but depend sensitively on $M_{Z'}$ ⁶. In particular they do not depend explicitly on whether S1 or S2 scenarios for $|V_{ub}|$ are considered. This dependence is hidden in the allowed shifts in $\Delta S(K)$ and $\Delta S(B_d)$ both in magnitudes and phases. We have then⁷

LHS Scenario

$$\frac{\Delta X_L(K)}{\sqrt{\Delta S(K)}} = \frac{\sqrt{2}\Delta_L^{\nu\bar{\nu}}(Z')}{M_{Z'}g_{\text{SM}}^2\sqrt{r^{\text{VLL}}}} = 0.597, \quad (107)$$

$$\frac{\Delta X_L(B_q)}{\sqrt{\Delta S(B_q)^*}} = \frac{\sqrt{2}\Delta_L^{\nu\bar{\nu}}(Z')}{M_{Z'}g_{\text{SM}}^2\sqrt{r^{\text{VLL}}}} = 0.597 \quad (108)$$

and

$$\Delta Y_A(K) = \Delta X_L(K) \frac{\Delta_A^{\mu\bar{\mu}}(Z')}{\Delta_L^{\nu\bar{\nu}}(Z')}, \quad \Delta Y_A(B_q) = \Delta X_L(B_q) \frac{\Delta_A^{\mu\bar{\mu}}(Z')}{\Delta_L^{\nu\bar{\nu}}(Z')}. \quad (109)$$

RHS Scenario

$$\Delta X_R(K) = \Delta X_L(K) = -\Delta Y_A(K) \frac{\Delta_L^{\nu\bar{\nu}}(Z')}{\Delta_A^{\mu\bar{\mu}}(Z')}, \quad (110)$$

$$\Delta X_R(B_q) = \Delta X_L(B_q) = -\Delta Y_A(B_q) \frac{\Delta_L^{\nu\bar{\nu}}(Z')}{\Delta_A^{\mu\bar{\mu}}(Z')}. \quad (111)$$

LRS Scenario

$$\frac{\Delta X_L(K)}{\sqrt{-\Delta S(K)}} = \frac{\Delta X_R(K)}{\sqrt{\Delta S(K)}} = \frac{\Delta_L^{\nu\bar{\nu}}(Z')}{M_{Z'}g_{\text{SM}}^2\sqrt{-r^{\text{VLL}} - r^{\text{LR}}(K)}} = 0.048, \quad (112)$$

$$\frac{\Delta X_L(B_q)}{\sqrt{-\Delta S(B_q)^*}} = \frac{\Delta X_R(B_q)}{\sqrt{-\Delta S(B_q)^*}} = \frac{\Delta_L^{\nu\bar{\nu}}(Z')}{M_{Z'}g_{\text{SM}}^2\sqrt{-r^{\text{VLL}} - r^{\text{LR}}(B_q)}} \quad (113)$$

with $\frac{\Delta X_L(B_d)}{\sqrt{-\Delta S(B_d)^*}} = 0.204$ and $\frac{\Delta X_L(B_s)}{\sqrt{-\Delta S(B_s)^*}} = 0.212$.

There are no NP contributions to Y_A functions in this scenario.

ALRS Scenario

$$\frac{\Delta Y_A(K)}{\sqrt{\Delta S(K)}} = 2 \frac{\Delta_A^{\mu\bar{\mu}}(Z')}{M_{Z'}g_{\text{SM}}^2\sqrt{r^{\text{VLL}} - r^{\text{LR}}(K)}} = 0.094, \quad (114)$$

⁶Similar relations have been derived in [35] in the context of $\overline{331}$ model but they involved only LHS scenario.

⁷The numerical values on the r.h.s of these equations correspond to $M_{Z'} = 1$ TeV.

$$\frac{\Delta Y_A(B_q)}{\sqrt{\Delta S(B_q)^*}} = 2 \frac{\Delta_A^{\mu\bar{\mu}}(Z')}{M_{Z'} g_{\text{SM}}^2 \sqrt{r^{\text{VLL}} - r^{\text{LR}}(B_q)}} \quad (115)$$

with $\frac{\Delta Y_A(B_d)}{\sqrt{\Delta S(B_d)^*}} = 0.337$ and $\frac{\Delta Y_A(B_s)}{\sqrt{\Delta S(B_s)^*}} = 0.346$.

There are no NP contributions to $X_{L,R}$ functions in this scenario.

General Scenario

Finally we give for completeness general formulae for the correlations in question that do not assume any particular relation between LH and RH couplings. To this end we write

$$\Delta_R^{ij} = a_{ij} \Delta_L^{ij}, \quad a_{ji} = a_{ij}^*, \quad (116)$$

where a_{ij} are complex numbers.

We find then in the K system

$$\frac{\Delta X_L(K)}{\sqrt{\Delta S(K)}} = \frac{\sqrt{2} \Delta_L^{\nu\bar{\nu}}(Z')}{M_{Z'} g_{\text{SM}}^2} \frac{1}{\sqrt{r^{\text{VLL}}(1 + a_{sd}^2) + 2a_{sd} r^{\text{LR}}(K)}}, \quad (117)$$

$$\Delta X_R(K) = a_{sd} \Delta X_L(K), \quad (118)$$

$$\frac{\Delta Y_A(K)}{\sqrt{\Delta S(K)}} = \frac{\sqrt{2} \Delta_A^{\mu\bar{\mu}}(Z')}{M_{Z'} g_{\text{SM}}^2} \frac{1 - a_{sd}}{\sqrt{r^{\text{VLL}}(1 + a_{sd}^2) + 2a_{sd} r^{\text{LR}}(K)}}. \quad (119)$$

Similarly in the $B_{s,d}$ systems we have

$$\frac{\Delta X_L(B_q)}{\sqrt{\Delta S(B_q)^*}} = \frac{\sqrt{2} \Delta_L^{\nu\bar{\nu}}(Z')}{M_{Z'} g_{\text{SM}}^2} \frac{1}{\sqrt{r^{\text{VLL}}(1 + a_{qb}^2) + 2a_{qb} r^{\text{LR}}(B_q)}}, \quad (120)$$

$$\Delta X_R(B_q) = a_{qb} \Delta X_L(B_q) \quad (121)$$

$$\frac{\Delta Y_A(B_q)}{\sqrt{\Delta S(B_q)^*}} = \frac{\sqrt{2} \Delta_A^{\mu\bar{\mu}}(Z')}{M_{Z'} g_{\text{SM}}^2} \frac{1 - a_{qb}}{\sqrt{r^{\text{VLL}}(1 + a_{qb}^2) + 2a_{qb} r^{\text{LR}}(B_q)}}, \quad (122)$$

Evidently these general relations involve more free parameters than in the scenarios considered in our paper but they could turn out to be useful in concrete Z' models and models with tree-level FCNC's mediated by Z boson.

5.3 Implications

Inspecting these formulae we observe that if the SM prediction for ε_K is very close to its experimental value $\Delta S(K)$ cannot be large and consequently at first sight the shifts $\Delta X_{L,R}(K)$ and $\Delta Y_A(K)$ cannot be large implying suppressed NP contributions to rare K decays unless Z' couplings to neutrinos and charged leptons in the final state are enhanced. The details depend on the value of $M_{Z'}$. However, as we will find below, the present theoretical and parametric uncertainties in ε_K and ΔM_K still allow for large effects in rare K decays both in S1 and S2 scenarios.

Similarly in the B_d and B_s systems if the SM predictions for $\Delta M_{s,d}$, $S_{\psi K_S}$ and $S_{\psi\phi}$ are very close to the data, it is unlikely that large NP contributions to rare B_d and B_s decays, in particular the asymmetries $S_{\mu^+\mu^-}^{s,d}$, will be found, unless again Z' couplings to neutrinos and charged leptons in the final state are enhanced. Here the situation concerning theoretical and parametric uncertainties is better than in the K system and the presence of several additional constraints from $b \rightarrow s$ transitions allows to reach in the B_s system clear cut conclusions.

In this context it is fortunate that within the SM there appears to be a tension between the values of ε_K and $S_{\psi K_S}$ so that some action from NP is required. Moreover, parallel to this tension, the values of $|V_{ub}|$ extracted from inclusive and exclusive decays differ significantly from each other. For a recent review see [101].

If one does not average the inclusive and exclusive values of $|V_{ub}|$ and takes into account the tensions mentioned above, one is lead naturally to two scenarios for NP:

- **Exclusive (small) $|V_{ub}|$ Scenario 1:** $|\varepsilon_K|$ is smaller than its experimental determination, while $S_{\psi K_S}$ is rather close to the central experimental value.
- **Inclusive (large) $|V_{ub}|$ Scenario 2:** $|\varepsilon_K|$ is consistent with its experimental determination, while $S_{\psi K_S}$ is significantly higher than its experimental value.

Thus dependently which scenario is considered we need either *constructive* NP contributions to $|\varepsilon_K|$ (Scenario 1) or *destructive* NP contributions to $S_{\psi K_S}$ (Scenario 2). However this NP should not spoil the agreement with the data for $S_{\psi K_S}$ (Scenario 1) and for $|\varepsilon_K|$ (Scenario 2).

While introducing these two scenarios, one should emphasize the following difference between them. In Scenario 1, the central value of $|\varepsilon_K|$ is visibly smaller than the very precise data but the still significant parametric uncertainty due to $|V_{cb}|^4$ dependence in $|\varepsilon_K|$ and a large uncertainty in the charm contribution found at the NNLO level in [61] does not make this problem as pronounced as this is the case of Scenario 2, where large $|V_{ub}|$ implies definitely a value of $S_{\psi K_S}$ that is by 3σ above the data.

Our previous discussion allows to expect larger NP effects in rare B_d decays in scenario S2 than in S1. This will be indeed confirmed by our numerical analysis. In the K

system one would expect larger NP effects in scenario S1 than S2 but the present uncertainties in ε_K and ΔM_K do not allow to see this clearly. The B_s system is not affected by the choice of these scenarios and in fact our results in S1 and S2 are basically indistinguishable from each other as long as there is no correlation with the B_d system. However, we will demonstrate that the imposition of $U(2)^3$ symmetry on Z' couplings will introduce such correlation with interesting implications for the B_s system.

We do not include $B \rightarrow \tau^+ \nu_\tau$ in this discussion as NP related to this decay has nothing to do with Z' . Moreover, the disagreement of the data with the SM in this case softened significantly with the new data from Belle Collaboration [102]. The new world average provided by the UTfit collaboration of $\mathcal{B}(B^+ \rightarrow \tau^+ \nu)_{\text{exp}} = (0.99 \pm 0.25) \times 10^{-4}$ [103] is in perfect agreement with the SM in scenario S2 and only by 1.5σ above the SM value in scenario S1.

Evidently $|V_{ub}|$ could be some average between the inclusive and exclusive values, in which significant NP effects will be in principle allowed simultaneously in K and B_d decays. This discussion shows how important is the determination of the value of $|V_{ub}|$.

As already remarked above, the case of B_s mesons is different as the $B_s^0 - \bar{B}_s^0$ system is not involved in the tensions discussed above. Here the visible deviation of the ΔM_s in the SM from the data and the asymmetry $S_{\psi\phi}$, still being not accurately measured, govern the possible size of NP contributions in rare decays.

With this general picture in mind we can now proceed to numerical analysis.

6 Strategy for Numerical Analysis

6.1 Preliminaries

Similarly to our analysis in [35] it is not the goal of the next section to present a full-fledged numerical analysis of all correlations including present theoretical, parametric and experimental uncertainties as this would only wash out the effects we want to emphasize. Yet, these uncertainties will be significantly reduced in the coming years [104, 105] and it is of interest to ask how the Z' scenarios considered here would face precision flavour data and the reduction of hadronic and CKM uncertainties. In this respect as emphasized above correlations between various observables are very important and we would like to exhibit these correlations by assuming reduced uncertainties in question. This strategy will also be used for the case of flavour violating Z -couplings.

Therefore, in our numerical analysis we will choose as nominal values for three out of four CKM parameters:

$$|V_{us}| = 0.2252, \quad |V_{cb}| = 0.0406, \quad \gamma = 68^\circ, \quad (123)$$

and instead of taking into account their uncertainties directly, we will take them effectively at a reduced level by increasing the experimental uncertainties in $\Delta M_{s,d}$ and ε_K .

$G_F = 1.16637(1) \times 10^{-5} \text{ GeV}^{-2}$ [106]	$m_{B_d} = 5279.5(3) \text{ MeV}$ [106]
$M_W = 80.385(15) \text{ GeV}$ [106]	$m_{B_s} = 5366.3(6) \text{ MeV}$ [106]
$\sin^2 \theta_W = 0.23116(13)$ [106]	$F_{B_d} = (190.6 \pm 4.6) \text{ MeV}$ [107]
$\alpha(M_Z) = 1/127.9$ [106]	$F_{B_s} = (227.7 \pm 6.2) \text{ MeV}$ [107]
$\alpha_s(M_Z) = 0.1184(7)$ [106]	$\hat{B}_{B_d} = 1.26(11)$ [107]
$m_u(2 \text{ GeV}) = (2.1 \pm 0.1) \text{ MeV}$ [107]	$\hat{B}_{B_s} = 1.33(6)$ [107]
$m_d(2 \text{ GeV}) = (4.73 \pm 0.12) \text{ MeV}$ [107]	$\hat{B}_{B_s}/\hat{B}_{B_d} = 1.05(7)$ [107]
$m_s(2 \text{ GeV}) = (93.4 \pm 1.1) \text{ MeV}$ [107]	$F_{B_d} \sqrt{\hat{B}_{B_d}} = 226(13) \text{ MeV}$ [107]
$m_c(m_c) = (1.279 \pm 0.013) \text{ GeV}$ [108]	$F_{B_s} \sqrt{\hat{B}_{B_s}} = 279(13) \text{ MeV}$ [107]
$m_b(m_b) = 4.19_{-0.06}^{+0.18} \text{ GeV}$ [106]	$\xi = 1.237(32)$ [107]
$m_t(m_t) = 163(1) \text{ GeV}$ [107, 109]	$\eta_B = 0.55(1)$ [58, 59]
$M_t = 172.9 \pm 0.6 \pm 0.9 \text{ GeV}$ [106]	$\Delta M_d = 0.507(4) \text{ ps}^{-1}$ [106]
$m_K = 497.614(24) \text{ MeV}$ [106]	$\Delta M_s = 17.73(5) \text{ ps}^{-1}$ [110, 111]
$F_K = 156.1(11) \text{ MeV}$ [107]	$S_{\psi K_S} = 0.679(20)$ [106]
$\hat{B}_K = 0.767(10)$ [107]	$S_{\psi\phi} = 0.0002 \pm 0.087$ [112]
$\kappa_\epsilon = 0.94(2)$ [62, 63]	$\mathcal{B}(B^+ \rightarrow \tau^+ \nu) = (1.64 \pm 0.34) \times 10^{-4}$ [106]
$\eta_1 = 1.87(76)$ [61]	$\tau_{B^\pm} = (1641 \pm 8) \times 10^{-3} \text{ ps}$ [106]
$\eta_2 = 0.5765(65)$ [58]	$ V_{us} = 0.2252(9)$ [106]
$\eta_3 = 0.496(47)$ [60]	$ V_{cb} = (40.6 \pm 1.3) \times 10^{-3}$ [106]
$\Delta M_K = 0.5292(9) \times 10^{-2} \text{ ps}^{-1}$ [106]	$ V_{ub}^{\text{incl.}} = (4.27 \pm 0.38) \times 10^{-3}$ [106]
$ \varepsilon_K = 2.228(11) \times 10^{-3}$ [106]	$ V_{ub}^{\text{excl.}} = (3.12 \pm 0.26) \times 10^{-3}$ [107]

Table 3: Values of the experimental and theoretical quantities used as input parameters.

Here the values for $|V_{us}|$ and $|V_{cb}|$ have been measured in tree level decays. The value for γ is consistent with CKM fits and as the ratio $\Delta M_d/\Delta M_s$ in the SM agrees well with the data, this choice is a legitimate one. Other inputs are collected in Table 3. For $|V_{ub}|$ we will use as two values

$$|V_{ub}| = 3.1 \cdot 10^{-3} \quad |V_{ub}| = 4.0 \cdot 10^{-3} \quad (124)$$

corresponding to central values of exclusive and inclusive determinations of this CKM element and representing thereby S1 and S2 scenarios, respectively.

Having fixed the three parameters of the CKM matrix to the values in (123), for a given $|V_{ub}|$ the “true” values of the angle β and of the element $|V_{td}|$ are obtained from the unitarity of the CKM matrix:

$$|V_{td}| = |V_{us}||V_{cb}|R_t, \quad R_t = \sqrt{1 + R_b^2 - 2R_b \cos \gamma}, \quad \cot \beta = \frac{1 - R_b \cos \gamma}{R_b \sin \gamma}, \quad (125)$$

where

$$R_b = \left(1 - \frac{\lambda^2}{2}\right) \frac{1 |V_{ub}|}{\lambda |V_{cb}|}. \quad (126)$$

	Scenario 1:	Scenario 2:	Experiment
$ \varepsilon_K $	$1.72(22) \cdot 10^{-3}$	$2.15(32) \cdot 10^{-3}$	$2.228(11) \times 10^{-3}$
$(\sin 2\beta)_{\text{true}}$	0.623(25)	0.770(23)	0.679(20)
$\Delta M_s [\text{ps}^{-1}]$	19.0(21)	19.0(21)	17.73(5)
$\Delta M_d [\text{ps}^{-1}]$	0.56(6)	0.56(6)	0.507(4)
$\mathcal{B}(B^+ \rightarrow \tau^+ \nu_\tau)$	$0.62(14) \cdot 10^{-4}$	$1.02(20) \cdot 10^{-4}$	$0.99(25) \times 10^{-4}$

Table 4: *SM prediction for various observables for $|V_{ub}| = 3.1 \cdot 10^{-3}$ and $|V_{ub}| = 4.0 \cdot 10^{-3}$ and $\gamma = 68^\circ$ compared to experiment.*

In Table 4 we summarize for completeness the SM results for $|\varepsilon_K|$, $\Delta M_{s,d}$, $(\sin 2\beta)_{\text{true}}$ and $\mathcal{B}(B^+ \rightarrow \tau^+ \nu_\tau)$, obtained from (125), setting $\gamma = 68^\circ$ and choosing the two values for $|V_{ub}|$ in (124). We observe that for both choices of $|V_{ub}|$ the data show significant deviations from the SM predictions but the character of the NP which could cure these tensions depends on the choice of $|V_{ub}|$ as already discussed in detail in [7] and in the previous section.

What is striking in this table is that the predicted central values of ΔM_s and ΔM_d , although slightly above the data, are both in good agreement with the latter when hadronic uncertainties are taken into account. In particular the central value of the ratio $\Delta M_s/\Delta M_d$ is very close to the data:

$$\left(\frac{\Delta M_s}{\Delta M_d}\right)_{\text{SM}} = 34.5 \pm 3.0 \quad \text{exp : } 35.0 \pm 0.3. \quad (127)$$

These results depend on the lattice input and in the case of ΔM_d on the value of γ . Therefore to get a better insight both lattice input and the tree level determination of γ have to improve.

In [35] we have analyzed a particular 331 model, the so-called $\overline{331}$ model. Because of suppressed contributions to ε_K , this model favoured the inclusive value of $|V_{ub}|$. Moreover only left-handed couplings of Z' to quarks were present. As already described in Section 2 the present analysis can be considered as the generalization of [35] to include also exclusive values of $|V_{ub}|$ and the right-handed couplings of Z' to quarks. Thus with two scenarios for $|V_{ub}|$ and four scenarios LHS, RHS, LRS, ALRS for flavour violating couplings of Z' to quarks we are led to eight scenarios of Z' -physics to be denoted by

$$\text{LHS1, LHS2, RHS1, RHS2, LRS1, LRS2, ALRS1, ALRS2} \quad (128)$$

with S1 and S2 indicating the $|V_{ub}|$ scenarios.

We should emphasize that in each case we have only two free parameters describing the Z' -quark couplings in each meson system except for the universal $M_{Z'}$. Therefore, as in the case of the $\overline{331}$ model it is possible to determine these couplings from flavour

observables (see Section 2) provided flavour conserving Z' couplings to neutrinos and muons are known. This was the case of the $\overline{331}$ model. Here these couplings are not fixed by the theory and have to be determined in purely leptonic processes. In principle one could also get some insight about them from semi-leptonic meson decays but determining them in purely leptonic processes increases the predictive power of the theory.

Following Step 2 of our general strategy of Section 2, in what follows we will assume that $\Delta_A^{\mu\bar{\mu}}(Z')$ and $\Delta_L^{\nu\bar{\nu}}(Z')$ have been determined in purely leptonic processes. For definiteness we set the lepton couplings at the following values

$$\Delta_L^{\nu\bar{\nu}}(Z') = 0.5, \quad \Delta_A^{\mu\bar{\mu}}(Z') = 0.5, \quad (129)$$

to be compared with $\Delta_L^{\nu\bar{\nu}}(Z') = 0.14$ and $\Delta_A^{\mu\bar{\mu}}(Z') = -0.26$ in the $\overline{331}$ model [35]. In the SM both couplings of Z are equal to 0.372.

The specification of signs in (129) is crucial for the identification of various enhancements and suppressions with respect to SM branching ratios and CP asymmetries and is at the basis of our search for successful oases in the space of parameters. If these signs will be identified in the future to be different from the ones assumed here, it will be straightforward to find out by inspecting our results how the landscape of oases changes for each of the four possibilities for the signs of leptonic couplings.

6.2 Dependence on $M_{Z'}$

The correlations between $\Delta F = 1$ and $\Delta F = 2$ derived in subsection 5.2 imply that when free NP parameters have been bounded by $\Delta F = 2$ constraints, the modifications of ΔX_i and ΔY_i are *inversely* proportional to $M_{Z'}$. This means that in the case of NP contributions significantly smaller than the SM contributions, the modifications of rare decay branching ratios due to NP will be governed by the interference of SM and NP contributions and consequently will also be inversely proportional to $M_{Z'}$. This is the case of all observables in B_s and B_d systems, but not in K system where NP contributions could be much larger than the SM contribution for sufficiently low values of $M_{Z'}$. In the latter case the NP modifications of branching ratios will decrease faster than $1/M_{Z'}$ ($1/M_{Z'}^2$ in the limit of full NP dominance) until NP contributions are sufficiently small so that the $1/M_{Z'}$ dependence is again valid.

Concerning the direct lower bound on $M_{Z'}$ from collider experiments, the most stringent bounds are provided by CMS experiment [113]. The precise value depends on the model considered. While for the so-called sequential Z' the lower bound for $M_{Z'}$ is in the ballpark of 2.5 TeV, in other models values as low as 1 TeV are still possible. In order to cover large set of models, we will choose as our nominal value $M_{Z'} = 1$ TeV. With the help of the formulae in subsection 5.2 it should be possible to estimate approximately, how our results would change for $1 \text{ TeV} \leq M_{Z'} \leq 3 \text{ TeV}$. For much larger values of $M_{Z'}$, considered mainly in K physics, explicit results will be provided.

6.3 Simplified Analysis

As in [35] we will perform a simplified analysis of ε_K , $\Delta M_{d,s}$, $S_{\psi K_S}$ and $S_{\psi\phi}$ in order to identify oases in the space of new parameters (see Section 2) for which these five observables are consistent with experiment. To this end we set all other input parameters at their central values but in order to take partially hadronic and experimental uncertainties into account we require the theory in each of the eight scenarios in (128) to reproduce the data for ε_K within $\pm 10\%$, $\Delta M_{s,d}$ within $\pm 5\%$ and the data on $S_{\psi K_S}$ and $S_{\psi\phi}$ within experimental 2σ . We choose larger uncertainty for ε_K than $\Delta M_{s,d}$ because of its strong $|V_{cb}|^4$ dependence. For ΔM_K we will only require the agreement within $\pm 25\%$ because of potential long distance uncertainties.

Specifically, our search is governed by the following allowed ranges:

$$16.9/\text{ps} \leq \Delta M_s \leq 18.7/\text{ps}, \quad -0.18 \leq S_{\psi\phi} \leq 0.18, \quad (130)$$

$$0.48/\text{ps} \leq \Delta M_d \leq 0.53/\text{ps}, \quad 0.64 \leq S_{\psi K_S} \leq 0.72. \quad (131)$$

$$0.75 \leq \frac{\Delta M_K}{(\Delta M_K)_{\text{SM}}} \leq 1.25, \quad 2.0 \times 10^{-3} \leq |\varepsilon_K| \leq 2.5 \times 10^{-3}. \quad (132)$$

The search for these oases in each of the scenarios in (128) is simplified by the fact that for fixed $M_{Z'}$ each of the pairs $(\Delta M_s, S_{\psi\phi})$, $(\Delta M_d, S_{\psi K_S})$ and $(\Delta M_K, |\varepsilon_K|)$ depend only on two variables. The fact that in the K system we have only one powerful constraint at present is rather unfortunate. The situation will improve by much when the branching ratios for $K^+ \rightarrow \pi^+ \nu \bar{\nu}$ and $K_L \rightarrow \pi^0 \nu \bar{\nu}$ will be measured.

In what follows we will first for each scenario identify the allowed oases. As in the case of the $\overline{331}$ model there will be several oases allowed by the constraints in (130)-(132) and we will have to invoke other observables, which are experimentally only weakly bounded at present in order to find the optimal oasis in each case. Yet, our plots will show that once these observables will be measured precisely one day not only unique oasis in the parameter space will be identified but the specific correlations in this oasis will provide a powerful test of the Z' scenarios.

As in [35], inspecting the expressions for various observables in different oases, we have identified the fastest route to the optimal oasis in each scenario. We will describe this route in each case below. We will also see how the correlations between various observables can give additional tests once the analysis is confined to a particular oasis.

It turns out that considerable progress in the search for the optimal oasis in each scenario can be made by identifying some special observables for whom the sign of departure from SM expectations is sufficient to identify this oasis uniquely. For instance in the case of LHS scenario, in the B_d and B_s meson systems these special observables turn out to be

$$\mathcal{B}(B_d \rightarrow \mu^+ \mu^-), \quad S_{\mu^+ \mu^-}^s, \quad (133)$$

respectively. Already the sign of shifts of them with respect to the SM values allows to make significant progress towards the identification of the optimal oasis in each scenario considered. However, in contrast to LHS scenario considered in [35], in the presence of RH currents the two observables will not be sufficient to identify optimal oasis. As already advertised, in the case of the B_s system, the rescue will come from $B \rightarrow K^* \mu^+ \mu^-$, $B \rightarrow K \mu^+ \mu^-$ and $b \rightarrow s \nu \bar{\nu}$ transitions.

7 An Excursion through Z' Scenarios

7.1 The LHS1 and LHS2 Scenarios

7.1.1 The B_s Meson System

We begin the search for the oases with the B_s system as here the choice of $|V_{ub}|$ is immaterial and the results for LHS1 and LHS2 scenarios are almost identical. Basically only the asymmetry $S_{\psi\phi}$ within the SM and $|V_{ts}|$ are slightly modified because of the unitarity of the CKM matrix. But this changes $S_{\psi\phi}$ in the SM from 0.032 to 0.042 and can be neglected.

The result of this search for $M_{Z'} = 1$ TeV is shown in Fig. 2, where we show the allowed ranges for $(\tilde{s}_{23}, \delta_{23})$. The *red* regions correspond to the allowed ranges for ΔM_s , while the *blue* ones to the corresponding ranges for $S_{\psi\phi}$. The overlap between red and blue regions identifies the oases we were looking for. We observe that the requirement of suppression of ΔM_s implies $\tilde{s}_{23} \neq 0$.

From these plots we extract several oases that are collected in Table 5. We denote by $A_i(S1)$ and $A_i(S2)$ the oases found for the two values of $|V_{ub}|$ but as in the B_s -case there is no change in these oases when moving from S1 to S2 we will show the results only for LHS1 scenario. We observe the following pattern:

- For each oasis with a given δ_{23} there is another oasis with δ_{23} shifted by 180° but the range for \tilde{s}_{23} is unchanged. This discrete ambiguity results from the fact that ΔM_s and $S_{\psi\phi}$ are governed by $2\delta_{23}$. However, as already seen in Table 5 and discussed below this ambiguity can be resolved by other observables. In this context we just investigate whether in a given oasis various branching ratios are enhanced or suppressed with respect to the SM or CP asymmetries modified. In the case of $S_{\mu^+\mu^-}^s$, that vanishes within the SM, we just look at its sign. In the last two columns of Table 5 we consider

$$\Delta\mathcal{B}_s^{\mu^+\mu^-} \equiv \Delta\mathcal{B}(B_s \rightarrow \mu^+\mu^-), \quad \Delta\mathcal{B}_s^{\nu\bar{\nu}} \equiv \Delta\mathcal{B}(B \rightarrow X_s\nu\bar{\nu}). \quad (134)$$

- The oases with $i = 2, 4$ are very small and imply very concrete predictions for various observables. In fact as we will soon see they are already ruled out by the

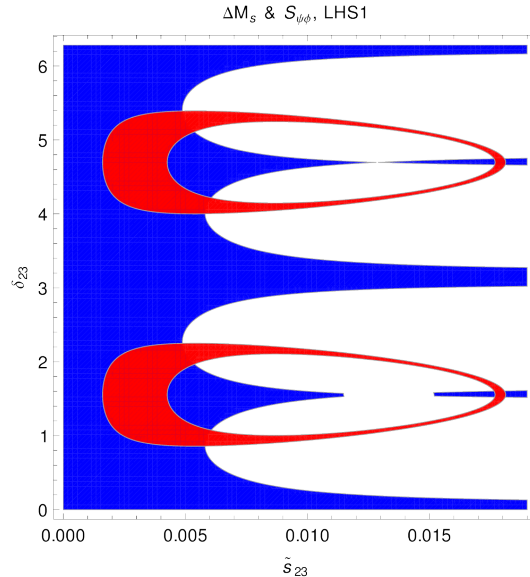


Figure 2: Ranges for ΔM_s (red region) and $S_{\psi\phi}$ (blue region) for $M_{Z'} = 1$ TeV in LHS1 satisfying the bounds in Eq. (130).

present data on $\mathcal{B}(B_s \rightarrow \mu^+ \mu^-)$. They correspond roughly to NP contribution to M_{12}^s twice as large as the SM one but carrying opposite sign.

- The increase of $M_{Z'}$ by a given factor allows to increase \tilde{s}_{23} by the same factor. This structure is evident from the formulae for $\Delta S(B_s)$. However, the inspection of the formulae for $\Delta F = 1$ transitions shows that this change will have impact on rare decays, making the NP effects in them with increased $M_{Z'}$ smaller. This is evident from the correlations derived in Section 5 and has been emphasized at the beginning of our paper.

We will next confine our numerical analysis to these oases, investigating whether some of them can be excluded by other constraints and studying correlations between various observables. To this end we set the lepton couplings as given in (129).

As a final comment, we observe that the oases reported in Table 5 and all other tables for other scenarios below actually describe squares in the spaces $(\tilde{s}_{23}, \delta_{23})$, $(\tilde{s}_{13}, \delta_{13})$ and $(\tilde{s}_{12}, \delta_{12})$, while the corresponding regions in Fig. 2 and analogous figures for other scenarios have more complicated shapes. Indeed, in our numerical analysis of the various observables we have varied the parameters in the *true* oases, requiring that constraints (130)-(132) are satisfied.

In Fig. 3 (left) we show $S_{\mu^+\mu^-}^s$ vs $S_{\psi\phi}$. The requirement of suppression of ΔM_s requires $S_{\mu^+\mu^-}^s$ to be non-zero. A *positive* value of $S_{\mu^+\mu^-}^s$ chooses scenario A_1 , while a *negative* one scenario A_3 . Note that in both scenarios the sign of $S_{\psi\phi}$ is not fixed yet but it will

	\tilde{s}_{23}	δ_{23}	$S_{\mu^+\mu^-}^s$	$\Delta S_{\psi\phi}$	$\Delta \mathcal{B}_s^{\mu^+\mu^-}$	$\Delta \mathcal{B}_s^{\nu\bar{\nu}}$
$A_1(S1)$	0.0016 – 0.0061	$49^\circ - 129^\circ$	+	\pm	\mp	\mp
$A_2(S1)$	0.0176 – 0.0181	$87^\circ - 92^\circ$				
$A_3(S1)$	0.0016 – 0.0061	$229^\circ - 309^\circ$	–	\pm	\pm	\pm
$A_4(S1)$	0.0176 – 0.0181	$267^\circ - 272^\circ$				

Table 5: *Oases in the space $(\tilde{s}_{23}, \delta_{23})$ for $M_{Z'} = 1$ TeV in LHS1. The sign of $S_{\mu^+\mu^-}^s$ chooses the oasis uniquely. The same applies to the pair $S_{\psi\phi}$ and $\Delta \mathcal{B}(B_s \rightarrow \mu^+\mu^-)$ as discussed in the text. Basically the same results are obtained in LHS2.*

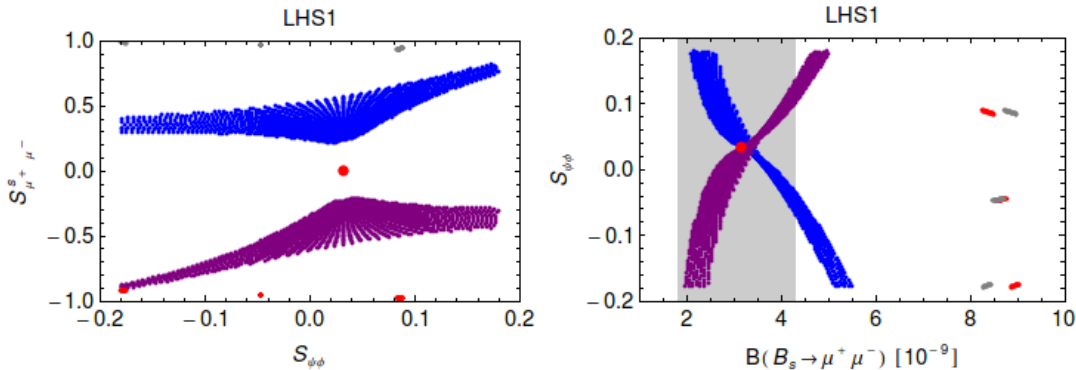


Figure 3: $S_{\mu^+\mu^-}^s$ versus $S_{\psi\phi}$ (left) and $S_{\psi\phi}$ versus $\mathcal{B}(B_s \rightarrow \mu^+\mu^-)$ (right) for $M_{Z'} = 1$ TeV in LHS1. A_1 : blue, A_3 : purple, A_2 : red, A_4 : gray. Gray region: $exp\ 1\sigma$ range $\mathcal{B}(B_s \rightarrow \mu^+\mu^-) = (2.9_{-1.1}^{+1.4}) \cdot 10^{-9}$. Red point: SM central value.

be fixed by invoking $\mathcal{B}(B_s \rightarrow \mu^+\mu^-)$ below. We note that in big oases for $M_{Z'} = 1$ TeV, $|S_{\mu^+\mu^-}^s|$ can reach values as high as 0.9 when $|S_{\psi\phi}| \approx 0.2$. Smaller values are found for larger $M_{Z'}$. We also observe that the small oases represented by gray and red areas are indeed very small and imply $|S_{\mu^+\mu^-}^s| \approx 1$.

The fact that $S_{\mu^+\mu^-}^s$ is very powerful in identifying the optimal oasis can be understood as follows. $S_{\mu^+\mu^-}^s$ is governed by the phase of the function $Y(B_s)$ that originates in the Z' contribution. It can distinguish between A_1 and A_3 oasis because the new phase δ_{23} in these two oases differs by 180° and consequently $\sin \delta_{23}$ relevant for this asymmetry differs by sign in these two oases. Calculating the imaginary part of $Y(B_s)$ in (36) and taking into account that it is Δ_L^{sb} and not Δ_L^{bs} that enters $Y(B_s)$ one can convince oneself about the definite sign of $S_{\mu^+\mu^-}^s$ in A_1 and A_3 oases as stated above.

The reason why $\mathcal{B}(B_s \rightarrow \mu^+\mu^-)$ cannot be presently powerful in the search for oases is the significant experimental error on $S_{\psi\phi}$ with which this branching ratio is correlated. However, inspecting this correlation in a given oasis constitutes an important test of the

model. We show this in Fig. 3 (right)⁸. While in the oasis A_1 $S_{\psi\phi}$ increases (decreases) uniquely with decreasing (increasing) $\mathcal{B}(B_s \rightarrow \mu^+\mu^-)$, in the oasis A_3 , the increase of $S_{\psi\phi}$ implies uniquely an increase of $\mathcal{B}(B_s \rightarrow \mu^+\mu^-)$. Therefore, while $\mathcal{B}(B_s \rightarrow \mu^+\mu^-)$ alone cannot uniquely determine the optimal oasis, it can do in collaboration with $S_{\psi\phi}$. Finding both these observables above or below their SM expectations, would select the oasis A_3 , while finding one of them enhanced and the other suppressed (opposite sign in the case of $S_{\psi\phi}$) would select A_1 as the optimal oasis. We indicate this pattern in Table 5. In fact in the coming years it will be $S_{\psi\phi}$ and $\mathcal{B}(B_s \rightarrow \mu^+\mu^-)$ which will be leading this search as $S_{\mu^+\mu^-}^s$ is much harder to measure.

If the favoured oasis will be found to differ from the one found by means of $S_{\mu^+\mu^-}^s$ one day the model in question will be in trouble. Indeed, let us assume that $\mathcal{B}(B_s \rightarrow \mu^+\mu^-)$ will be found below its SM value. Then the measurement of $S_{\psi\phi}$ will uniquely tell us whether A_1 or A_3 is the optimal scenario and consequently as seen in Fig. 3 (left) and Table 5 we will be able to predict the sign of $S_{\mu^+\mu^-}^s$. Moreover, in the case of $S_{\psi\phi}^s$ sufficiently different from zero, we will be able to determine not only the sign but also the magnitude of $S_{\mu^+\mu^-}^s$.

Probably the most important message from Fig. 3 (right) is the following one. If NP is dominated by Z' in the LHS1 scenario, then departure of $S_{\psi\phi}$ from the SM implies automatically the departure of $\mathcal{B}(B_s \rightarrow \mu^+\mu^-)$ from its SM value and vice versa. Moreover, for $M_{Z'} = 1$ TeV and $|S_{\psi\phi}| \approx 0.2$, $\mathcal{B}(B_s \rightarrow \mu^+\mu^-)$ can deviate from the SM value by $\pm 60\%$. We also note that the small oases are inconsistent with the LHCb data on $\mathcal{B}(B_s \rightarrow \mu^+\mu^-)$ and are already ruled out. Consequently $|S_{\mu^+\mu^-}^s| \approx 1$ is also ruled out. Therefore we will omit the results for small oases in the subsequent plots for B_s meson system.

In Fig. 4 (left) we plot $\mathcal{A}_{\Delta\Gamma}^\lambda$ vs $S_{\psi\phi}$. We observe that for $M_{Z'} = 1$ TeV and $S_{\psi\phi}$ significantly different from zero, $\mathcal{A}_{\Delta\Gamma}^\lambda$ can differ significantly from unity. With $\mathcal{A}_{\Delta\Gamma}^\lambda$ as low as 0.6 the effect of $\Delta\Gamma_s$ on $\mathcal{B}(B_s \rightarrow \mu^+\mu^-)$ becomes smaller.

In Fig. 4 (right) we show $\mathcal{B}(B \rightarrow X_s\nu\bar{\nu})$ vs $\mathcal{B}(B_s \rightarrow \mu^+\mu^-)$. This correlation is valid in any oasis due to the assumed equal sign of the leptonic couplings in (129). However, as seen in the plot the size of NP contribution may depend on the oasis considered. We note that NP effects of 50% are still possible and suppression of $\mathcal{B}(B_s \rightarrow \mu^+\mu^-)$ below the SM value will also imply the suppression of $\mathcal{B}(B \rightarrow X_s\nu\bar{\nu})$. Yet, one should note that if the future data will disagree with this pattern, the rescue could come from the flip of the signs in $\nu\bar{\nu}$ or $\mu^+\mu^-$ couplings provided this is allowed by leptonic decays of Z' .

In Fig. 5 we show $\mathcal{B}(B \rightarrow X_s\nu\bar{\nu})$ vs $S_{\psi\phi}$ which could turn out to be informative when $S_{\psi\phi}$ will be measured precisely one day.

⁸ The central values for $\mathcal{B}(B_d \rightarrow \mu^+\mu^-)^{\text{SM}} = 1.0 \times 10^{-10}$ and $\mathcal{B}(B_s \rightarrow \mu^+\mu^-)^{\text{SM}} = 3.1 \times 10^{-9}$ shown in the plots correspond to fixed CKM parameters chosen by us and differ from the ones listed in (62) and (63) but are fully consistent with them.

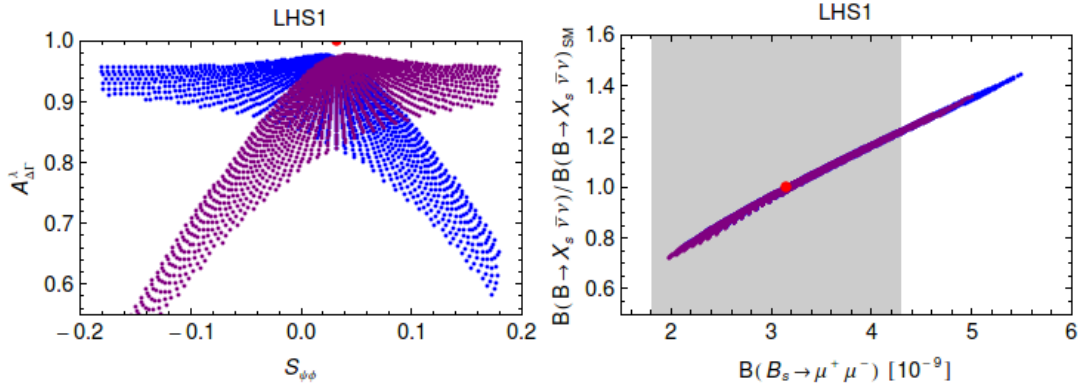


Figure 4: $A_{\Delta\Gamma}^\lambda$ versus $S_{\psi\phi}$ (left) and $\mathcal{B}(B \rightarrow X_s \nu \bar{\nu})$ versus $\mathcal{B}(B_s \rightarrow \mu^+ \mu^-)$ (right) for $M_{Z'} = 1$ TeV in LHS1. A_1 : blue, A_3 : purple. Gray region: exp 1σ range $\mathcal{B}(B_s \rightarrow \mu^+ \mu^-) = (2.9_{-1.1}^{+1.4}) \cdot 10^{-9}$. Red point: SM central value.

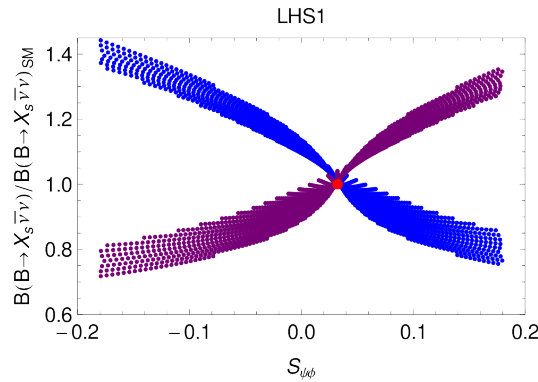


Figure 5: $\mathcal{B}(B \rightarrow X_s \nu \bar{\nu})$ versus $\mathcal{B}(B_s \rightarrow \mu^+ \mu^-)$ for $M_{Z'} = 1$ TeV in LHS1. A_1 : blue, A_3 : purple, A_2 : red, A_4 : gray. Red point: SM central value.

7.1.2 The B_d Meson System

We begin by searching for the allowed oases in this case. The result is shown in Fig. 6 and Table 6. The general structure of the discrete ambiguities is as in Table 5 but now as expected the selected oases in S1 and S2 differ significantly from each other.

Let us first concentrate on S2 scenario that corresponds to the one already analyzed in [35]. In the right panel of Fig. 7 we show $S_{\psi K_S}$ vs $\mathcal{B}(B_d \rightarrow \mu^+ \mu^-)$. The requirement on $S_{\psi K_S}$ and ΔM_d forces $\mathcal{B}(B_d \rightarrow \mu^+ \mu^-)$ to differ from the SM value but the sign of this departure depends on the oasis considered. Here distinction is made between B_1 and B_3 for which $\mathcal{B}(B_d \rightarrow \mu^+ \mu^-)$ is suppressed and enhanced with respect to the SM, respectively. These enhancements and suppressions amount up to $\pm 50\%$ for $M_{Z'} = 1$ TeV. They increase with decreasing $S_{\psi K_S}$.

Note that because of the correlation between $\mathcal{B}(B_d \rightarrow \mu^+ \mu^-)$ and $S_{\psi K_S}$ and the fact that

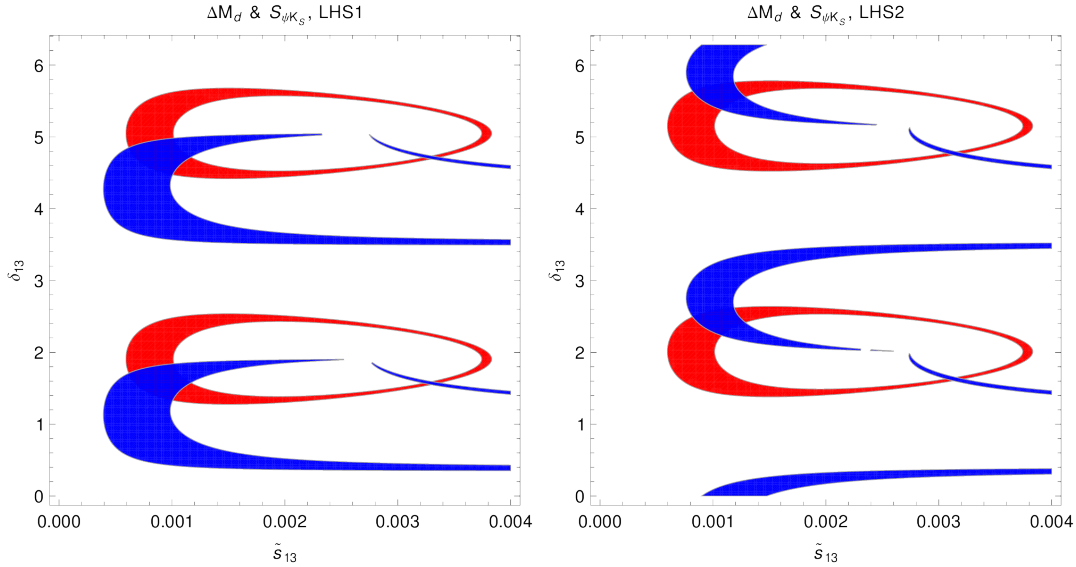


Figure 6: Ranges for ΔM_d (red region) and $S_{\psi K_S}$ (blue region) for $M_{Z'} = 1$ TeV in LHS1 (left) and LHS2 (right) satisfying the bounds in Eq. (131).

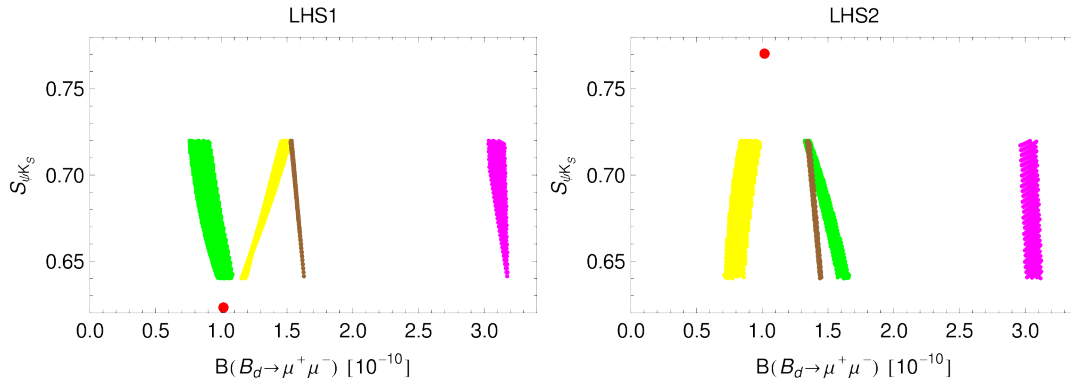


Figure 7: $S_{\psi K_S}$ versus $\mathcal{B}(B_d \rightarrow \mu^+ \mu^-)$ for $M_{Z'} = 1$ TeV in LHS1 (left) and LHS2 (right). B_1 : yellow, B_3 : green, B_2 : magenta, B_4 : brown. Red point: SM central value.

the latter is already well determined, the range of δ_{13} cannot be large. $\mathcal{B}(B_d \rightarrow \mu^+ \mu^-)$ can then distinguish between B_1 and B_3 oases because $\cos \delta_{13}$ differs by sign in these two oases. We find then destructive interference of Z' contribution with the SM contribution in oasis B_1 and constructive one in oasis B_3 implying the results summarized in Table 6 for this $|V_{ub}|$ scenario.

We also observe in Table 6 that $S_{\mu^+ \mu^-}^d$ can also help by means of its sign to distinguish between different oases. Fig. 8 (right panel) also shows that in LHS2 the sign of $S_{\mu^+ \mu^-}^d$

	\tilde{s}_{13}	δ_{13}	$\Delta\mathcal{B}(B_d \rightarrow \mu^+\mu^-)$	$S_{\mu^+\mu^-}^d$
$B_1(S1)$	0.00062 – 0.00117	$76^\circ - 105^\circ$	+(0)	+
$B_2(S1)$	0.00322 – 0.00337	$89^\circ - 91^\circ$		+
$B_3(S1)$	0.00062 – 0.00117	$256^\circ - 285^\circ$	-(0)	-
$B_4(S1)$	0.00322 – 0.00337	$269^\circ - 271^\circ$		-
$B_1(S2)$	0.00081 – 0.00128	$128^\circ - 150^\circ$	-	+
$B_2(S2)$	0.00306 – 0.00322	$92^\circ - 95^\circ$		+
$B_3(S2)$	0.00081 – 0.00128	$308 - 330^\circ$	+	-
$B_4(S2)$	0.00306 – 0.00322	$272^\circ - 275^\circ$		-

Table 6: *Oases in the space* $(\tilde{s}_{13}, \delta_{13})$ *for* $M_{Z'} = 1$ *TeV in LHS and two scenarios for* $|V_{ub}|$. *The enhancement or suppression of* $\mathcal{B}(B_d \rightarrow \mu^+\mu^-)$ *with respect to the SM value chooses the oasis uniquely in LHS2. The sign of* $S_{\mu^+\mu^-}^d$ *chooses the oasis for both LHS1 and LHS2.*

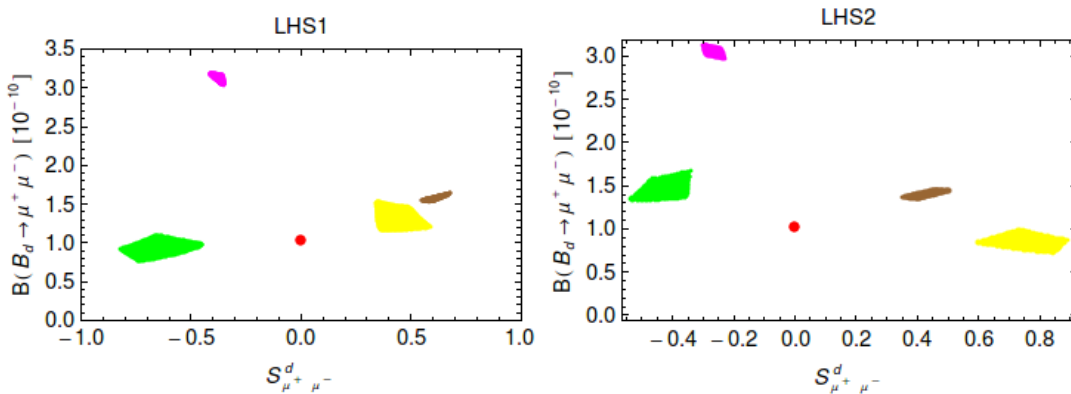


Figure 8: $\mathcal{B}(B_d \rightarrow \mu\bar{\mu})$ versus $S_{\mu^+\mu^-}^d$ for $M_{Z'} = 1$ TeV in LHS1 (left) and LHS2 (right). B_1 : yellow, B_3 : green, B_2 : magenta, B_4 : brown. Red point: SM central value.

is opposite to the sign of the shift in the corresponding branching ratio (except for the small oasis $B_2(S2)$), which can easily be understood by inspecting the ranges of δ_{13} . Moreover, the predictions for $S_{\mu^+\mu^-}^d$ are rather precise. This is in particular the case for small oases, which in the B_d -system cannot be ruled out. In fact in the B_2 oasis $\mathcal{B}(B_d \rightarrow \mu^+\mu^-)$ can still be by a factor of three enhanced with respect to its SM value. Finally, we observe that $S_{\mu^+\mu^-}^d$ can be large, although not as large as $S_{\mu^+\mu^-}^s$.

We next turn to LHS1 scenario for $|V_{ub}|$ which is novel with respect to the analysis in [35]. We observe that the phase δ_{13} is lower for big oases than in the case of scenario S2 but \tilde{s}_{13} is basically the same. We observe that while the sign of $S_{\mu^+\mu^-}^d$ can still

distinguish between the big oases, $B_d \rightarrow \mu^+ \mu^-$ cannot do it as well. This is related to the fact that with $|V_{ub}|$ as low as 0.0031 we have to enhance slightly $S_{\psi K_S}$ in certain range of parameters involved. These features are seen in the left panels in Figs. 7 and 8.

What distinguishes LHS1 from LHS2 is the sign of the correlation between $S_{\mu^+ \mu^-}^d$ and $\mathcal{B}(B_d \rightarrow \mu^+ \mu^-)$. A positive $S_{\mu^+ \mu^-}^d$ implies enhancement of $\mathcal{B}(B_d \rightarrow \mu^+ \mu^-)$ in LHS1 but suppression in LHS2. Note that this pattern is independent of the sign of $Z' \mu^+ \mu^-$ coupling as this coupling enters both observables. On the other hand the flip of this sign would also flip signs in the last two columns in Table 6 and thereby interchange colours in Figs. 7 and 8.

7.1.3 The K Meson System

In the $\overline{331}$ model, which was governed by S2 scenario, NP effects in rare K decays were very small due to suppression of both $\bar{s}dZ'$ and $\bar{\nu}\nu Z'$ couplings in this model.

However in a general Z' model the possibility for S1 scenario for $|V_{ub}|$ and enhanced values of leptonic couplings with respect to the ones found in the $\overline{331}$ model allow to find large NP effects in rare K decays. This allows to find interesting correlations between relevant branching ratios that we would like to exhibit here.

As seen in (132) the constraints from $\Delta F = 2$ observables are weaker than in previous cases. Yet as seen in Fig. 9 it is possible to identify the allowed oases. These plots have the same structure as the plot in Fig. 2 of [34] with the S1 and S2 scenario for $|V_{ub}|$ on the left and on the right, respectively. We observe that the small oases are absent now as ε_K and ΔM_K are governed respectively by imaginary and real parts of M_{12}^K and not by their absolute values like in the case of $\Delta M_{s,d}$. Therefore the solutions with very large NP contributions but opposite signs to the SM contributions corresponding to small oases in the latter case are not allowed here.

Due to weaker constraints in the K system the oases are rather large. We have two oases in S1:

$$C_1(S1) : 0^\circ \leq \delta_{12} \leq 90^\circ, \quad C_2(S1) : 180^\circ \leq \delta_{12} \leq 270^\circ \quad (135)$$

and only one oasis in S2:

$$C_1(S2) : 0^\circ \leq \delta_{12} \leq 360^\circ. \quad (136)$$

As emphasized in [34] of particular interest are the values

$$\delta_{12} = n \frac{\pi}{2}, \quad n = 0, 1, 2, 3 \quad (137)$$

for which NP contributions to ε_K vanish. As seen in Fig. 9 this is only allowed for scenario S2 for which SM agrees well with the data and NP contributions are not required. In this scenario \tilde{s}_{12} can even vanish. In scenario S1, in which NP contributions

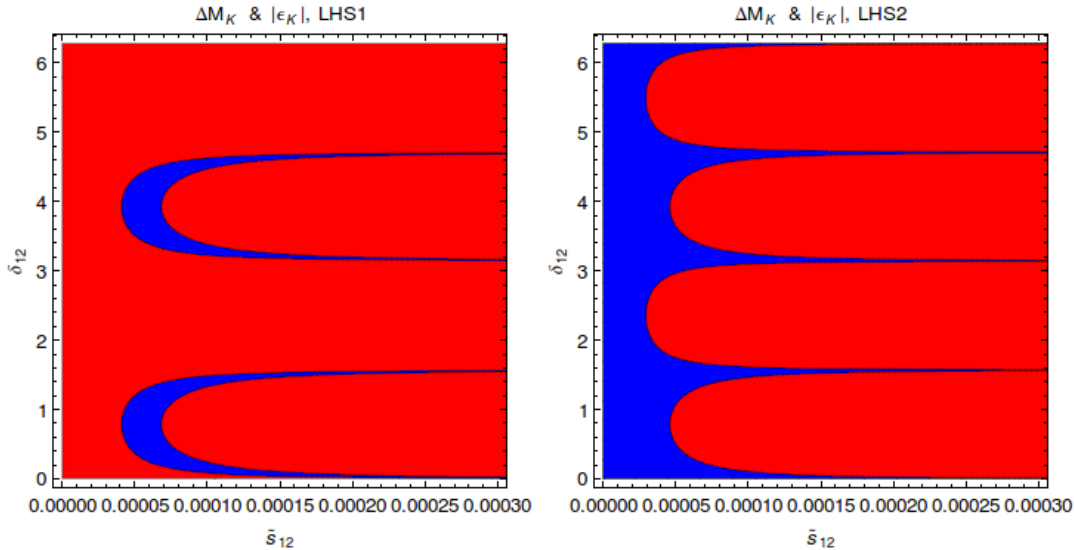


Figure 9: Ranges for ΔM_K (red region) and ε_K (blue region) (LHS1: left, LHS2: right) for $M_{Z'} = 1$ TeV satisfying the bounds in Eq. (132).

are required to reproduce the data, \tilde{s}_{12} is bounded from below and δ_{12} cannot satisfy (137) but for sufficiently large \tilde{s}_{12} can satisfy it approximately. As at these values of δ_{12} , the mass difference ΔM_K is non-zero, \tilde{s}_{12} is bounded from above but due to the weak ΔM_K -constraint this is not seen in the plot.

In [34] an extensive analysis of the interplay between ε_K and in $K \rightarrow \pi\nu\bar{\nu}$ in different NP scenarios has been performed but the case of tree-level Z' contributions has not been discussed. As the latter contributions are much more specific and simpler than the NP models discussed in [34], it will be interesting to see how correlations between ε_K and $K \rightarrow \pi\nu\bar{\nu}$ in the eight scenarios in (128) compare with the findings of [34].

To this end for the LHS scenarios we find for the quantities defined in [34]⁹

$$\phi_{K \rightarrow \pi\nu\bar{\nu}} = \phi_{\Delta S=2} = -\delta_{12} \quad (138)$$

$$R_{K \rightarrow \pi\nu\bar{\nu}} = -\frac{\Delta_L^{\nu\bar{\nu}}(Z')\tilde{s}_{12}}{g_{\text{SM}}^2 M_{Z'}^2}, \quad R_{\Delta S=2} = -\frac{2\sqrt{\tilde{r}}\tilde{s}_{12}}{g_{\text{SM}} M_{Z'}}, \quad (139)$$

implying

$$\rho \equiv \frac{R_{K \rightarrow \pi\nu\bar{\nu}}}{R_{\Delta S=2}} = \frac{1}{2\sqrt{\tilde{r}}} \frac{\Delta_L^{\nu\bar{\nu}}(Z')}{g_{\text{SM}} M_{Z'}} = 1.2 \Delta_L^{\nu\bar{\nu}}(Z') \frac{1 \text{ TeV}}{M_{Z'}}. \quad (140)$$

For our choice of $\Delta_L^{\nu\bar{\nu}}(Z')$ we find $\rho \approx 0.6$ for $M_{Z'} = 1$ TeV. On the basis of [34] we expect for this value of ρ strict correlation between $\mathcal{B}(K^+ \rightarrow \pi^+\nu\bar{\nu})$ and $\mathcal{B}(K_L \rightarrow \pi^0\nu\bar{\nu})$ familiar from the LHT model [32]. It is interesting that ρ depends only on the size of

⁹In [34] ρ was denoted by ϵ .

$\Delta_L^{\nu\bar{\nu}}(Z')$ and $M_{Z'}$. This will have important implications for the study of flavour-violating Z couplings considered in Section 9.

In the upper panels of Fig. 10 we show this correlation in LHS1 and LHS2 for $M_{Z'} = 1$ TeV. We observe the following pattern of deviations from the SM expectations:

- There are two branches in both scenarios. The difference between LHS1 and LHS2 originates from required NP contributions in LHS1 in order to agree with the data on ε_K and the fact that in LHS1 there are two oases and only one in LHS2.
- The horizontal branch in both plots corresponds to $n = 0, 2$ in (137), for which NP contribution to $K \rightarrow \pi\nu\bar{\nu}$ is real and vanishes in the case of $K_L \rightarrow \pi^0\nu\bar{\nu}$.
- The second branch corresponds to $n = 1, 3$ in (137), for which NP contribution is purely imaginary. It is parallel to the Grossman-Nir (GN) bound [114] that is represented by the solid line.

This pattern agrees with general results of [34]. In fact the structure of plots in the Fig. 3 and 4 of the latter paper agrees for $\rho \approx 1$ very well with our findings for LHS2 and LHS1 scenarios, respectively. What is striking is the fact that still large deviations from the SM predictions are allowed, significantly larger than in the case of rare B decays. This is a consequence of the weaker constraint from $\Delta S = 2$ processes than $\Delta B = 2$ and the fact that rare K decays are stronger suppressed than rare B decays within the SM. Yet as we will soon see some of these large values will be ruled out through the correlation with $K_L \rightarrow \mu^+\mu^-$.

In the left panel of Fig. 11 we show the correlation between $\mathcal{B}(K^+ \rightarrow \pi^+\nu\bar{\nu})$ and $\mathcal{B}(K_L \rightarrow \mu^+\mu^-)$ for LHS1. We note a correlation analogous to the one found in the LHT model [32] but due to fewer free parameters in Z' model this correlation depends whether oasis C_1 or C_2 is considered. Very similar correlation is found in LHS2 scenario but as here only one very big oasis is present only *cyan* regions appear. We will return to the right panel in this figure in the context of RHS1 scenario below.

While at first sight the correlation in Fig. 11 is similar in shape to the one in Fig. 10, one should note that $K_L \rightarrow \mu^+\mu^-$ is governed by the real part of the involved master function and not imaginary part as was the case of $K_L \rightarrow \pi^0\nu\bar{\nu}$. Therefore the horizontal line in Fig. 11 corresponds this time to $n = 1, 3$ in (137), for which NP contribution is purely imaginary, while the other branches correspond to $n = 0, 2$ in (137), for which NP contribution to $K \rightarrow \pi\nu\bar{\nu}$ is real and vanishes in the case of $K_L \rightarrow \pi^0\nu\bar{\nu}$.

We observe again that NP effects in both decays can be large and the upper bound on $\mathcal{B}(K_L \rightarrow \mu^+\mu^-)$ in (68) represented by the horizontal black line can easily be violated. The impact of this bound on the results in Fig. 10 is represented by the black areas that violate this bound.

Combining the information from Figs. 10 and 11 we obtain the following result:

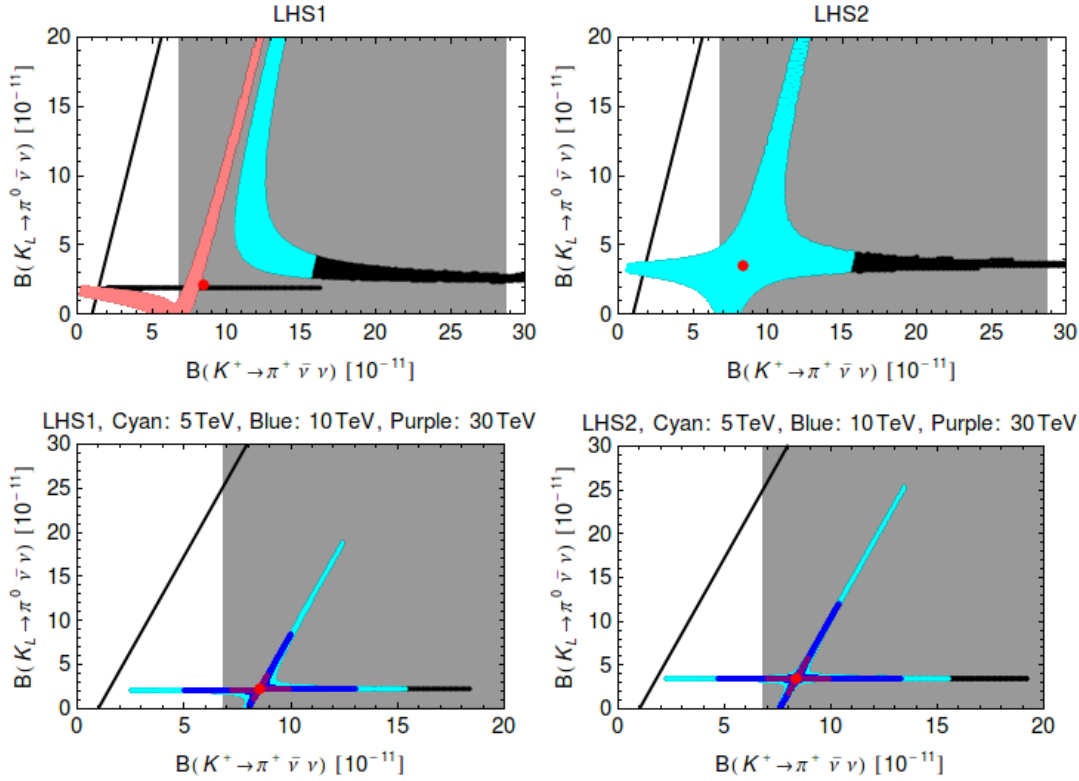


Figure 10: $\mathcal{B}(K_L \rightarrow \pi^0 \nu \bar{\nu})$ versus $\mathcal{B}(K^+ \rightarrow \pi^+ \nu \bar{\nu})$ for $M_{Z'} = 1$ TeV (upper panels, C_1 : cyan, C_2 : pink.) and $M_{Z'} = 5$ TeV (cyan), 10 TeV (blue) and 30 TeV (purple) (lower panels) in LHS1 (left) and LHS2 (right). Black regions are excluded by the upper bound $\mathcal{B}(K_L \rightarrow \mu^+ \mu^-) \leq 2.5 \cdot 10^{-9}$. Red point: SM central value. Gray region: experimental range of $\mathcal{B}(K^+ \rightarrow \pi^+ \nu \bar{\nu})$.

- In the case of the dominance of real NP contributions we find in $C_1(S1)$ for $M_{Z'} = 1$ TeV

$$\mathcal{B}(K^+ \rightarrow \pi^+ \nu \bar{\nu}) \leq 16 \cdot 10^{-11}. \quad (141)$$

In this case $K_L \rightarrow \pi^0 \nu \bar{\nu}$ is SM-like and $\mathcal{B}(K_L \rightarrow \mu^+ \mu^-)$ reaches the upper bound in (68). On the other hand $C_2(S1)$ oasis in this case is excluded through the simultaneous consideration of both decays.

- In the case of the dominance of imaginary NP contributions the bound on $\mathcal{B}(K_L \rightarrow \mu^+ \mu^-)$ is ineffective and both $\mathcal{B}(K^+ \rightarrow \pi^+ \nu \bar{\nu})$ and $\mathcal{B}(K_L \rightarrow \pi^0 \nu \bar{\nu})$ can be significantly larger than the SM predictions and $\mathcal{B}(K^+ \rightarrow \pi^+ \nu \bar{\nu})$ can also be larger than its present experimental central value. We also find that for such large values the branching ratios are strongly correlated. Inspecting in the LHS2 scenario when the branch parallel to the GN bound leaves the grey region corresponding to the

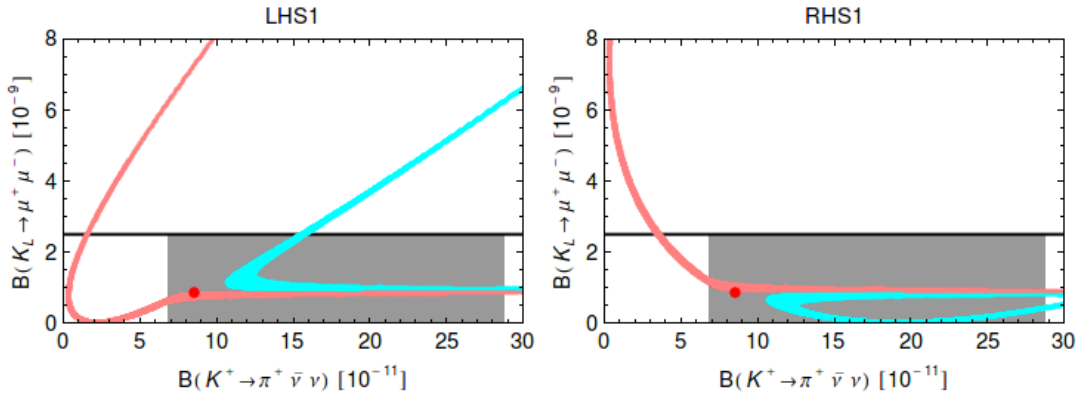


Figure 11: $\mathcal{B}(K_L \rightarrow \mu^+ \mu^-)$ versus $\mathcal{B}(K^+ \rightarrow \pi^+ \nu \bar{\nu})$ for $M_{Z'} = 1$ TeV in LHS1 (left) and RHS1 (right). C_1 : cyan, C_2 : pink. Red point: SM central value. Gray region: experimental range of $\mathcal{B}(K^+ \rightarrow \pi^+ \nu \bar{\nu})$ and horizontal black line: upper bound of $\mathcal{B}(K_L \rightarrow \mu^+ \mu^-)$.

1σ region in (74) we find a rough upper bound

$$\mathcal{B}(K_L \rightarrow \pi^0 \nu \bar{\nu}) \leq 85 \cdot 10^{-11}, \quad (142)$$

which is much stronger than the present experimental upper bound in (75).

We conclude therefore that $K \rightarrow \pi \nu \bar{\nu}$ decays provide an important portal to flavour-violating Z' with masses outside the reach of the LHC before its upgrade and even in its second phase. In the lower part of Fig. 10 we show therefore how the plots in the upper part of this figure would look like for $M_{Z'} = 5$ TeV, 10 TeV and 30 TeV. We observe that even at $M_{Z'} = 10$ TeV both branching ratios can still differ by much from SM predictions and for $M_{Z'} \leq 20$ TeV NP effects in these decays, in particular $K_L \rightarrow \pi^0 \nu \bar{\nu}$ should be detectable in the flavour precision era. For $M_{Z'} = 30$ TeV and higher scales it will be very difficult.

In the left panel of Fig. 12 we show the correlation between $\mathcal{B}(K_L \rightarrow \pi^0 e^+ e^-)$ and $\mathcal{B}(K_L \rightarrow \pi^0 \mu^+ \mu^-)$ that has first been investigated in [89, 91, 92]. We have shown only the results in LHS2 as our main goal here is to find out whether large enhancements of the branching ratios for $K_L \rightarrow \pi^0 \nu \bar{\nu}$ and $K^+ \rightarrow \pi^+ \nu \bar{\nu}$ can be affected by these decays. To this end we have also assumed constructive interference between SM and NP contributions.

We observe a strong correlation between $\mathcal{B}(K_L \rightarrow \pi^0 e^+ e^-)$ and $\mathcal{B}(K_L \rightarrow \pi^0 \mu^+ \mu^-)$, similar to the case of LHT [31] and RSc [33] models. Indeed such a correlation is common to all models with no scalar operators contributing to the decays in question [89, 91, 92]. We also observe that both branching ratios can be in principle enhanced by an order of magnitude over the SM values in (86). However, the correlation with $K^+ \rightarrow \pi^+ \nu \bar{\nu}$ and

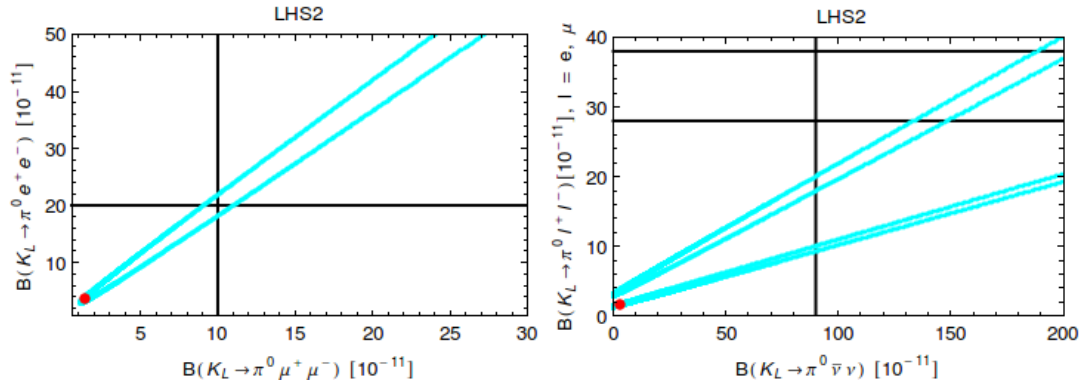


Figure 12: $\mathcal{B}(K_L \rightarrow \pi^0 e^+ e^-)$ as a function of $\mathcal{B}(K_L \rightarrow \pi^0 \mu^+ \mu^-)$ (left panel) and $\mathcal{B}(K_L \rightarrow \pi^0 e^+ e^-)$ (upper curve) and $\mathcal{B}(K_L \rightarrow \pi^0 \mu^+ \mu^-)$ (lower curve) as functions of $\mathcal{B}(K_L \rightarrow \pi^0 \nu \bar{\nu})$ (right panel) in LHS2 for $M_{Z'} = 1$ TeV. The red points represent SM predictions.

$K_L \rightarrow \pi^0 \nu \bar{\nu}$ does not allow for such large values. Indeed the experimental upper bound on $\mathcal{B}(K^+ \rightarrow \pi^+ \nu \bar{\nu})$ implies in a given scenario an upper bound on $\mathcal{B}(K_L \rightarrow \pi^0 \nu \bar{\nu})$ as given in (142) and this in turn implies upper bounds on $\mathcal{B}(K_L \rightarrow \pi^0 e^+ e^-)$ and $\mathcal{B}(K_L \rightarrow \pi^0 \mu^+ \mu^-)$ that are strongly correlated with $\mathcal{B}(K_L \rightarrow \pi^0 \nu \bar{\nu})$. This correlation is evident in Z' scenarios if one compares the expressions for the relevant amplitudes.

In the right panel of Fig. 12 we show this correlation that has already been found in the LHT model [31] and in the RSc model [33]. We note that a large enhancement of $\mathcal{B}(K_L \rightarrow \pi^0 \nu \bar{\nu})$ automatically implies significant enhancements of $\mathcal{B}(K_L \rightarrow \pi^0 \ell^+ \ell^-)$, although the NP effects in $K_L \rightarrow \pi^0 \nu \bar{\nu}$ are stronger. This is related to the fact that small or moderate NP effects in $K_L \rightarrow \pi^0 \ell^+ \ell^-$ are shadowed by the dominant indirectly CP-violating contribution. However, for large NP contributions when the directly CP-violating contribution becomes more important NP effects in $\mathcal{B}(K_L \rightarrow \pi^0 \nu \bar{\nu})$ and $\mathcal{B}(K_L \rightarrow \pi^0 \ell^+ \ell^-)$ are comparable in size. The correlations in Fig. 12 constitute a powerful test of the model considered.

The vertical solid line in the right panel of Fig. 12 corresponds to the rough bound in (142). It implies upper bounds on $\mathcal{B}(K_L \rightarrow \pi^0 \ell^+ \ell^-)$ that are stronger than the present experimental bounds. We indicate these bounds by horizontal and vertical solid lines in the left panel of this figure.

This analysis shows that in LHS scenarios the present upper bounds on $\mathcal{B}(K_L \rightarrow \pi^0 \ell^+ \ell^-)$ do not preclude large NP effects found in $\mathcal{B}(K^+ \rightarrow \pi^+ \nu \bar{\nu})$ and $\mathcal{B}(K_L \rightarrow \pi^0 \nu \bar{\nu})$ but the bounds on the latter branching ratios have an impact on $\mathcal{B}(K_L \rightarrow \pi^0 \ell^+ \ell^-)$. This property remains for higher values of $M_{Z'}$.

7.2 The RHS1 and RHS2 Scenarios

7.2.1 First Observations

We will now investigate Z' scenario with exclusively RH couplings to quarks. We should emphasize that such scenario is not artificial as in certain extensions of the SM, the corrections to left-handed neutral gauge boson couplings are suppressed due to some custodial symmetries. This is for instance the case of the ordinary Z gauge boson in Randall-Sundrum scenarios with custodial symmetry in the bulk (RSc). In such a case the phenomenology of flavour violation is dominated by right-handed couplings [33].

Now in the RHS1 and RHS2 scenarios only RH couplings to quarks are present in Z' contributions. As QCD is parity conserving, the hadronic matrix elements for operators with RH currents as well as QCD corrections remain unchanged. The expressions for $\Delta F = 2$ observables in RHS1 and RHS2 scenarios as well as the corresponding constraints have precisely the same structure as in the LHS1 and LHS2 cases just discussed. Therefore the oases in the space of parameters related to RH currents are precisely the same as those given in Tables 5 and 6, except that the parameters \tilde{s}_{ij} and δ_{ij} parametrize now RH and not LH currents. Anticipating this result we have not introduced separate description of LH and RH oases. Yet, in the case of $\Delta F = 1$ observables several changes are present which allow in principle to distinguish the RHS1 and RHS2 scenarios from the corresponding LHS1 and LHS2, which we just analyzed in detail.

In what follows we will list all changes in the three meson systems one by one. We use for the oases the same notation as in the LHS cases. The basic rule for modifications of correlations between various observables is as follows:

- In $\Delta F = 2$ observables nothing changes as stated above. Therefore we do not show any plots for allowed oases.
- In $\Delta F = 1$ observables governed by the functions Y , that is processes with muons in the final state, there is *a change of sign* of NP contributions in a given oasis. See (35) and (36).
- In $\Delta F = 1$ observables governed by the functions X , that is processes with neutrinos in the final state, there is *no change of sign* of NP contributions in a given oasis. The consequences of it are straightforward in the case of $K^+ \rightarrow \pi^+ \nu \bar{\nu}$ and $K_L \rightarrow \pi^0 \nu \bar{\nu}$ but in the case of $b \rightarrow s \nu \bar{\nu}$ transitions the implications are richer as we have four observables to our disposal that are sensitive to the RH currents in a different manner. See (78)-(80) and (82). The same comments apply to $B \rightarrow K^* \mu^+ \mu^-$ and $B \rightarrow K \mu^+ \mu^-$ which now receive contributions from primed operators Q'_9 and Q'_{10} .

7.2.2 The B_s Meson System

In Fig. 3 we have shown $S_{\mu^+\mu^-}^s$ vs $S_{\psi\phi}$ in the LHS1 scenario. This plot is also valid for RHS1 scenario except that now a *negative* value of $S_{\mu^+\mu^-}^s$ chooses scenario A_1 , while a *positive* one scenario A_3 . The size of NP effects is the same in LHS1 and RHS1, only the oases are interchanged. The same comments apply to large $|V_{ub}|$ scenario.

We conclude therefore that on the basis of $S_{\mu^+\mu^-}^s$ and $S_{\psi\phi}$ alone it is not possible to distinguish between LHS1 and RHS1 scenarios because in the RHS1 scenario one can simply interchange the two big oases or two small oases to obtain the same physical results as in LHS1 scenario. Therefore let us look at other observables.

In Fig. 3 (right) we have shown $S_{\psi\phi}$ vs $\mathcal{B}(B_s \rightarrow \mu^+\mu^-)$ in the LHS1 scenario. This plot is also valid for the RHS1 scenario but again the oases A_1 and A_3 are interchanged. While in the oasis A_1 $S_{\psi\phi}$ increases (decreases) uniquely with increasing (decreasing) $\mathcal{B}(B_s \rightarrow \mu^+\mu^-)$, in the oasis A_3 , the increase of $S_{\psi\phi}$ implies uniquely a decrease of $\mathcal{B}(B_s \rightarrow \mu^+\mu^-)$.

Clearly as in the LHS1 scenario this result represents a test of the RHS1 scenario but if one day we will have precise measurements of $S_{\mu^+\mu^-}^s$, $S_{\psi\phi}$ and $\mathcal{B}(B_s \rightarrow \mu^+\mu^-)$ we will still not be able to distinguish for instance whether we deal with LHS1 scenario in oasis A_1 or RHS1 scenario in oasis A_3 .

Fortunately, as we will see in subsection 7.5, we will be able to make a clear distinction between LHS and RHS scenarios by considering model independent bounds from $B \rightarrow K^*\mu^+\mu^-$ and $B \rightarrow K\mu^+\mu^-$ on the Wilson coefficients of primed operator Q'_{10} . Also, as seen in (78)-(80) and (82), $b \rightarrow s\nu\bar{\nu}$ transitions being sensitive to RH currents will be very helpful in this respect. In LHS scenarios the first three observables were affected in the same manner and F_L was unaffected. Therefore the comparison of these different structures in RHS and LHS scenarios will give us a powerful insight in the Z' couplings. As these issues will also be relevant for LR and ALR scenarios, we will discuss $b \rightarrow s\nu\bar{\nu}$ observables in the four scenarios in a separate subsection at the end of this section.

7.2.3 The B_d Meson System

Similarly to the B_s case the structure of oases is as in Fig. 6 and Table 6. In Fig. 7 we have shown $S_{\psi K_S}$ vs $\mathcal{B}(B_d \rightarrow \mu^+\mu^-)$ for the LHS2 scenario. This plot is also valid for RHS2 scenario and $\mathcal{B}(B_d \rightarrow \mu^+\mu^-)$ can distinguish between B_1 and B_3 oases. But now the behaviour of $\mathcal{B}(B_d \rightarrow \mu^+\mu^-)$ in these two oases is interchanged. It is enhanced and suppressed with respect to the SM in B_1 and B_3 , respectively. Thus we cannot distinguish between LHS2 and RHS2 on the basis of these observables. Clearly the study of $b \rightarrow d\mu^+\bar{\mu}^-$ and $b \rightarrow d\nu\bar{\nu}$ transitions could help in this context but they are more challenging both theoretically and experimentally.

Analogous comments apply to RHS1 which cannot be distinguished from LHS1 on the basis of observables considered.

7.2.4 The K Meson System

In Fig. 10 we have shown the correlation between $\mathcal{B}(K^+ \rightarrow \pi^+ \nu \bar{\nu})$ and $\mathcal{B}(K_L \rightarrow \pi^0 \nu \bar{\nu})$ in the LHS1 and LHS2 scenario. It is evident from (73) that this plot applies identically to RHS1 and RHS2 scenarios as well. Thus $K^+ \rightarrow \pi^+ \nu \bar{\nu}$ and $K_L \rightarrow \pi^0 \nu \bar{\nu}$ decays are not useful for the search of RH currents as they are sensitive only the vector parts of Z' couplings to quarks. As expected, we also find that the results for $K_L \rightarrow \pi^0 \ell^+ \ell^-$ decays are the same as in LHS scenarios.

However, as known already from different studies, in particular in RSc scenario [33], the correlation between $\mathcal{B}(K^+ \rightarrow \pi^+ \nu \bar{\nu})$ and $\mathcal{B}(K_L \rightarrow \mu^+ \mu^-)$ brings the rescue to this problematic as the latter decay is sensitive to the axial-vector couplings. In the right panel of Fig. 11 we show this correlation for the RHS1 scenario. Indeed the correlations in both cases differ from the ones in LHS1.

We also note that in the case of the dominance of imaginary NP contributions corresponding to the horizontal line, $\mathcal{B}(K^+ \rightarrow \pi^+ \nu \bar{\nu})$ and $\mathcal{B}(K_L \rightarrow \pi^0 \nu \bar{\nu})$ can be large. But otherwise $\mathcal{B}(K^+ \rightarrow \pi^+ \nu \bar{\nu})$ is suppressed with respect to its SM value and $\mathcal{B}(K_L \rightarrow \pi^0 \nu \bar{\nu})$ is SM-like.

We should emphasize at this point that the impact of $K_L \rightarrow \mu^+ \mu^-$ on $K^+ \rightarrow \pi^+ \nu \bar{\nu}$ and $K_L \rightarrow \pi^0 \nu \bar{\nu}$ and its correlation with them depends on the sign of leptonic couplings. For a negative $\Delta_A^{\mu\bar{\mu}}$ the results in LHS and RHS scenarios would be interchanged.

7.3 The LRS1 and LRS2 Scenarios

7.3.1 First Observations

If both LH and RH currents are present in NP contributions, the pattern of flavour violation can differ from the scenarios considered until now in a profound manner. If the LH and RH couplings differ from each other, the number of parameters increases and it is harder to get clear cut conclusions without some underlying fundamental theory. On the other hand some of the ‘‘symmetries’’ between LHS and RHS scenarios identified above are broken and the effect of RH currents in certain cases could in principle be better visible.

Here in order to keep the same number of parameters as in previous scenarios we will assume a left-right symmetry in the Z' -couplings to quarks. That is the LH couplings Δ_L are equal in magnitudes and phases to the corresponding RH couplings Δ_R . In this manner we can also keep the same parametrization of couplings as in previous scenarios.

Before entering the details let us emphasize two new features relative to the cases in which either LH or RH couplings in NP contributions were present:

- NP contributions to $\Delta F = 2$ observables are dominated now by new LR operators, whose contributions are enhanced through renormalization group effects relative

to LL and RR operators and in the case of ε_K also through chirally enhanced hadronic matrix elements. Consequently the oases will differ from the previous ones.

- NP contributions to $B_{d,s} \rightarrow \mu^+\mu^-$ and $K_L \rightarrow \mu^+\mu^-$ vanish eliminating in this manner $S_{\mu^+\mu^-}^{s,d}$ and $\mathcal{B}(B_{s,d} \rightarrow \mu^+\mu^-)$ as basic observables in the identification of acceptable oases. On the other hand $B \rightarrow K^*\mu^+\mu^-$ and $B \rightarrow K\mu^+\mu^-$ receive still NP contributions and can help in this context.
- Also NP contributions to decays with neutrinos in the final state, that is $K^+ \rightarrow \pi^+\nu\bar{\nu}$, $K_L \rightarrow \pi^0\nu\bar{\nu}$ and the $b \rightarrow s\nu\bar{\nu}$ transitions are important for testing the LRS1 and LRS2 scenarios.

While $S_{\mu^+\mu^-}^{s,d}$ cannot help in the identification of the optimal oasis in the LR scenarios they are non-vanishing as seen in (59) and (61):

$$S_{\mu^+\mu^-}^q = -\sin(2\varphi_{B_q}). \quad (143)$$

While rather small they offer a clean test of LR scenarios.

7.3.2 The B_s Meson System

We begin the search for the oases with the B_s system proceeding with input parameters as in the previous scenarios. The result of this search for $M_{Z'} = 1$ TeV is shown in Fig. 13, where we show the allowed ranges for $(\tilde{s}_{23}, \delta_{23})$. The *red* regions correspond to the allowed ranges for ΔM_s , while the *blue* ones to the corresponding ranges for $S_{\psi\phi}$. The overlap between red and blue regions identifies the oases we were looking for.

From these plots we extract several oases that are collected in Table 7. The notations are as in previous cases but it should be kept in mind that the parameters $(\tilde{s}_{23}, \delta_{23})$ describe both LH and RH couplings. Note that the entries related to $B_{s,d} \rightarrow \mu^+\mu^-$ are absent now as in this scenario there are no NP contributions to these decays. Consequently the $\Delta\Gamma_s$ effects in $B_s \rightarrow \mu^+\mu^-$ are as in the SM: $\mathcal{A}_{\Delta\Gamma}^\lambda = 1$.

In order to understand the structure of oases in Table 7, that differs from the ones found so far, we note that the matrix element of the dominant Q_1^{LR} operator has the sign opposite to SM operators. Therefore, this operator naturally suppresses ΔM_s with the phase δ_{23} centered in the ballpark of 0° and 180° , that is shifted down by roughly 90° relatively to the LHS scenarios. As the matrix element of Q_1^{LR} is larger than that of the SM operator in LHS and RHS scenarios, \tilde{s}_{23} has to be sufficiently small to agree with data.

The crucial role in the B_s meson system in this scenario, in the absence of NP contributions to $B_{s,d} \rightarrow \mu^+\mu^-$ decays, is now played by $B \rightarrow K^*\mu^+\mu^-$, $B \rightarrow K\mu^+\mu^-$ and $b \rightarrow s\nu\bar{\nu}$ transitions. We will discuss the latter decays at the end of this section.

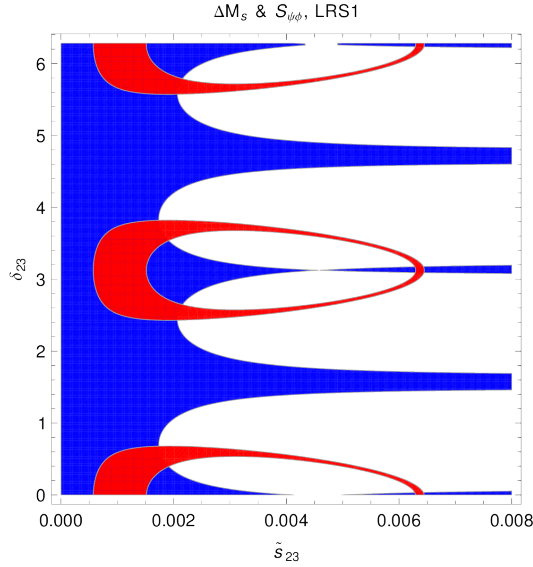


Figure 13: Ranges for ΔM_s (red region) and $S_{\psi\phi}$ (blue region) for $M_{Z'} = 1$ TeV in LRS1 satisfying the bounds in Eq. (130).

	\tilde{s}_{23}	δ_{23}	$\Delta S_{\psi\phi}$	$\Delta \mathcal{B}_s^{\nu\bar{\nu}}$
$A_1(S1)$	0.00059 – 0.00216	$139^\circ - 219^\circ$	\pm	\mp
$A_2(S1)$	0.00628 – 0.00644	$177^\circ - 182^\circ$		
$A_3(S1)$	0.00059 – 0.00216	$-41^\circ - 39^\circ$	\pm	\pm
$A_4(S1)$	0.00628 – 0.00644	$-3^\circ - 2^\circ$		

Table 7: Oases in the space $(\tilde{s}_{23}, \delta_{23})$ for $M_{Z'} = 1$ TeV in LRS1. Basically the same results are obtained for LRS2 scenario.

7.3.3 The B_d Meson System

The structure of oases in this case is given in Fig. 14 and Table 8. As we do not have $\mathcal{B}(B_d \rightarrow \mu^+ \mu^-)$ to our disposal and $b \rightarrow d\nu\bar{\nu}$ decays are challenging this system is not very useful to provide tests of LRS scenarios without some fundamental theory.

Due to the sign of the matrix element of the dominant Q_1^{LR} operator in both LRS1 and LRS2 the mass difference ΔM_d is naturally suppressed. The requested size of this suppression together with significant suppression of $S_{\psi K_S}$ in LRS2 and slight enhancement of it in LRS1 governs the structure of the phases.

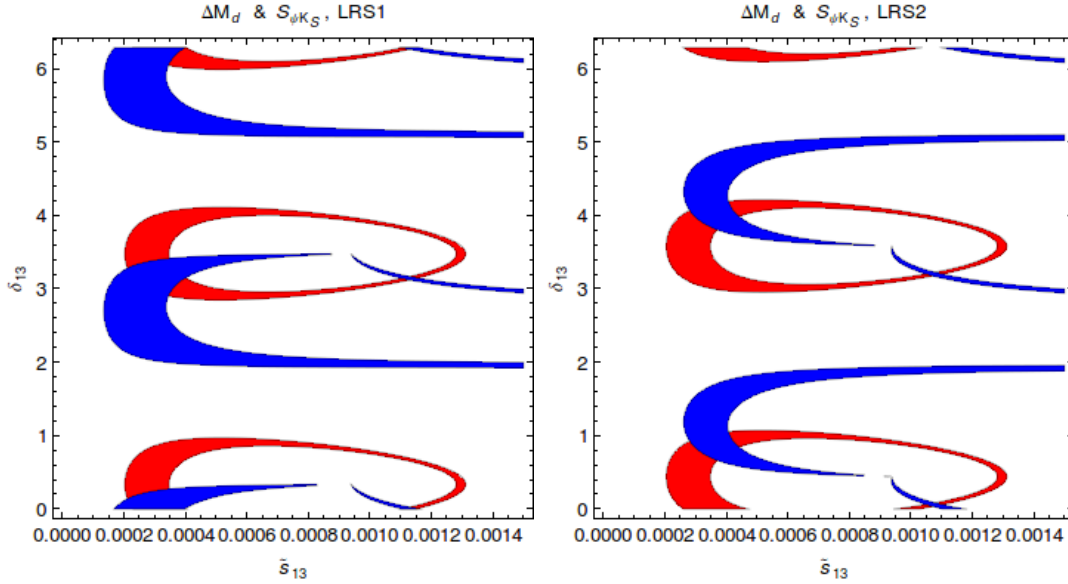


Figure 14: Ranges for ΔM_d (red region) and $S_{\psi K_S}$ (blue region) for $M_{Z'} = 1$ TeV in LRS1 (left) and LRS2 (right) satisfying the bounds in Eq. (131).

	\tilde{s}_{13}	δ_{13}
$B_1(S1)$	0.00021 – 0.00040	$166^\circ - 195^\circ$
$B_2(S1)$	0.00111 – 0.00117	$179^\circ - 180^\circ$
$B_3(S1)$	0.00021 – 0.00040	$-14^\circ - 15^\circ$
$B_4(S1)$	0.00111 – 0.00117	$-1^\circ - 0^\circ$
$B_1(S2)$	0.00028 – 0.00044	$38^\circ - 60^\circ$
$B_2(S2)$	0.00106 – 0.00111	$2^\circ - 5^\circ$
$B_3(S2)$	0.00028 – 0.00044	$218^\circ - 240^\circ$
$B_4(S2)$	0.00106 – 0.00111	$182^\circ - 185^\circ$

Table 8: Oases in the space $(\tilde{s}_{13}, \delta_{13})$ for $M_{Z'} = 1$ TeV and two scenarios for $|V_{ub}|$ in LR scenarios.

7.3.4 The K Meson System

In Fig. 15 we show the oases in this system that due to the presence of LR operators have a different structure than in previous scenarios. While the shape of the single oasis in the LRS2 case is similar to the LHS2, for LRS1 the oases are shifted by 90° :

$$C_1(S1) : 90^\circ \leq \delta_{12} \leq 180^\circ, \quad C_2(S1) : 270^\circ \leq \delta_{12} \leq 360^\circ. \quad (144)$$

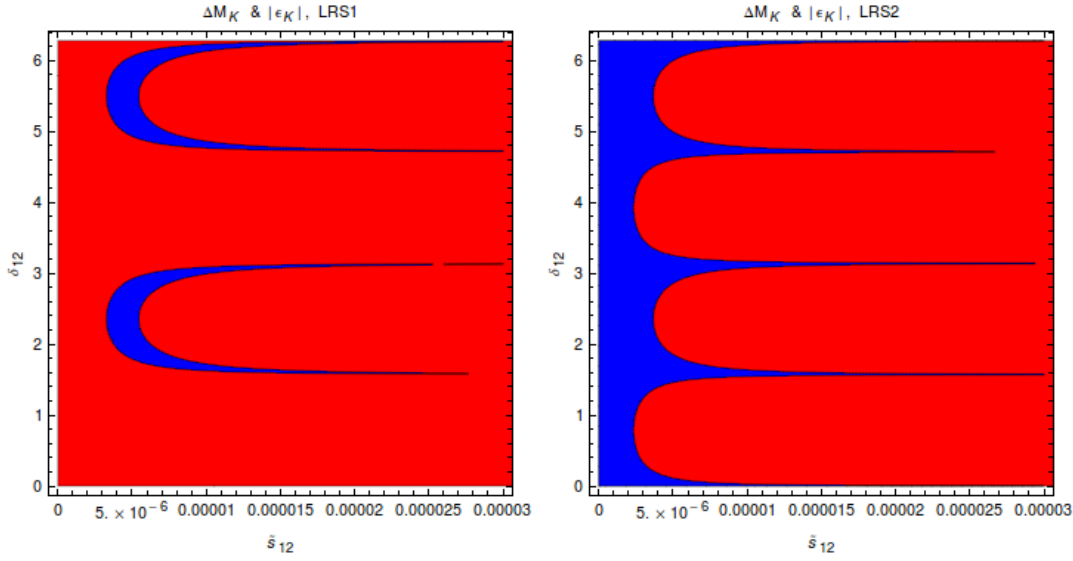


Figure 15: Ranges for ΔM_K (red region) and ε_K (LRS1: left, LRS2: right) for $M_{Z'} = 1$ TeV satisfying the bounds in Eq. (132).

In Fig. 16 we show the correlation between $\mathcal{B}(K^+ \rightarrow \pi^+ \nu \bar{\nu})$ and $\mathcal{B}(K_L \rightarrow \pi^0 \nu \bar{\nu})$ in the LRS1 and LRS2 scenarios. Even if this correlation has similar structure to the one found in previous scenarios, there are differences:

- Concentrating first on the $M_{Z'} = 1$ TeV case we observe that the branches in both scenarios are much thinner than in the LHS1 and LHS2 cases which originates in the fact that NP contributions to ε_K have to be kept under control in the presence of LR operators.
- In the LRS1 case the new structure of phases in (144) implies definite predictions for both branching ratios in $C_1(S1)$ and $C_2(S1)$ respectively ($M_{Z'} = 1$ TeV):

$$3 \cdot 10^{-11} \leq \mathcal{B}(K^+ \rightarrow \pi^+ \nu \bar{\nu}) \leq 12 \cdot 10^{-11}, \quad 2 \cdot 10^{-11} \leq \mathcal{B}(K_L \rightarrow \pi^0 \nu \bar{\nu}) \leq 14 \cdot 10^{-11}, \quad (145)$$

$$8 \cdot 10^{-11} \leq \mathcal{B}(K^+ \rightarrow \pi^+ \nu \bar{\nu}) \leq 16 \cdot 10^{-11}, \quad 0 \leq \mathcal{B}(K_L \rightarrow \pi^0 \nu \bar{\nu}) \leq 3 \cdot 10^{-11}. \quad (146)$$

- In LRS2 the effects are slightly larger than in LRS1 and in fact on the horizontal line $\mathcal{B}(K^+ \rightarrow \pi^+ \nu \bar{\nu})$ can be larger than in LHS2 in Fig. 10 as in LRS2 the $K_L \rightarrow \mu^+ \mu^-$ bound is ineffective.
- However, otherwise the effects in LRS1 and LRS2 scenarios are much smaller than in LHS1 and LHS2 scenarios in accordance with the correlations between $\Delta F = 1$ and $\Delta F = 2$ transitions derived in Subsection 5.2. This is clearly seen in lower

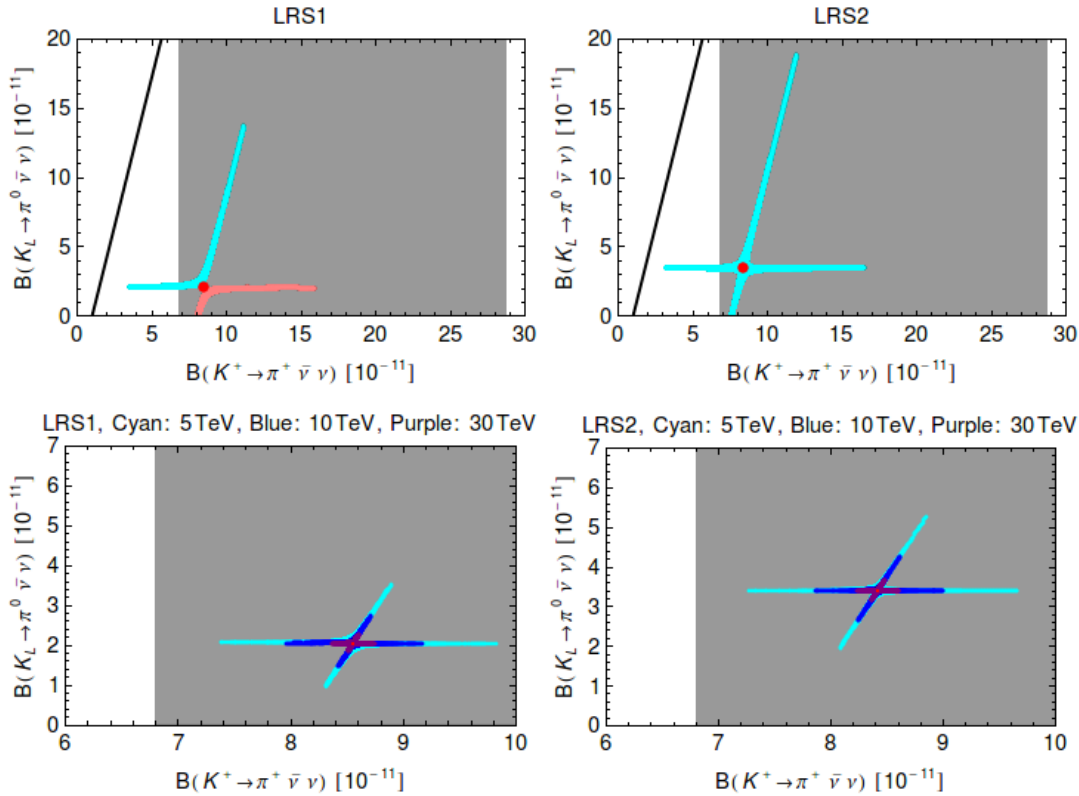


Figure 16: $\mathcal{B}(K_L \rightarrow \pi^0 \nu \bar{\nu})$ versus $\mathcal{B}(K^+ \rightarrow \pi^+ \nu \bar{\nu})$ for $M_{Z'} = 1$ TeV in LRS1 and LRS2 (upper panels, C_1 : cyan, C_2 : pink.) and $M_{Z'} = 5$ TeV (cyan), 10 TeV (blue) and 30 TeV (purple) in LRS1 and LRS2. Red point: SM central value. Gray region: experimental range of $\mathcal{B}(K^+ \rightarrow \pi^+ \nu \bar{\nu})$.

panels in Fig. 16, where we show the results for higher values of $M_{Z'}$. While for $M_{Z'} = 5$ TeV NP effects in both branching ratio can still be distinguished in the future from SM values, for higher masses of $M_{Z'}$ this will be very difficult. Note that the SM values of $\mathcal{B}(K_L \rightarrow \pi^0 \nu \bar{\nu})$ in LRS1 are visibly smaller than in LRS2 which is a clear consequence of the change of $|V_{ub}|$.

This discussion shows that if $M_{Z'} \geq 5$ TeV and both branching ratios will be found significantly larger than SM values the LRS1 and LRS2 scenarios will be favoured over LRS1 and LRS2.

These results have been obtained under the assumptions of the exact LR symmetry. However, as already shown in [115] and also discussed in [34] if the phase structure of LL and RR and LR contributions in $\Delta S = 2$ transitions is not related to each other the correlation between $\mathcal{B}(K^+ \rightarrow \pi^+ \nu \bar{\nu})$ and $\mathcal{B}(K_L \rightarrow \pi^0 \nu \bar{\nu})$ can change profoundly. This is for instance seen in Fig. 3 of [115], where for such a general scenario one can find a decrease of $\mathcal{B}(K_L \rightarrow \pi^0 \nu \bar{\nu})$ with increasing $\mathcal{B}(K^+ \rightarrow \pi^+ \nu \bar{\nu})$, the property which

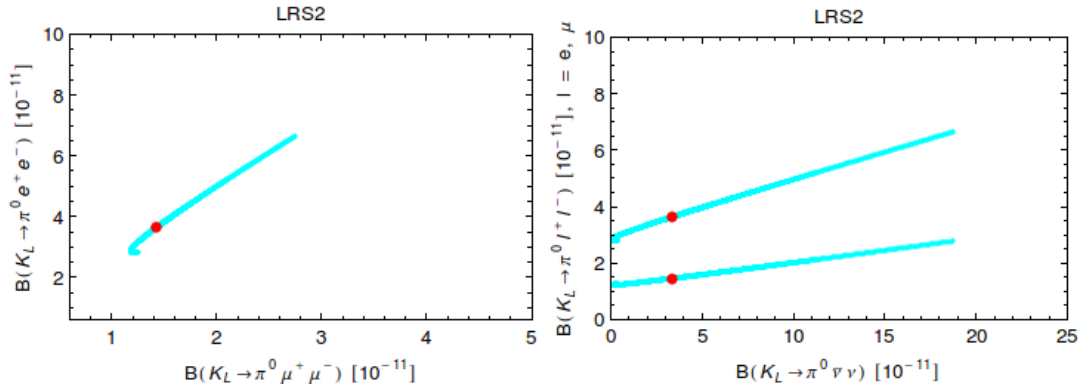


Figure 17: $\mathcal{B}(K_L \rightarrow \pi^0 e^+ e^-)$ as a function of $\mathcal{B}(K_L \rightarrow \pi^0 \mu^+ \mu^-)$ (left panel) and $\mathcal{B}(K_L \rightarrow \pi^0 e^+ e^-)$ (upper curve) and $\mathcal{B}(K_L \rightarrow \pi^0 \mu^+ \mu^-)$ (lower curve) as functions of $\mathcal{B}(K_L \rightarrow \pi^0 \nu \bar{\nu})$ (right panel) in LRS2 at $M_{Z'} = 1$ TeV. The red points represent SM predictions.

is absent in the results presented so far. Indeed in this case the leading NP contribution in $\Delta S = 2$ amplitudes is not proportional to the square of NP contribution to $\Delta S = 1$ amplitudes implying a different correlation. As such a study can be more efficiently performed in a concrete model, we leave it for the future.

Finally we discuss $K_L \rightarrow \pi^0 \ell^+ \ell^-$ decays in this scenario. In Fig. 17 we show the results corresponding to those in Figs. 12 obtained in LHS2. We observe that NP effects in $K_L \rightarrow \pi^0 \ell^+ \ell^-$ in this scenario can be large but much smaller than in LHS2 in accordance with the correlations derived in Subsection 5.2. We have also checked that the present bounds on these decays do not remove sizable NP effects found in LRS2 scenario for $K^+ \rightarrow \pi^+ \nu \bar{\nu}$ and $K_L \rightarrow \pi^0 \nu \bar{\nu}$ decays. Similar results are found for LRS1.

7.4 The ALRS1 and ALRS2 Scenarios

We include this case as well because it has not been discussed in the literature but it is an interesting NP scenario for the following reasons:

- NP contributions to $\Delta F = 2$ observables are dominated as in LRS scenarios by new LR operators but as the sign of LR interference is flipped some differences arise.
- NP contributions to $B_{d,s} \rightarrow \mu^+ \mu^-$ enter again with full power. Therefore these decays together with $S_{\mu^+ \mu^-}^q$ offer as in the LHS and RHS scenarios some help in the identification of acceptable oases.
- The phase structure of the oases is as in LHS scenario but due to enhanced hadronic matrix elements of LR operators the mixing parameters \tilde{s}_{ij} are decreased typically by a factor of 3.5.

- NP contributions to $K^+ \rightarrow \pi^+ \nu \bar{\nu}$, $K_L \rightarrow \pi^0 \nu \bar{\nu}$ and $K_L \rightarrow \pi^0 \ell^+ \ell^-$ vanish in this scenario but the $b \rightarrow s \nu \bar{\nu}$ transitions can still offer important tests.

In view of this simple structure of modifications with respect to LHS scenario, all plots with the exception of decays with neutrinos in the final state have the same structure as LH scenarios but NP effects are smaller. This is also seen by inspecting (107), (108), (114) and (115). Therefore we will not show these plots. However when we will move to consider flavour-violating Z couplings this suppression of NP effects in ALRS relative to LHS will turn out to be fortunate and ALRS will be doing better than LHS.

Concerning NP contributions to $K \rightarrow \pi \nu \bar{\nu}$ decays this scenario could turn out one day to be interesting if the data on observables in B_s and B_d systems will show the presence of RH currents but negligible NP effects in $K \rightarrow \pi \nu \bar{\nu}$. On the other hand as we will discuss soon $b \rightarrow s \nu \bar{\nu}$ transitions can help to distinguish this scenario from the previous ones.

7.5 Implications of $b \rightarrow s \ell^+ \ell^-$ Constraints

Presently the NP effects found by us are consistent with the experimental data on $B_{s,d} \rightarrow \mu^+ \mu^-$, although a range of values above the SM estimate of $\mathcal{B}(B_s \rightarrow \mu^+ \mu^-)$ already slightly violates the existing upper bound. However, also the data on $B \rightarrow X_s \ell^+ \ell^-$, $B \rightarrow K^* \ell^+ \ell^-$ and $B \rightarrow K \ell^+ \ell^-$ improved recently by much and it is of interest to see whether they have an impact on our results. A very extensive model independent analysis of the impact of the recent LHCb data on the Wilson coefficients $C_9^{(\prime)}$ and $C_{10}^{(\prime)}$ has been performed in [36] and we can use these results in our case.

As seen in Subsection 3.2.3 the Wilson coefficients $C_9^{(\prime)}$ depend on $\Delta_V^{\mu\bar{\mu}}(Z')$ couplings which did not enter our analysis. They can be chosen to satisfy the constraints in question. Therefore we will only check whether for the ranges of parameters considered by us the resulting coefficients $C_{10}^{(\prime)}$ satisfy the model independent bounds in [36]. As these coefficients are scale independent we can use the formulae in Subsection 3.2.3 and compare the resulting coefficients with those in the latter paper. The allowed 2σ ranges of $C_{10}^{(\prime)}$ are shown in Figs. 1 and 2 of [36]. They are given approximately as follows:

$$-2 \leq \Re(C'_{10}) \leq 0, \quad -2.5 \leq \Im(C'_{10}) \leq 2.5, \quad (147a)$$

$$-0.8 \leq \Re(C_{10}^{\text{NP}}) \leq 1.8, \quad -3 \leq \Im(C_{10}) \leq 3. \quad (147b)$$

Especially, the new data on $B \rightarrow K^* \mu^+ \mu^-$ allow only for *negative* values of the real part of C'_{10}

$$\Re(C'_{10}) \leq 0 \quad (148)$$

and this has an impact on our results in RH and LR scenarios.

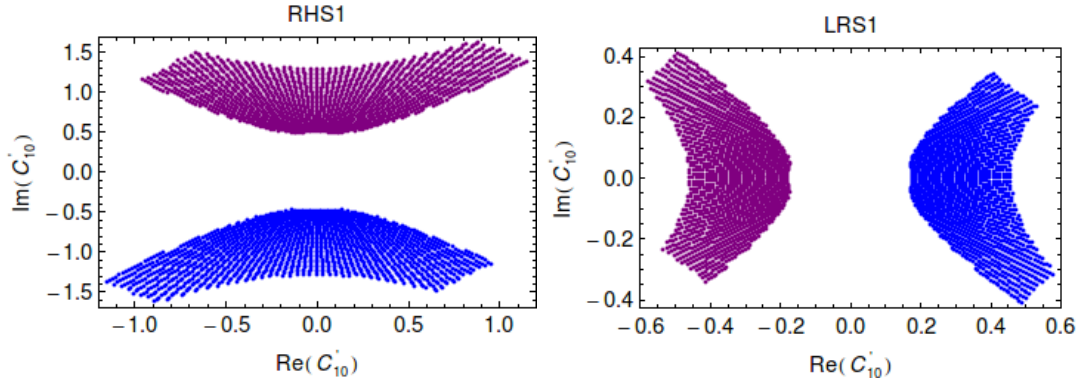


Figure 18: C'_{10} for $M_{Z'} = 1 \text{ TeV}$ in *RHS1* (left) and *LRS1* (right). A_1 : blue, A_3 : purple.

We find that the NP effects in C_{10} are within the 2σ bounds presented in [36] even if with improved data one will be able to remove certain range of parameters. Some footprints of this can already been seen in Figs. 3 and 4.

In Fig. 18 we show the results on C'_{10} in RH and LR scenarios without the constraint in Eq. (148). We observe that imposing it removes roughly half of each of oases A_1 and A_3 in the RH case and the oasis A_1 (blue) in the case of LR. We will now investigate the implications of this finding on the comparison between LHS and RHS scenarios.

The most interesting impact of this constraint at present is on the correlation of $S_{\psi\phi}$ and $\mathcal{B}(B_s \rightarrow \mu^+\mu^-)$ that for the LHS is given in Fig. 3. As we discussed previously the same result is obtained in the RHS with the two oases A_1 (blue) and A_3 (purple) interchanged. However taking the constraint (148) into account results in a modified correlation within RH scenario that we show in Fig. 19. The black areas are excluded and in the RH scenario an enhancement of $\mathcal{B}(B_s \rightarrow \mu^+\mu^-)$ relative to the SM is excluded. This feature distinguishes LH and RH scenarios. For $\mathcal{B}(B_s \rightarrow \mu^+\mu^-)$ below its SM value, the measurement of these two observables cannot distinguish between LH and RH scenarios as one can always move to the other oasis to obtain the same result.

7.6 $b \rightarrow s\nu\bar{\nu}$ Observables in Different Scenarios.

In view of the important role of these transitions in the search for RH currents we devote to them a separate subsection. We begin with the $\epsilon - \eta$ plane proposed in [83]. In Fig. 20 we show the results for all four scenarios considered by us. Indeed they can be clearly distinguished in this plane. Indeed a future determination of ϵ and η will tell us whether the nature chooses one of the scenario considered by us or a linear combination of them.

With four observables and four scenarios for Z' -couplings there is a multitude of results for specific observables one could present at this stage. Here we present only some of them that we consider most interesting.

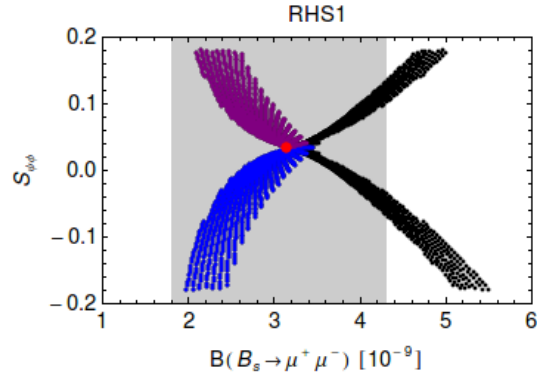


Figure 19: $S_{\psi\phi}$ and $\mathcal{B}(B_s \rightarrow \mu^+\mu^-)$ for $M_{Z'} = 1$ TeV in RHS1. A_1 : blue, A_3 : purple, A_2 : red, A_4 : gray. Black: excluded due to $\Re(C'_{10}) \geq 0$. Gray region: $exp\ 1\sigma$ range $\mathcal{B}(B_s \rightarrow \mu^+\mu^-) = (2.9^{+1.4}_{-1.1}) \cdot 10^{-9}$. Red point: SM central value.

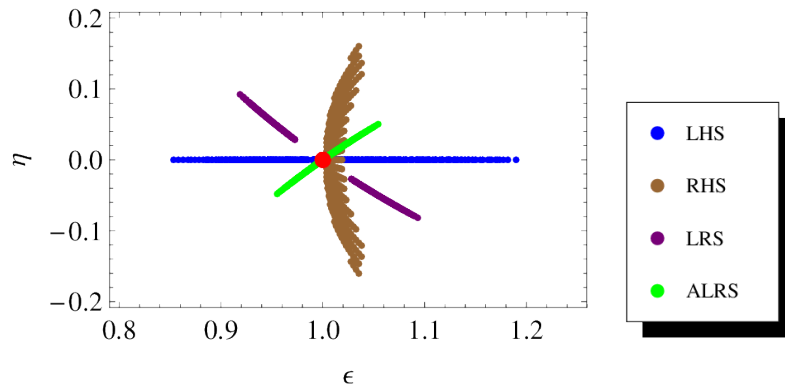


Figure 20: η versus ϵ for scenario LHS1, RHS1, LRS1 and ALRS1.

On the left in Fig. 21 we show $\mathcal{B}(B \rightarrow K\nu\bar{\nu})$ versus $\mathcal{B}(B_s \rightarrow \mu^+\mu^-)$ in LHS1 and RHS1 scenarios. Even without the (148) constraint which eliminates the black region in the RH scenario, there is a clear distinction between these two scenarios so that the measurement of these two observables can uniquely tell us whether we deal with LHS or RHS case. Imposing (148) we find that in the RH scenario $\mathcal{B}(B \rightarrow K\nu\bar{\nu})$ can only be enhanced and $\mathcal{B}(B_s \rightarrow \mu^+\mu^-)$ suppressed. In the case of $\mathcal{B}(B \rightarrow K^*\nu\bar{\nu})$ as seen on the right in the same figure its branching ratio can only be suppressed relative to the SM in RHS but otherwise the distinction between LHS and RHS is not as pronounced as for $\mathcal{B}(B \rightarrow K\nu\bar{\nu})$.

In Fig. 22 we show the correlations between $\mathcal{B}(B \rightarrow K\nu\bar{\nu})$ and $S_{\psi\phi}$ (top) and $\mathcal{B}(B \rightarrow K^*\nu\bar{\nu})$ and $S_{\psi\phi}$ (down) in LHS and RH scenarios with the black regions excluded by the constraint in (148). We note in particular that in the RHS the measurement of $S_{\psi\phi}$, if different from the SM value, will uniquely determine the allowed oasis.

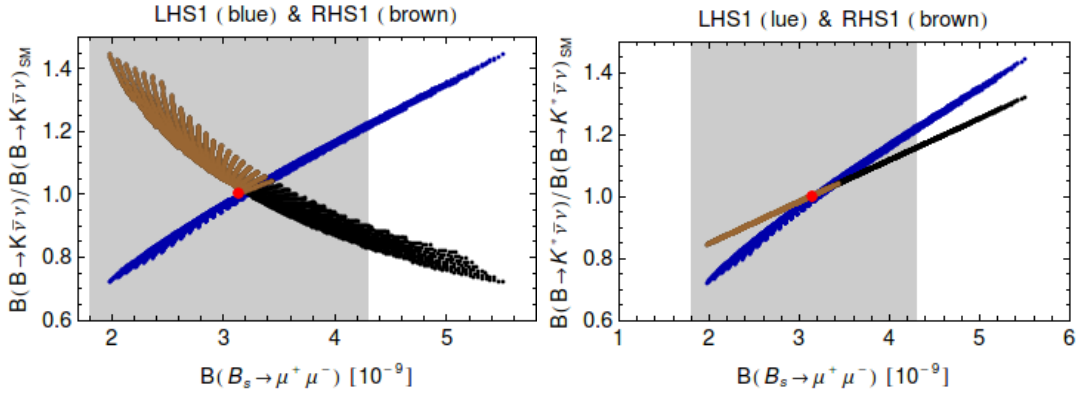


Figure 21: $\mathcal{B}(B \rightarrow K\nu\bar{\nu})$ versus $\mathcal{B}(B_s \rightarrow \mu^+\mu^-)$ (left) and $\mathcal{B}(B \rightarrow K^*\nu\bar{\nu})$ versus $\mathcal{B}(B_s \rightarrow \mu^+\mu^-)$ (right) for $M_{Z'} = 1$ TeV in LHS1 (blue for both oases $A_{1,3}$) and RHS1 (brown for both oases $A_{1,3}$), black points excluded by $b \rightarrow s\ell^+\ell^-$. Gray region: exp 1 σ range $\mathcal{B}(B_s \rightarrow \mu^+\mu^-) = (2.9^{+1.4}_{-1.1}) \cdot 10^{-9}$. Red point: SM central value.

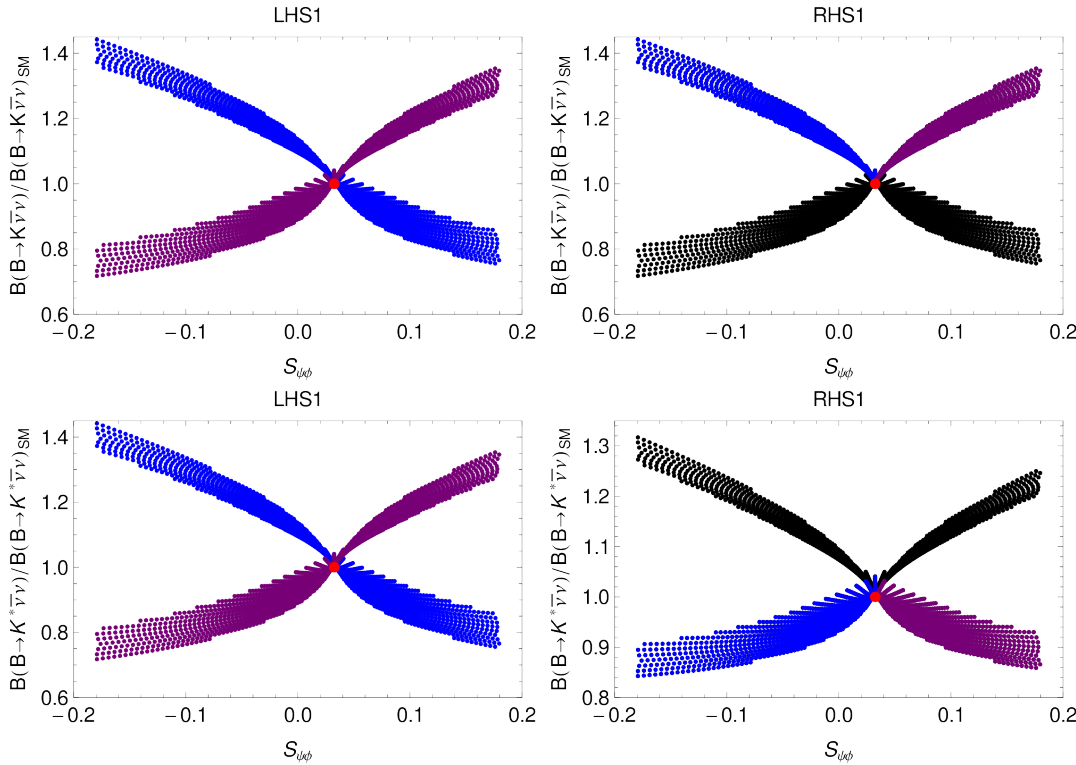


Figure 22: $\mathcal{B}(B \rightarrow K\nu\bar{\nu})$ versus $S_{\psi\phi}$ (top) and $\mathcal{B}(B \rightarrow K^*\nu\bar{\nu})$ versus $S_{\psi\phi}$ (down) for $M_{Z'} = 1$ TeV in LHS1 (left) and RHS1 (right). A_1 : blue, A_3 : purple, A_2 : red, A_4 : gray. Black points excluded by $b \rightarrow s\ell^+\ell^-$. Red point: SM central value.

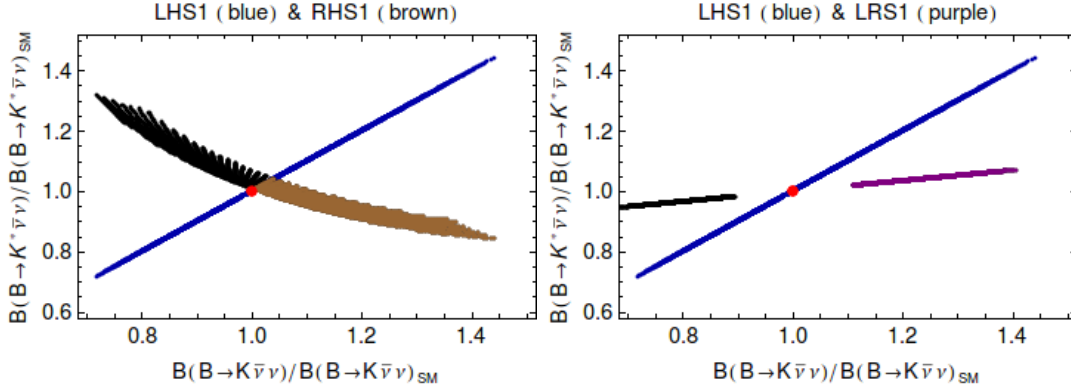


Figure 23: $\mathcal{B}(B \rightarrow K^* \nu \bar{\nu})$ versus $\mathcal{B}(B \rightarrow K \nu \bar{\nu})$ for $M_{Z'} = 1$ TeV in LHS1 (blue for both oases $A_{1,3}$), RHS1 (brown for both oases $A_{1,3}$) and LRS1 (purple for both oases $A_{1,3}$), black points excluded by $b \rightarrow s \ell^+ \ell^-$. Red point: SM central value.

Finally, in Fig. 23 we show $\mathcal{B}(B \rightarrow K^* \nu \bar{\nu})$ versus $\mathcal{B}(B \rightarrow K \nu \bar{\nu})$ in RH and LR scenarios compared to LH scenario with black regions excluded by the constraint in (148). Also these plots will test the presence of RH currents as emphasized in [115].

The observable F_L being dependent only on η can in principle serve to identify the presence of RH currents. However in our case, as seen in Fig. 20, $|\eta| \leq 0.16$, and NP effects in F_L turn out to be small as can be deduced from Fig. 4 in [83].

8 The $U(2)^3$ Limit

We have investigated how the parameter space is further constrained when the flavour $U(2)^3$ symmetry [23–29] is imposed on the Z' couplings. As pointed out in [30] in this case $\varphi_{B_d} = \varphi_{B_s}$ which in turn implies not only the correlation between CP asymmetries $S_{\psi K_S}$ and $S_{\psi \phi}$ but also a triple $S_{\psi K_S} - S_{\psi \phi} - |V_{ub}|$ correlation.

As in [30] we will only consider the case of $U(2)^3$ broken by the minimal set of spurions: the $MU(2)^3$ case. Then only the LHS1 and LHS2 are involved. We find then that \tilde{s}_{ij} and δ_{ij} are constrained at the fundamental level as follows.

In the K system we have

$$\tilde{s}_{12} = a|V_{td}||V_{ts}|, \quad \delta_{12} = \beta - \beta_s, \quad (149)$$

where $a \geq 0$ and real. Thus NP effects in ε_K , $K^+ \rightarrow \pi^+ \nu \bar{\nu}$, $K_L \rightarrow \pi^0 \nu \bar{\nu}$ and $K_L \rightarrow \mu^+ \mu^-$ are described for fixed leptonic couplings by a single real and positive definite parameter. Once this parameter is fixed through one of these observables, the others are uniquely predicted. Note that this is even more predictive than CMFV in which except for common CKM couplings there is no relation between $\Delta F = 2$ and $\Delta F = 1$ transitions unless some ratios are constructed [116].

The observables in B_d and B_s systems are correlated with each other due to the relations:

$$\frac{\tilde{s}_{13}}{|V_{td}|} = \frac{\tilde{s}_{23}}{|V_{ts}|}, \quad \delta_{13} - \delta_{23} = \beta - \beta_s. \quad (150)$$

Thus, once the allowed oases in the B_d system are fixed, the oases in B_s system are determined. Moreover, all observables in both systems are described by only one real positive parameter and one phase, e.g. $(\tilde{s}_{23}, \delta_{23})$.

In Fig. 24 we combine Figs. 2 and 6 using the $U(2)^3$ symmetry relations in (150). In the $U(2)^3$ limit the small oases are eliminated and the big oases get smaller. This decrease turns out to be not very pronounced in the case of $(\tilde{s}_{13}, \delta_{13})$ oases as they were already small as seen in Fig. 6 but has a significant impact on $(\tilde{s}_{23}, \delta_{23})$ oases which were much larger as seen in Fig. 2. Moreover the fact that the results in the B_d system depend on whether LHS1 or LHS2 is considered is now transferred through the relations in (150) into the B_s system. This is clearly seen in Fig. 24, in particular the final oases (magenta) in LHS2 are smaller than in LHS1 due to the required shift of $S_{\psi K_S}$.

This change of allowed oases in the B_s system has a profound impact on the correlation between $S_{\psi\phi}$ and $\mathcal{B}(B_s \rightarrow \mu^+\mu^-)$. We show this in Fig. 25 that should be compared with the corresponding correlation in Fig. 3. We observe that already the sign of $S_{\psi\phi}$ will decide whether LHS1 or LHS2 is favoured. Moreover if $\mathcal{B}(B_s \rightarrow \mu^+\mu^-)$ will turn out to be suppressed relatively to the SM then only one oasis will survive in each scenario. Comparison with future precise values of $|V_{ub}|$ will confirm or rule out this scenario of NP. These correlations are particular examples of the correlations in $MU(2)^3$ models pointed out in [30]. What is new here is that in a specific model considered by us the $|V_{ub}| - S_{\psi\phi}$ correlation has now also implications for $\mathcal{B}(B_s \rightarrow \mu^+\mu^-)$.

We also note that in this case [30]

$$S_{\mu^+\mu^-}^s = S_{\mu^+\mu^-}^d = \sin(2\theta_Y - 2\varphi_{\text{new}}), \quad (151)$$

where

$$\theta_Y = \theta_Y^d = \theta_Y^s, \quad \varphi_{\text{new}} = \varphi_{B_d} = \varphi_{B_s}. \quad (152)$$

Moreover, as the CMFV relations for $\mathcal{B}(B_{s,d} \rightarrow \mu^+\mu^-)$, also apply in this case the result in (65) allows to find [30]

$$\mathcal{B}(B_d \rightarrow \mu^+\mu^-) = (1.0_{-0.3}^{+0.5}) \times 10^{-10}, \quad (\text{CMFV, } MU(2)^3). \quad (153)$$

Finally we remark that within the $\overline{331}$ model, analyzed by us in [35], the imposition of $U(2)^3$ symmetry implies the relations:

$$\tilde{s}_{13} = b|V_{td}|, \quad \tilde{s}_{23} = b|V_{ts}|, \quad \delta_1 - \delta_2 = \beta - \beta_s + \pi, \quad (154)$$

where $b \geq 0$ and real. Consequently NP in all three systems is described by only one real positive definite parameter and one phase.

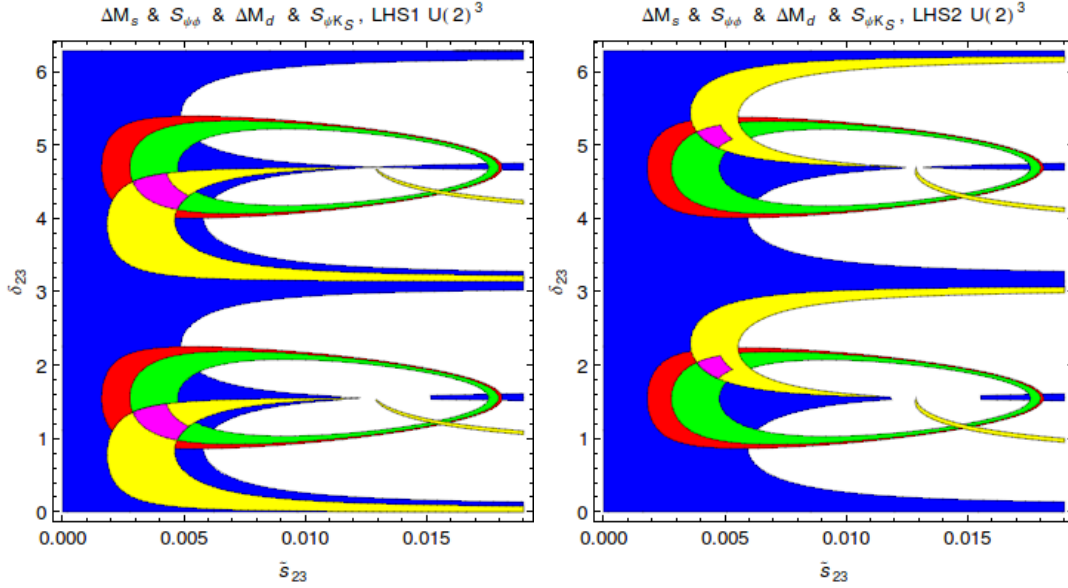


Figure 24: Ranges for ΔM_s (red region), $S_{\psi\phi}$ (blue region), ΔM_d (green region) and $S_{\psi K_S}$ (yellow region) for $M_{Z'} = 1$ TeV in LHS1 (left) and LHS2 (right) in the $U(2)^3$ limit satisfying the bounds in Eq. (130) and (131). The overlap region of all four regions is shown in magenta.

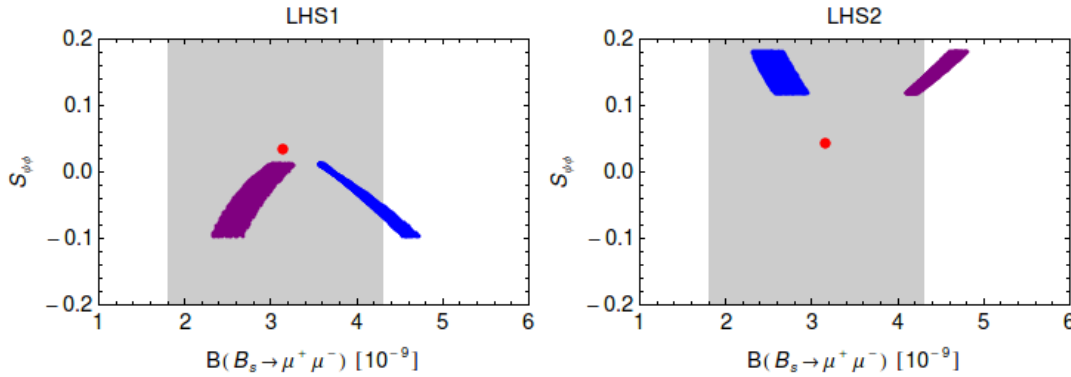


Figure 25: $S_{\psi\phi}$ versus $\mathcal{B}(B_s \rightarrow \mu^+\mu^-)$ for $M_{Z'} = 1$ TeV in LHS1 (left) and LHS2 (right) in the $U(2)^3$ limit. Blue region corresponds to the lower magenta oases in Fig. 24 (former A_1) and the purple region corresponds to the upper magenta oases (former A_3). Gray region: $\exp 1\sigma$ range $\mathcal{B}(B_s \rightarrow \mu^+\mu^-) = (2.9^{+1.4}_{-1.1}) \cdot 10^{-9}$.

9 Flavour Violating SM Z Boson

9.1 Preliminaries

We will now turn our attention to flavour violating Z -couplings that can be generated in the presence of other neutral gauge bosons and or new heavy vectorial fermions with $+2/3$ and $-1/3$ electric charges. RSc is an explicit model of this type [33, 117]. See also [18]. Recently, an extensive analysis of flavour violation in the presence of a vectorial $+2/3$ quark has been presented in [118], where references to previous literature can be found. In the case considered by us, new quarks with $-1/3$ charges are essential for generating flavour violating couplings to SM down-quarks but the presence of heavy quarks with $+2/3$ charges could be relevant for charm physics. Moreover, such heavy fermions could contribute to rare K and B decays through loop diagrams. In what follows we will assume that these loop contributions can be neglected in comparison with the tree-level effects discussed by us. Of course in a concrete model one has to check whether this assumption is justified.

The strategy and formalism developed in the previous sections can be used in a straightforward manner for the case of Z flavour-violating couplings to quarks. In this case we have

$$M_Z = 91.2 \text{ GeV}, \quad \Delta_L^{\nu\bar{\nu}}(Z) = \Delta_A^{\mu\bar{\mu}}(Z) = 0.372, \quad \Delta_V^{\mu\bar{\mu}}(Z) = -0.028 \quad (155)$$

The implications of these changes are as follows:

- The decrease of the neutral gauge boson mass by an order of magnitude relatively to the nominal value $M_{Z'} = 1 \text{ TeV}$ used by us decreases the couplings \tilde{s}_{ij} by the same amount without any impact on the phases δ_{ij} when the constraints from $\Delta F = 2$ processes are imposed.
- As already noticed in [35] and discussed at the beginning of our paper once the parameters \tilde{s}_{ij} are constrained through $\Delta F = 2$ observables the decrease of neutral gauge boson mass enhances NP effects in rare K and B decays. This follows from the structure of tree-level contributions to FCNC processes and is not generally the case when NP contributions are governed by penguin and box diagrams. The formulae in Section 5 exhibit this feature transparently.
- The latter fact implies that already the present experimental bounds on $\mathcal{B}(K^+ \rightarrow \pi^+ \nu\bar{\nu})$ and $\mathcal{B}(B_{s,d} \rightarrow \mu^+ \mu^-)$ as well as the data on $B \rightarrow X_s \ell^+ \ell^-$, $B \rightarrow K^* \ell^+ \ell^-$ and $B \rightarrow K \ell^+ \ell^-$ decays become more powerful than the $\Delta F = 2$ transitions in constraining flavour violating couplings of Z so that effects in $\Delta F = 2$ processes cannot be as large as in Z' case.

We will now investigate how the flavour-violating Z couplings perform in the three meson systems.

9.2 The B_s Meson System

We used first only the ΔM_s and $S_{\psi\phi}$ constraints finding that small oases are excluded by the data on $B_s \rightarrow \mu^+\mu^-$. However, also in big oases $\mathcal{B}(B_s \rightarrow \mu^+\mu^-)$ is always larger than its SM value and mostly above the data except in LRS case where NP contributions vanish. In Fig. 26 (in the case of the LHS1 scenario) we show the region allowed by ΔM_s and $S_{\psi\phi}$ constraint together with the yellow region allowed by $\mathcal{B}(B_s \rightarrow \mu^+\mu^-) = (2.9_{-1.1}^{+1.4}) \cdot 10^{-9}$. We observe no overlap between these regions. A small orange region is still left when 2σ range for $\mathcal{B}(B_s \rightarrow \mu^+\mu^-)$ is considered. Thus at first sight one could conclude that in contrast to the Z' scenarios $\mathcal{B}(B_s \rightarrow \mu^+\mu^-)$ could reach values 2σ away from its experimental value.

However, when the values of C_{10}^{NP} and C'_{10} are considered the situation gets worse. The 2σ bounds on these coefficients from [36] (see Eq. (147)) are violated in LHS and RHS cases and for the LRS scenario only small room is left. Indeed we find

$$|\Im(C_{10})| \geq 3.5 \quad (\text{LHS1}), \quad |\Im(C_{10}')| \geq 3.5 \quad (\text{RHS1}) \quad (156)$$

and

$$|\Re(C_{10}^{\text{NP}})| \geq 1.5 \quad (\text{LRS1}), \quad |\Re(C_{10}')| \geq 1.5 \quad (\text{LRS1}). \quad (157)$$

Therefore, the main message from this exercise is that when the above constraints are taken into account it is very difficult to suppress ΔM_s sufficiently in LHS, LRS and RHS scenarios without violating the constraints from $b \rightarrow s\mu^+\mu^-$ transitions. We conclude therefore that this NP scenario appears to be strongly disfavoured even if not fully ruled out because of assumed small hadronic uncertainties.

In ALR scenario we find

$$|\Re(C_{10}^{\text{NP}})| \geq 1.5 \quad (\text{ALRS1}), \quad |\Im(C_{10}')| \geq 1.0 \quad (\text{ALRS1}). \quad (158)$$

While this scenario is in a slightly better shape most of the allowed space is ruled out as well.

We have also calculated C_9 and C'_9 coefficients. Due to the smallness of $\Delta_V^{\mu\bar{\mu}}$ in the SM, the present 2σ bounds are satisfied in all scenarios. Yet, in view of the results for C_{10} it does not look that we should expect much from flavour-violating Z couplings in B_s system and consequently we will not consider $b \rightarrow s\nu\bar{\nu}$ transitions. Similar conclusions have been reached in [36, 37].

9.3 The B_d Meson System

In the B_d system using the same constraints as before we find the allowed oases shown in Fig. 27. While the magenta regions in this plot are also allowed by the upper bound on $\mathcal{B}(B_d \rightarrow \mu^+\mu^-)$, Fig. 28 shows that the latter bound has already and impact on

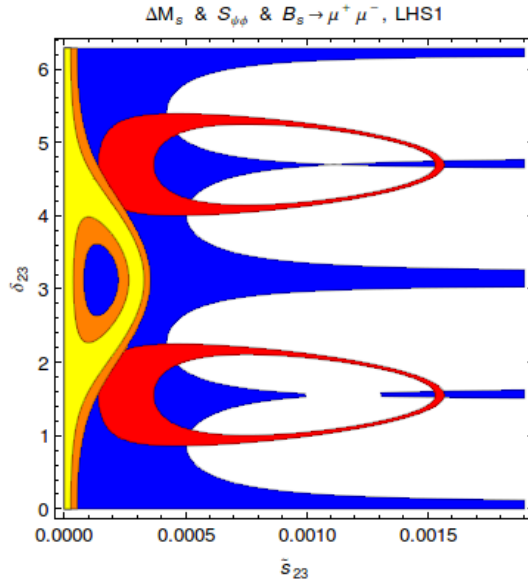


Figure 26: Ranges for ΔM_s (red region), $S_{\psi\phi}$ (blue region) and $B_s \rightarrow \mu^+ \mu^-$ (yellow) in LHS1 satisfying the bounds in Eq. (130) and $\mathcal{B}(B_s \rightarrow \mu^+ \mu^-)$ in 1σ range $[1.8, 4.3] \cdot 10^{-9}$ (yellow) and $[0.7, 5.7] \cdot 10^{-9}$ (orange).

the LHS1 and LHS2 scenarios. This should be compared with the Z' case in Fig. 7, where NP effects were much smaller. This time we show also the results in ALRS1 and ALRS2 scenarios in which NP effects are smaller than in LHS1 and LHS2 scenarios. We only show the results for big oases as small oases imply typically values for $\mathcal{B}(B_d \rightarrow \mu^+ \mu^-)$ of $8 \cdot 10^{-9}$ and $4 \cdot 10^{-9}$ for LHS and ALRS, respectively and are ruled out.

We observe that $\mathcal{B}(B_d \rightarrow \mu^+ \mu^-)$ can strongly be enhanced in all shown scenarios so that with improved bound on this branching ratio LHS1 and LHS2 scenarios could be put into difficulties, while in ALRS1 and ALRS2 one could easier satisfy these bounds. If such a situation really took place and NP effects would be observed in this decay, this would mean that both LH and RH Z' -couplings in the B_d system would be required but with opposite sign.

Fig. 29 shows that not only $\mathcal{B}(B_d \rightarrow \mu^+ \mu^-)$ but also the CP-asymmetry $S_{\mu^+ \mu^-}^d$ can deviate significantly from SM expectation.

9.4 The K Meson System

The effects of flavour violating Z couplings in $K^+ \rightarrow \pi^+ \nu \bar{\nu}$ and $K_L \rightarrow \pi^0 \nu \bar{\nu}$ can be very large in LHS, RHS and LRS but they can be bounded by the upper bound on $K_L \rightarrow \mu^+ \mu^-$ except for the LR scenarios and the case of purely imaginary NP contributions in all these scenarios where this bound is ineffective.

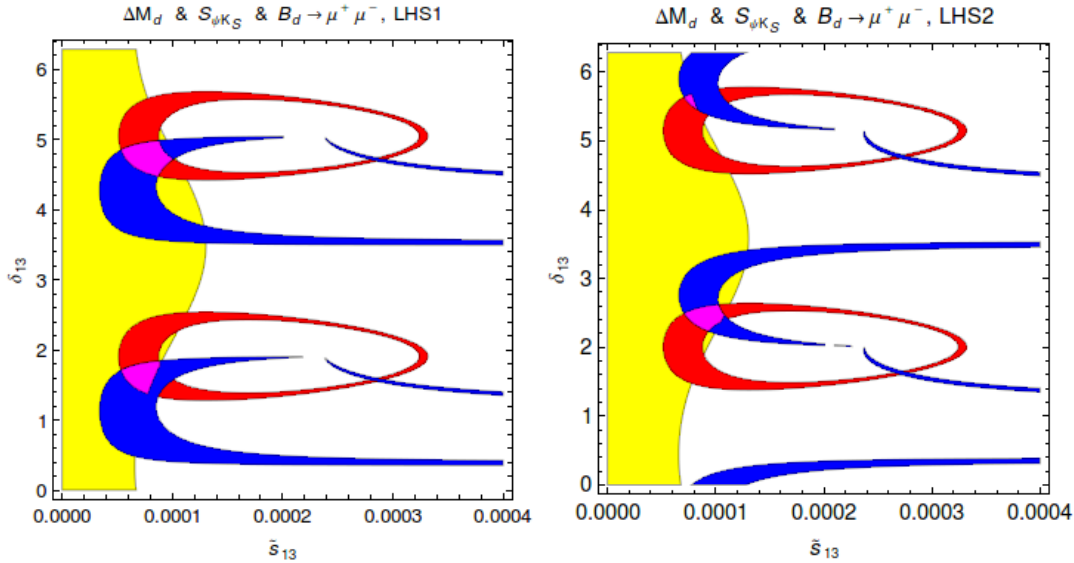


Figure 27: Ranges for ΔM_d (red region), $S_{\psi K_S}$ (blue region) and $B_d \rightarrow \mu^+ \mu^-$ (yellow) in LHS1 (left) and LHS2 (right) satisfying the bounds in Eq. (131) and $\mathcal{B}(B_d \rightarrow \mu^+ \mu^-) \leq 9.4 \cdot 10^{-10}$.

We begin therefore with LRS1 and LRS2 scenarios and show in Fig. 30 $\mathcal{B}(K_L \rightarrow \pi^0 \nu \bar{\nu})$ vs $\mathcal{B}(K^+ \rightarrow \pi^+ \nu \bar{\nu})$. Indeed the NP effects can be much larger than in the Z' case shown in Fig. 16.

In Fig. 31 we show analogous result for LHS1 and LHS2 case imposing the $K_L \rightarrow \mu^+ \mu^-$ constraint. We observe that in both scenarios only the branch unaffected by the $K_L \rightarrow \mu^+ \mu^-$ constraint survives. This is $C_2(S1)$ and $C_1(S2)$. In $C_1(S1)$ $\mathcal{B}(K^+ \rightarrow \pi^+ \nu \bar{\nu}) \geq 3.5 \cdot 10^{-10}$ and this case is ruled out. In Fig. 32 we show the corresponding results for RHS1 and RHS2 where the $K_L \rightarrow \mu^+ \mu^-$ constraint has a different impact than in LHS cases. Also here NP effects can be very large.

Finally we discuss $K_L \rightarrow \pi^0 \ell^+ \ell^-$ decays. In Figs. 33 and 34 we show the results corresponding to the ones found for Z' LHS and LRS scenarios. As the results for S1 scenarios turn out to be very similar we only show the results for S2 scenarios. The meaning of the curves is the same as in the case of Z' results in Figs. 12 and 17. We observe that NP effects in $K_L \rightarrow \pi^0 \ell^+ \ell^-$ decays can be very large but they are bounded by the upper bound on $\mathcal{B}(K_L \rightarrow \pi^0 \nu \bar{\nu})$ which follows from the present bound on $\mathcal{B}(K^+ \rightarrow \pi^+ \nu \bar{\nu})$. We note that in LHS scenarios the upper bound on $\mathcal{B}(K_L \rightarrow \pi^0 \nu \bar{\nu})$ practically coincides with the GN bound and amounts to

$$\mathcal{B}(K_L \rightarrow \pi^0 \nu \bar{\nu}) \leq 115 \cdot 10^{-11}. \quad (159)$$

It is slightly weaker in LRS scenarios. In any case the the present upper bounds on $\mathcal{B}(K_L \rightarrow \pi^0 \ell^+ \ell^-)$ do not preclude large NP effects found in $\mathcal{B}(K^+ \rightarrow \pi^+ \nu \bar{\nu})$ and

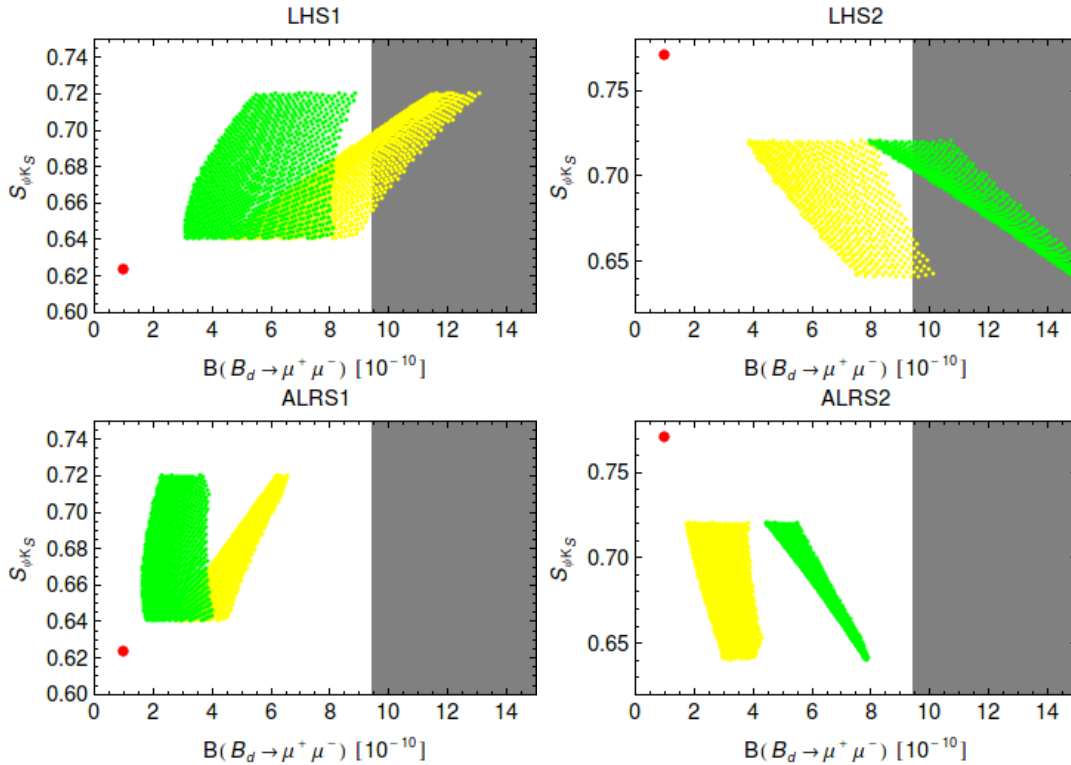


Figure 28: $S_{\psi K_S}$ versus $\mathcal{B}(B_d \rightarrow \mu^+ \mu^-)$ in LHS1, LHS2 (upper row) and ALRS1, ALRS2 (lower row). B_1 : yellow, B_3 : green. Red point: SM central value. Gray region: excluded by $\mathcal{B}(B_d \rightarrow \mu^+ \mu^-) \leq 9.4 \cdot 10^{-10}$.

$\mathcal{B}(K_L \rightarrow \pi^0 \nu \bar{\nu})$.

9.5 Comments on ε'/ε

The large NP effects in $K^+ \rightarrow \pi^+ \nu \bar{\nu}$ and $K_L \rightarrow \pi^0 \nu \bar{\nu}$ both through Z' and Z tree level exchanges belong clearly to highlights of our paper. Yet we would like to emphasize at this point that in principle these large effects could be eliminated by the ratio ε'/ε if the relevant hadronic matrix elements were precisely known. As already pointed out in [44, 45] there is a strong correlation between $K^+ \rightarrow \pi^+ \nu \bar{\nu}$ and $K_L \rightarrow \pi^0 \nu \bar{\nu}$ and ε'/ε because electroweak penguin contributions that are relevant for ε'/ε govern $K^+ \rightarrow \pi^+ \nu \bar{\nu}$ and $K_L \rightarrow \pi^0 \nu \bar{\nu}$ even if operators are different. The strongest correlation is between $\mathcal{B}(K_L \rightarrow \pi^0 \nu \bar{\nu})$ and ε'/ε because they are both CP-violating. However, if $\mathcal{B}(K_L \rightarrow \pi^0 \nu \bar{\nu})$ is bounded by ε'/ε then automatically $\mathcal{B}(K^+ \rightarrow \pi^+ \nu \bar{\nu})$ is bounded on the branch parallel to the GN bound on which their ratio is approximately constant. On the second branch $\mathcal{B}(K^+ \rightarrow \pi^+ \nu \bar{\nu})$ is less affected but there the bound from $K_L \rightarrow \mu^+ \mu^-$ plays a role unless we work in LRS scenario.

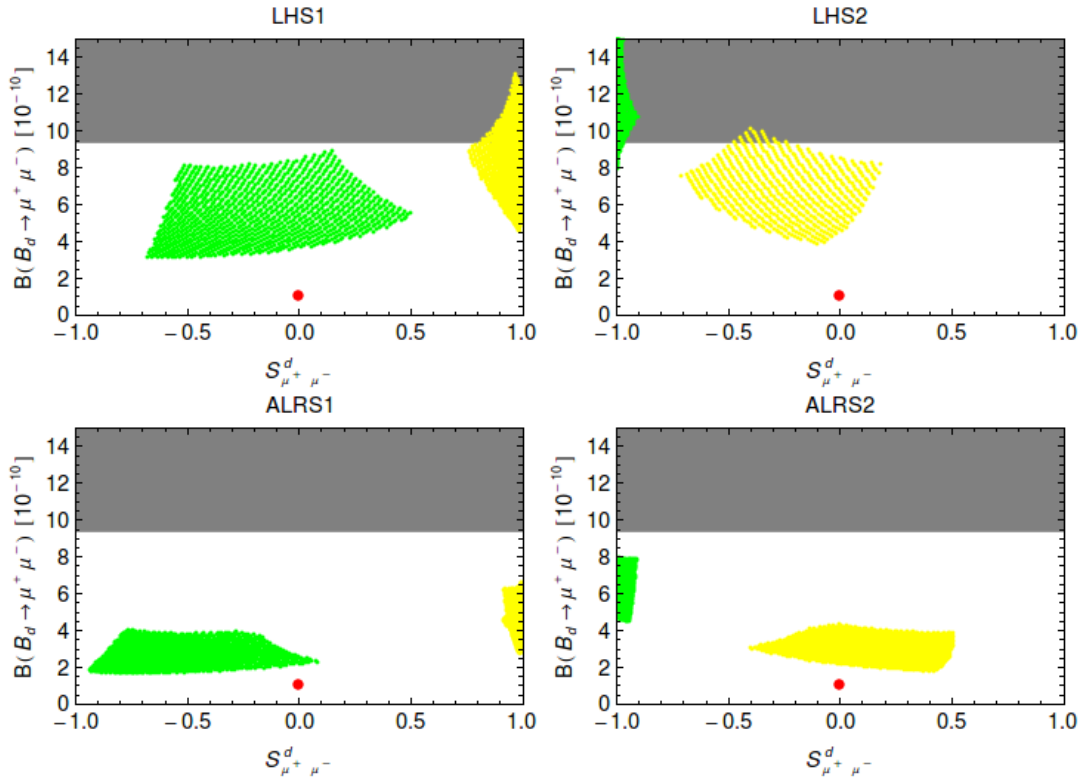


Figure 29: $\mathcal{B}(B_d \rightarrow \mu^+\mu^-)$ versus $S_{\mu^+\mu^-}^d$ in LHS1, LHS2 (upper row) and ALRS1, ALRS2 (lower row). B_1 : yellow, B_3 : green. Red point: SM central value. Gray region: excluded by $\mathcal{B}(B_d \rightarrow \mu^+\mu^-) \leq 9.4 \cdot 10^{-10}$.

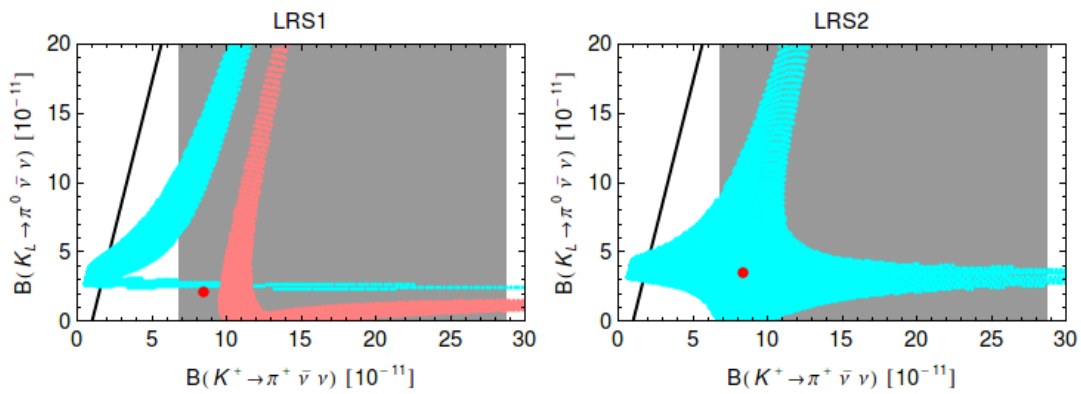


Figure 30: $\mathcal{B}(K_L \rightarrow \pi^0 \nu \bar{\nu})$ versus $\mathcal{B}(K^+ \rightarrow \pi^+ \nu \bar{\nu})$ in LRS1 (left) and LRS2 (right). C_1 : cyan, C_2 : pink. Red point: SM central value. Gray region: experimental range of $\mathcal{B}(K^+ \rightarrow \pi^+ \nu \bar{\nu})$.

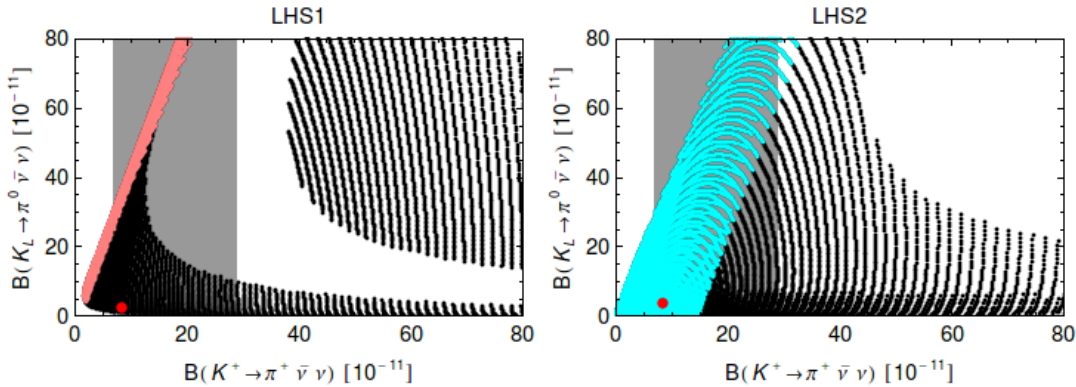


Figure 31: $\mathcal{B}(K_L \rightarrow \pi^0 \nu \bar{\nu})$ versus $\mathcal{B}(K^+ \rightarrow \pi^+ \nu \bar{\nu})$ in LHS1 (left) and LHS2 (right). C_1 : cyan, C_2 : pink. Black points excluded due to $\mathcal{B}(K_L \rightarrow \mu^+ \mu^-) \leq 2.5 \cdot 10^{-9}$ constraint. Red point: SM central value. Gray region: experimental range of $\mathcal{B}(K^+ \rightarrow \pi^+ \nu \bar{\nu})$.

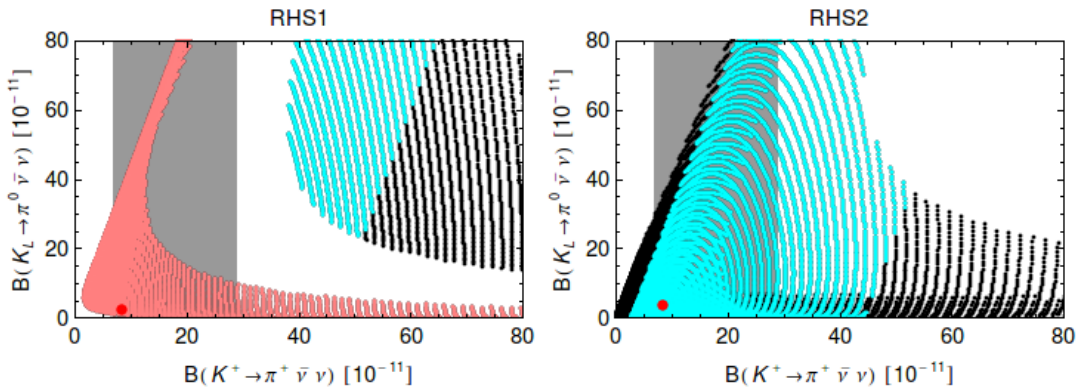


Figure 32: $\mathcal{B}(K_L \rightarrow \pi^0 \nu \bar{\nu})$ versus $\mathcal{B}(K^+ \rightarrow \pi^+ \nu \bar{\nu})$ in RHS1 (left) and RHS2 (right). C_1 : cyan, C_2 : pink. Black points excluded due to $\mathcal{B}(K_L \rightarrow \mu^+ \mu^-) \leq 2.5 \cdot 10^{-9}$ constraint. Red point: SM central value. Gray region: experimental range of $\mathcal{B}(K^+ \rightarrow \pi^+ \nu \bar{\nu})$.

Unfortunately, in spite of the recent progress on the calculation of the hadronic matrix elements relevant for ε'/ε [119–121], the hadronic uncertainties in ε'/ε are still too large for reaching a clear cut conclusion on the impact of this ratio on rare K decays. An analysis of ε'/ε in the LHT model demonstrates this problem in explicit terms [46]. If one uses hadronic matrix elements of QCD and electroweak penguin operators obtained in the large N approach, $(\varepsilon'/\varepsilon)_{\text{SM}}$ is in the ballpark of the experimental data and sizable departures of $\mathcal{B}(K_L \rightarrow \pi^0 \nu \bar{\nu})$ from its SM value are not allowed. $K^+ \rightarrow \pi^+ \nu \bar{\nu}$ being CP conserving and consequently not as strongly correlated with ε'/ε as $\mathcal{B}(K_L \rightarrow \pi^0 \nu \bar{\nu})$ could still be enhanced by 50% in LHT. On the other hand if hadronic matrix elements in question differ significantly from their large N values, $(\varepsilon'/\varepsilon)_{\text{SM}}$ disagrees with experiment

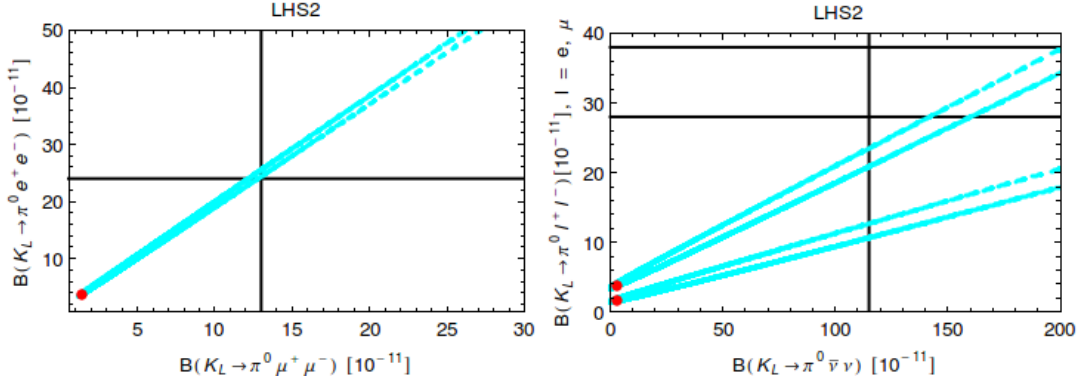


Figure 33: $\mathcal{B}(K_L \rightarrow \pi^0 e^+ e^-)$ as a function of $\mathcal{B}(K_L \rightarrow \pi^0 \mu^+ \mu^-)$ (left panel) and $\mathcal{B}(K_L \rightarrow \pi^0 e^+ e^-)$ (upper curve) and $\mathcal{B}(K_L \rightarrow \pi^0 \mu^+ \mu^-)$ (lower curve) as functions of $\mathcal{B}Br(K_L \rightarrow \pi^0 \nu \bar{\nu})$ (right panel) in LHS2. The red points represent SM predictions.

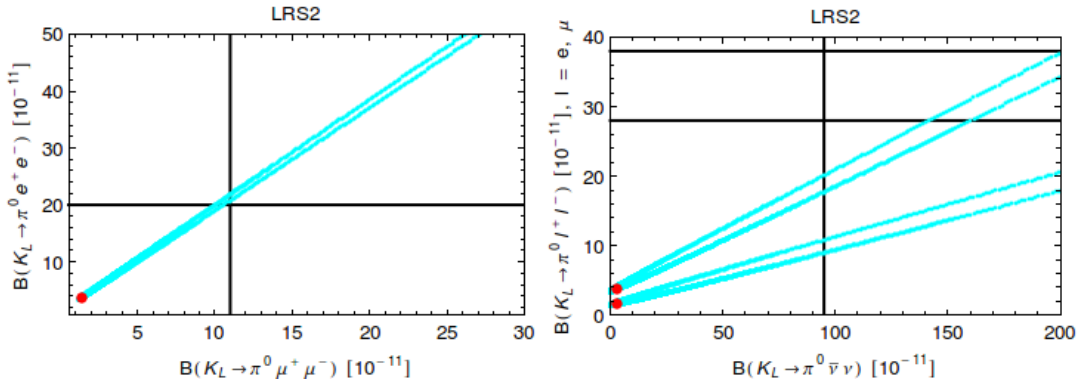


Figure 34: $\mathcal{B}(K_L \rightarrow \pi^0 e^+ e^-)$ as a function of $\mathcal{B}(K_L \rightarrow \pi^0 \mu^+ \mu^-)$ (left panel) and $\mathcal{B}(K_L \rightarrow \pi^0 e^+ e^-)$ (upper curve) and $\mathcal{B}(K_L \rightarrow \pi^0 \mu^+ \mu^-)$ (lower curve) as functions of $\mathcal{B}Br(K_L \rightarrow \pi^0 \nu \bar{\nu})$ (right panel) in LRS2. The red points represent SM predictions.

and much more room for enhancements of rare K decay branching ratios through NP contributions is available.

10 Summary and Conclusions

In this paper we exhibited the pattern of flavour violation in models in which NP effects are dominated by tree-level Z' exchanges under the assumption that the theoretical and experimental errors on various input parameters will decrease with time. In particular we have identified a number of correlations between $\Delta F = 2$ and $\Delta F = 1$ processes that will enable in due time to test this NP scenario. Our detailed analysis of these correlations in Section 7 shows that in the three meson systems considered significant

$B_{d,s}$ systems: observables	scenarios	Figure	comments
ΔM_s & $S_{\psi\phi}$ oases	LHS/RHS Z'	2	oases (A_1, A_2, A_3, A_4) found
	LRS Z'	13	oases (A_1, A_2, A_3, A_4) found
	LHS $U(2)^3 Z'$	24	two common oases for B_s and B_d
	LHS Z	26	no oases found
$S_{\psi\phi}$ vs. $B_s \rightarrow \mu^+\mu^-$	LHS Z'	3	excludes (A_2, A_4) (anti)correlation found in A_3 (A_1)
	RHS Z'	19	(anti)correlation found in A_1 (A_3)
	LHS $U(2)^3 Z'$	25	
$S_{\mu^+\mu^-}^s$ vs. $S_{\psi\phi}$	LHS Z'	3	$S_{\mu^+\mu^-}^s > 0 (< 0)$ in A_1 (A_3)
$B \rightarrow X_s \bar{\nu}\nu$ vs. $B_s \rightarrow \mu^+\mu^-$	LHS Z'	4	correlation found in A_3, A_1
$B \rightarrow X_s \bar{\nu}\nu$ vs. $S_{\psi\phi}$	LHS Z'	5	(anti)correlation found in A_3 (A_1)
$B \rightarrow K^{(*)}\bar{\nu}\nu$ vs. $B_s \rightarrow \mu^+\mu^-$	LHS/RHS Z'	21	$B \rightarrow K\bar{\nu}\nu$: (anti)correlation in LHS(RHS) $B \rightarrow K^*\bar{\nu}\nu$: correlation in LHS and RHS
$B \rightarrow K^{(*)}\bar{\nu}\nu$ vs. $S_{\psi\phi}$	LHS/RHS Z'	22	LHS: (anti)correlation in A_3 (A_1) RHS: K case: above SM, (anti)correlation in A_3 (A_1); opposite in K^* case: below SM
$B \rightarrow K^*\bar{\nu}\nu$ vs. $B \rightarrow K\bar{\nu}\nu$	LHS/RHS/LRS Z'	23	(anti)correlation in LHS and LRS (RHS)
$Im(C'_{10})$ vs. $Re(C'_{10})$	RHS/LRS Z'	18	RHS: $Im(C'_{10}) > 0 (< 0)$ in A_3 (A_1) $Re(C'_{10}) > 0 (< 0)$ in A_1 (A_3)
η vs. ϵ ($b \rightarrow s\bar{\nu}\nu$)	LHS/RHS/LRS/ALRS Z'	20	$\eta = 0$ in LHS; no dependence on ϵ in RHS (anti)correlation in ALRS(LRS)
ΔM_d & $S_{\psi K_S}$ oases	LHS/RHS Z'	6	oases (B_1, B_2, B_3, B_4) found
	LRS Z'	14	oases (B_1, B_2, B_3, B_4) found
	LHS $U(2)^3 Z'$	24	two common oases for B_s and B_d
	LHS Z	27	only two oases found
$S_{\psi K_S}$ vs. $B_d \rightarrow \mu^+\mu^-$	LHS Z'	7	$B(B_d \rightarrow \mu^+\mu^-)$ above SM in B_2, B_4 and in B_1 (LHS1) or in B_3 (LHS2)
	LHS/ALRS Z	28	$B_d \rightarrow \mu^+\mu^-$ always above SM;
$B_d \rightarrow \mu^+\mu^-$ vs. $S_{\mu^+\mu^-}^d$ $B_d \rightarrow \mu^+\mu^-$ vs. $S_{\mu^+\mu^-}^d$	LHS Z'	8	$S_{\mu^+\mu^-}^d > 0 (< 0)$ in B_1, B_4 (B_2, B_3)
	LHS/ALRS Z	29	

Table 9: Overview of correlation plots in B_d and B_s sectors.

foot prints of Z' will be seen provided $M_{Z'} \leq 5$ TeV. But only in the K system these effects can be detected if $M_{Z'}$ is larger and outside the LHC reach.

In view of these findings we have investigated whether larger effects could be found if the SM Z boson couplings were flavour violating. Indeed, in this case the stronger constraints come from $\Delta F = 1$ and not $\Delta F = 2$ processes. We find then that imposition

K system: observables	scenarios	Figure	comments
ΔM_K & ε_K oases	LHS/RHS Z'	9	oases (C_1, C_2) found in S1; only C_1 in S2
	LRS Z'	15	oases (C_1, C_2) found in S1; only C_1 in S2
$K_L \rightarrow \pi^0 \bar{\nu} \nu$ vs. $K^+ \rightarrow \pi^+ \bar{\nu} \nu$	LHS Z'	10	two branch structure
	LRS Z'	16	two branch structure
	LHS Z	31	only one branch allowed
	LRS Z	30	two branch structure
	RHS Z	32	two branch structure
$K_L \rightarrow \mu^+ \mu^-$ vs. $K^+ \rightarrow \pi^+ \bar{\nu} \nu$	LHS/RHS Z'	11	(anti)correlation in LHS (RHS)
$K_L \rightarrow \pi^0 e^+ e^-$ vs. $K_L \rightarrow \pi^0 \mu^+ \mu^-$	LHS Z'	12	correlation
	LRS Z'	17	correlation
	LHS Z	33	correlation
	LRS Z	34	correlation
$K_L \rightarrow \pi^0 \ell^+ \ell^-$ vs. $K_L \rightarrow \pi^0 \bar{\nu} \nu$	LHS Z'	12	correlation
	LRS Z'	17	correlation
	LHS Z	33	correlation
	LRS Z	34	correlation

Table 10: *Overview of correlation plots in the K sector.*

of the present constraints from $b \rightarrow s\mu^+\mu^-$ transitions makes NP effects in $\Delta F = 2$ transitions in the B_s system very small precluding also large NP effects in $b \rightarrow s\nu\bar{\nu}$ transitions.

The situation is different in the B_d system and in particular in the K system where effects from flavour-violating Z couplings are still allowed to be large.

Our results are summarized in a number of plots that have been obtained in various scenarios for the Z' couplings and for inclusive and exclusive values of $|V_{ub}|$. Also a number of plots have been shown for the case of flavour-violating Z - couplings. The overview of all correlations found by us and of the related figures is given in Tables 9 and 10. There we collect a short description of all those plots, in particular stressing whether correlations or anticorrelations are found among the various observables. We list here only few highlights:

- For each scenario we have identified allowed oases in the parameter space of the model. In each oasis particular structure of correlations between various observables will in the future either favour or exclude a given oasis.
- For the near future the correlations involving $S_{\psi\phi}$ and $\mathcal{B}(B_{s,d} \rightarrow \mu^+\mu^-)$ will be most interesting as the data on these three observables will be improved in the coming months sharpening the outcome of our analysis, possibly ruling out some

oases and scenarios of the couplings. The plots in Figs. 3, 19 and 7 will be helpful in monitoring these developments.

- Of particular interest will be the study of the effects of right-handed currents. Here the recent constraints on the Wilson coefficients of primed operators from $b \rightarrow s\mu^+\mu^-$ transitions had already impact on our results. In the future an important role in testing RH currents will be played by $b \rightarrow s\nu\bar{\nu}$ transitions. The plots in Fig. 21, 22 and 23 exhibit the power of these decays in this context.
- While in $B_{s,d}$ decays for $M_{Z'} \geq 5$ TeV Z' effects are predicted to be small, in $K^+ \rightarrow \pi^+\nu\bar{\nu}$ and $K_L \rightarrow \pi^0\nu\bar{\nu}$ decays they can be important in LHS and RHS scenarios even at $M_{Z'} = 10$ TeV and slightly larger scales. This is seen in Fig. 10. On the other hand as seen in Fig. 16 in LRS scenarios for $M_{Z'} \geq 5$ TeV it will be difficult to identify NP in these decays.
- We have demonstrated that the imposition of $U(2)^3$ symmetry on the Z' couplings has a profound impact on the correlation of $S_{\psi\phi}$ with $B_s \rightarrow \mu^+\mu^-$ sharpening the predictions significantly. We show this in Fig. 25.
- Our analysis of flavour-violating Z -couplings shows that in the case of B_d and K system they could constitute an important portal to NP with only small effects still allowed in the B_s system. The plots in Figs. 27, 28, 29, 30, 31, 32, 33 and 34 illustrate these findings.
- We have reemphasized, following [44–46], that large NP effects in rare K decays could be softened by the correlations with ε'/ε if the hadronic matrix elements relevant for this ratio were better known.

We are aware of the fact that some of the correlations presented by us would be washed out if we included all existing uncertainties. Yet, our simplified numerical analysis had as the main goal to illustrate how the decrease of theoretical, parametric and experimental uncertainties in the coming years might allow to exhibit certain features of NP, even if deviations from the SM will be only moderate. In this manner we have uncovered a world of correlations present in NP scenario, where new effects are dominated by flavour-violating couplings of a heavy neutral gauge bosons and/or SM Z boson. In fact within the coming years the size of the assumed uncertainties in our analysis could likely become reality.

We are looking forward to improved experimental data and improved lattice calculations. The correlations identified in this paper will allow to monitor how the simple NP scenarios discussed by us face the future precision flavour data.

Acknowledgements

We thank Pietro Colangelo, Robert Fleischer, Robert Knegjens, and Robert Ziegler for discussions. This research was financially supported by the ERC Advanced Grant project “FLAVOUR” (267104).

References

- [1] S. L. Glashow, J. Iliopoulos, and L. Maiani, *Weak Interactions with Lepton-Hadron Symmetry*, *Phys. Rev.* **D2** (1970) 1285–1292.
- [2] A. J. Buras, P. Gambino, M. Gorbahn, S. Jager, and L. Silvestrini, *Universal unitarity triangle and physics beyond the standard model*, *Phys. Lett.* **B500** (2001) 161–167, [[hep-ph/0007085](#)].
- [3] A. J. Buras, *Minimal flavor violation*, *Acta Phys. Polon.* **B34** (2003) 5615–5668, [[hep-ph/0310208](#)].
- [4] M. Blanke, A. J. Buras, D. Guadagnoli, and C. Tarantino, *Minimal Flavour Violation Waiting for Precise Measurements of ΔM_s , $S_{\psi\phi}$, A_{SL}^s , $|V_{ub}|$, γ and $B_{s,d}^0 \rightarrow \mu^+\mu^-$* , *JHEP* **10** (2006) 003, [[hep-ph/0604057](#)].
- [5] G. D’Ambrosio, G. F. Giudice, G. Isidori, and A. Strumia, *Minimal flavour violation: An effective field theory approach*, *Nucl. Phys.* **B645** (2002) 155–187, [[hep-ph/0207036](#)].
- [6] G. Isidori, Y. Nir, and G. Perez, *Flavor Physics Constraints for Physics Beyond the Standard Model*, *Ann.Rev.Nucl.Part.Sci.* **60** (2010) 355, [[arXiv:1002.0900](#)].
- [7] A. J. Buras and J. Girrbach, *BSM models facing the recent LHCb data: A First look*, *Acta Phys.Polon.* **B43** (2012) 1427, [[arXiv:1204.5064](#)].
- [8] P. Langacker and M. Plumacher, *Flavor changing effects in theories with a heavy Z' boson with family nonuniversal couplings*, *Phys.Rev.* **D62** (2000) 013006, [[hep-ph/0001204](#)].
- [9] G. Buchalla, G. Hiller, and G. Isidori, *Phenomenology of non-standard Z couplings in exclusive semileptonic $b \rightarrow s$ transitions*, *Phys. Rev.* **D63** (2001) 014015, [[hep-ph/0006136](#)].
- [10] F. del Aguila, M. Perez-Victoria, and J. Santiago, *Observable contributions of new exotic quarks to quark mixing*, *JHEP* **0009** (2000) 011, [[hep-ph/0007316](#)].
- [11] V. Barger, C.-W. Chiang, P. Langacker, and H.-S. Lee, *Z' mediated flavor changing neutral currents in B meson decays*, *Phys.Lett.* **B580** (2004) 186–196, [[hep-ph/0310073](#)].
- [12] V. Barger, C.-W. Chiang, J. Jiang, and P. Langacker, *$B_s - \bar{B}_s$ mixing in Z' models with flavor-changing neutral currents*, *Phys.Lett.* **B596** (2004) 229–239, [[hep-ph/0405108](#)].
- [13] C.-W. Chiang, N. Deshpande, and J. Jiang, *Flavor changing effects in family nonuniversal Z' models*, *JHEP* **0608** (2006) 075, [[hep-ph/0606122](#)].

- [14] S. Baek, J. H. Jeon, and C. Kim, $B_s^0 - \bar{B}_s^0$ Mixing in Leptophobic Z' Model, *Phys.Lett.* **B641** (2006) 183–188, [[hep-ph/0607113](#)].
- [15] K. Cheung, C.-W. Chiang, N. Deshpande, and J. Jiang, Constraints on flavor-changing Z' models by B_s mixing, Z' production, and $B_s \rightarrow \mu^+ \mu^-$, *Phys.Lett.* **B652** (2007) 285–291, [[hep-ph/0604223](#)].
- [16] X.-G. He and G. Valencia, $B_s^0 - \bar{B}_s^0$ Mixing constraints on FCNC and a non-universal Z' , *Phys.Rev.* **D74** (2006) 013011, [[hep-ph/0605202](#)].
- [17] V. Barger, L. L. Everett, J. Jiang, P. Langacker, T. Liu, *et. al.*, $b \rightarrow s$ Transitions in Family-dependent $U(1)'$ Models, *JHEP* **0912** (2009) 048, [[arXiv:0906.3745](#)].
- [18] F. del Aguila, J. de Blas, P. Langacker, and M. Perez-Victoria, Impact of extra particles on indirect Z' limits, *Phys.Rev.* **D84** (2011) 015015, [[arXiv:1104.5512](#)].
- [19] X.-Q. Li, Y.-M. Li, G.-R. Lu, and F. Su, $B_s^0 - \bar{B}_s^0$ mixing in a family non-universal Z' model revisited, *JHEP* **1205** (2012) 049, [[arXiv:1204.5250](#)].
- [20] Q. Chang, X.-Q. Li, and Y.-D. Yang, $B \rightarrow K^* l^+ l^-$, $K l^+ l^-$ decays in a family non-universal Z' model, *JHEP* **1004** (2010) 052, [[arXiv:1002.2758](#)].
- [21] Q. Chang, X.-Q. Li, and Y.-D. Yang, Family Non-universal Z' effects on $\bar{B}_q - B_q$ mixing, $B \rightarrow X_s \mu^+ \mu^-$ and $B_s \rightarrow \mu^+ \mu^-$ Decays, *JHEP* **1002** (2010) 082, [[arXiv:0907.4408](#)].
- [22] P. Langacker, *The Physics of Heavy Z' Gauge Bosons*, *Rev.Mod.Phys.* **81** (2009) 1199–1228, [[arXiv:0801.1345](#)].
- [23] R. Barbieri, G. Isidori, J. Jones-Perez, P. Lodone, and D. M. Straub, $U(2)$ and Minimal Flavour Violation in Supersymmetry, *Eur.Phys.J.* **C71** (2011) 1725, [[arXiv:1105.2296](#)].
- [24] R. Barbieri, P. Campli, G. Isidori, F. Sala, and D. M. Straub, B -decay CP -asymmetries in SUSY with a $U(2)^3$ flavour symmetry, *Eur.Phys.J.* **C71** (2011) 1812, [[arXiv:1108.5125](#)].
- [25] R. Barbieri, D. Buttazzo, F. Sala, and D. M. Straub, Flavour physics from an approximate $U(2)^3$ symmetry, *JHEP* **1207** (2012) 181, [[arXiv:1203.4218](#)].
- [26] R. Barbieri, D. Buttazzo, F. Sala, and D. M. Straub, Less Minimal Flavour Violation, [arXiv:1206.1327](#).
- [27] A. Crivellin, L. Hofer, and U. Nierste, *The MSSM with a softly broken $U(2)^3$ flavor symmetry*, [arXiv:1111.0246](#).

- [28] A. Crivellin, L. Hofer, U. Nierste, and D. Scherer, *Phenomenological consequences of radiative flavor violation in the MSSM*, *Phys.Rev.* **D84** (2011) 035030, [[arXiv:1105.2818](#)].
- [29] A. Crivellin and U. Nierste, *Supersymmetric renormalisation of the CKM matrix and new constraints on the squark mass matrices*, *Phys.Rev.* **D79** (2009) 035018, [[arXiv:0810.1613](#)].
- [30] A. J. Buras and J. Girrbach, *On the Correlations between Flavour Observables in Minimal $U(2)^3$ Models*, *JHEP* **1301** (2013) 007, [[arXiv:1206.3878](#)].
- [31] M. Blanke *et. al.*, *Rare and CP-violating K and B decays in the Littlest Higgs model with T-parity*, *JHEP* **01** (2007) 066, [[hep-ph/0610298](#)].
- [32] M. Blanke, A. J. Buras, B. Duling, S. Recksiegel, and C. Tarantino, *FCNC Processes in the Littlest Higgs Model with T-Parity: a 2009 Look*, *Acta Phys.Polon.* **B41** (2010) 657–683, [[arXiv:0906.5454](#)].
- [33] M. Blanke, A. J. Buras, B. Duling, K. Gemmler, and S. Gori, *Rare K and B Decays in a Warped Extra Dimension with Custodial Protection*, *JHEP* **03** (2009) 108, [[arXiv:0812.3803](#)].
- [34] M. Blanke, *Insights from the Interplay of $K \rightarrow \pi\nu\bar{\nu}$ and ϵ_K on the New Physics Flavour Structure*, *Acta Phys.Polon.* **B41** (2010) 127, [[arXiv:0904.2528](#)].
- [35] A. J. Buras, F. De Fazio, J. Girrbach, and M. V. Carlucci, *The Anatomy of Quark Flavour Observables in 331 Models in the Flavour Precision Era*, [arXiv:1211.1237](#).
- [36] W. Altmannshofer and D. M. Straub, *Cornering New Physics in $b \rightarrow s\gamma$ Transitions*, *JHEP* **1208** (2012) 121, [[arXiv:1206.0273](#)].
- [37] F. Beaujean, C. Bobeth, D. van Dyk, and C. Wacker, *Bayesian Fit of Exclusive $b \rightarrow s\bar{l}l$ Decays: The Standard Model Operator Basis*, *JHEP* **1208** (2012) 030, [[arXiv:1205.1838](#)].
- [38] A. J. Buras, L. Merlo, and E. Stamou, *The Impact of Flavour Changing Neutral Gauge Bosons on $\bar{B} \rightarrow X_s\gamma$* , *JHEP* **1108** (2011) 124, [[arXiv:1105.5146](#)].
- [39] W. Altmannshofer, A. J. Buras, S. Gori, P. Paradisi, and D. M. Straub, *Anatomy and Phenomenology of FCNC and CPV Effects in SUSY Theories*, *Nucl.Phys.* **B830** (2010) 17–94, [[arXiv:0909.1333](#)].
- [40] W. Altmannshofer, P. Paradisi, and D. M. Straub, *Model-Independent Constraints on New Physics in $b \rightarrow s\gamma$ Transitions*, *JHEP* **1204** (2012) 008, [[arXiv:1111.1257](#)].

- [41] M. Blanke, A. J. Buras, K. Gemmler, and T. Heidsieck, $\Delta F = 2$ observables and $B \rightarrow X_q \gamma$; in the Left-Right Asymmetric Model: Higgs particles striking back, *JHEP* **1203** (2012) 024, [arXiv:1111.5014].
- [42] K. De Bruyn, R. Fleischer, R. Knegjens, P. Koppenburg, M. Merk, *et. al.*, Branching Ratio Measurements of B_s Decays, *Phys.Rev.* **D86** (2012) 014027, [arXiv:1204.1735].
- [43] K. De Bruyn, R. Fleischer, R. Knegjens, P. Koppenburg, M. Merk, *et. al.*, Probing New Physics via the $B_s^0 \rightarrow \mu^+ \mu^-$ Effective Lifetime, *Phys.Rev.Lett.* **109** (2012) 041801, [arXiv:1204.1737].
- [44] A. J. Buras and L. Silvestrini, Upper bounds on $k \rightarrow \pi \nu \bar{\nu}$ and $k_l \rightarrow \pi^0 e^+ e^-$ from ε'/ε and $k_l \rightarrow \mu^+ \mu^-$, *Nucl. Phys.* **B546** (1999) 299–314, [hep-ph/9811471].
- [45] A. J. Buras, G. Colangelo, G. Isidori, A. Romanino, and L. Silvestrini, Connections between ε'/ε and rare kaon decays in supersymmetry, *Nucl. Phys.* **B566** (2000) 3–32, [hep-ph/9908371].
- [46] M. Blanke, A. J. Buras, S. Recksiegel, C. Tarantino, and S. Uhlig, Correlations between ε'/ε and Rare K Decays in the Littlest Higgs Model with T -Parity, *JHEP* **06** (2007) 082, [0704.3329].
- [47] A. J. Buras, S. Jager, and J. Urban, Master formulae for $\Delta F = 2$ NLO QCD factors in the standard model and beyond, *Nucl.Phys.* **B605** (2001) 600–624, [hep-ph/0102316].
- [48] A. J. Buras and J. Girschbach, Complete NLO QCD Corrections for Tree Level Delta $F = 2$ FCNC Processes, *JHEP* **1203** (2012) 052, [arXiv:1201.1302].
- [49] **RBC and UKQCD Collaborations** Collaboration, P. Boyle, N. Garron, and R. Hudspith, Neutral kaon mixing beyond the standard model with $n_f = 2 + 1$ chiral fermions, *Phys.Rev.* **D86** (2012) 054028, [arXiv:1206.5737].
- [50] V. Bertone, N. Carrasco, M. Ciuchini, P. Dimopoulos, R. Frezzotti, *et. al.*, Kaon Mixing Beyond the SM from $N_f=2$ tmQCD and model independent constraints from the UTA, arXiv:1207.1287.
- [51] C. Bouchard, E. Freeland, C. Bernard, A. El-Khadra, E. Gamiz, *et. al.*, Neutral B mixing from $2 + 1$ flavor lattice-QCD: the Standard Model and beyond, arXiv:1112.5642.
- [52] G. Buchalla and A. J. Buras, The rare decays $k \rightarrow \pi \nu \bar{\nu}$, $b \rightarrow x \nu \bar{\nu}$ and $b \rightarrow \ell^+ \ell^-$: An update, *Nucl. Phys.* **B548** (1999) 309–327, [hep-ph/9901288].
- [53] M. Misiak and J. Urban, QCD corrections to FCNC decays mediated by Z penguins and W boxes, *Phys.Lett.* **B451** (1999) 161–169, [hep-ph/9901278].

- [54] M. Blanke *et. al.*, *Particle antiparticle mixing, ε_K , $\Delta\Gamma_q$, A_{SL}^q , $A_{CP}(B_d \rightarrow \psi K_S)$, $A_{CP}(B_s \rightarrow \psi\phi)$ and $B \rightarrow X_{s,d}\gamma$ in the Littlest Higgs model with T -parity*, *JHEP* **12** (2006) 003, [[hep-ph/0605214](#)].
- [55] S. Herrlich and U. Nierste, *Enhancement of the $K_L - K_S$ mass difference by short distance QCD corrections beyond leading logarithms*, *Nucl. Phys.* **B419** (1994) 292–322, [[hep-ph/9310311](#)].
- [56] S. Herrlich and U. Nierste, *Indirect CP violation in the neutral kaon system beyond leading logarithms*, *Phys. Rev.* **D52** (1995) 6505–6518, [[hep-ph/9507262](#)].
- [57] S. Herrlich and U. Nierste, *The Complete $|\Delta S| = 2$ Hamiltonian in the Next-To-Leading Order*, *Nucl. Phys.* **B476** (1996) 27–88, [[hep-ph/9604330](#)].
- [58] A. J. Buras, M. Jamin, and P. H. Weisz, *Leading and next-to-leading QCD corrections to ε parameter and $B^0 - \bar{B}^0$ mixing in the presence of a heavy top quark*, *Nucl. Phys.* **B347** (1990) 491–536.
- [59] J. Urban, F. Krauss, U. Jentschura, and G. Soff, *Next-to-leading order QCD corrections for the $B^0 - \bar{B}^0$ mixing with an extended Higgs sector*, *Nucl. Phys.* **B523** (1998) 40–58, [[hep-ph/9710245](#)].
- [60] J. Brod and M. Gorbahn, *ε_K at Next-to-Next-to-Leading Order: The Charm-Top-Quark Contribution*, *Phys.Rev.* **D82** (2010) 094026, [[arXiv:1007.0684](#)].
- [61] J. Brod and M. Gorbahn, *Next-to-Next-to-Leading-Order Charm-Quark Contribution to the CP Violation Parameter ε_K and ΔM_K* , *Phys.Rev.Lett.* **108** (2012) 121801, [[arXiv:1108.2036](#)].
- [62] A. J. Buras and D. Guadagnoli, *Correlations among new CP violating effects in $\Delta F = 2$ observables*, *Phys. Rev.* **D78** (2008) 033005, [[arXiv:0805.3887](#)].
- [63] A. J. Buras, D. Guadagnoli, and G. Isidori, *On ε_K beyond lowest order in the Operator Product Expansion*, *Phys.Lett.* **B688** (2010) 309–313, [[arXiv:1002.3612](#)].
- [64] S. Descotes-Genon, J. Matias, and J. Virto, *An analysis of $B_{d,s}$ mixing angles in presence of New Physics and an update of $B_s \rightarrow K^{0*}\bar{K}^{0*}$* , *Phys.Rev.* **D85** (2012) 034010, [[arXiv:1111.4882](#)].
- [65] R. Fleischer, *On Branching Ratios of B_s Decays and the Search for New Physics in $B_s^0 \rightarrow \mu^+\mu^-$* , [arXiv:1208.2843](#).
- [66] **LHCb collaboration** Collaboration, R. Aaij *et. al.*, *Strong constraints on the rare decays $B_s \rightarrow \mu^+\mu^-$ and $B^0 \rightarrow \mu^+\mu^-$* , [arXiv:1203.4493](#).

- [67] **LHCb collaboration** Collaboration, R. Aaij *et. al.*, *First evidence for the decay $B_s \rightarrow \mu^+ \mu^-$* , [arXiv:1211.2674](#).
- [68] A. J. Buras, J. Girrbach, D. Guadagnoli, and G. Isidori, *On the Standard Model prediction for $BR(Bs, d \text{ to } \mu^+ \mu^-)$* , *Eur.Phys.J.* **C72** (2012) 2172, [[arXiv:1208.0934](#)].
- [69] A. J. Buras, R. Fleischer, S. Recksiegel, and F. Schwab, *Anatomy of prominent B and K decays and signatures of CP-violating new physics in the electroweak penguin sector*, *Nucl. Phys.* **B697** (2004) 133–206, [[hep-ph/0402112](#)].
- [70] M. Gorbahn and U. Haisch, *Charm quark contribution to $K_L \rightarrow \mu^+ \mu^-$ at next-to-next-to-leading order*, *Phys. Rev. Lett.* **97** (2006) 122002, [[hep-ph/0605203](#)].
- [71] G. Isidori and R. Unterdorfer, *On the short-distance constraints from $K_{L,S} \rightarrow \mu^+ \mu^-$* , *JHEP* **01** (2004) 009, [[hep-ph/0311084](#)].
- [72] A. J. Buras, F. Schwab, and S. Uhlig, *Waiting for precise measurements of $K^+ \rightarrow \pi^+ \nu \bar{\nu}$ and $K_L \rightarrow \pi^0 \nu \bar{\nu}$* , *Rev. Mod. Phys.* **80** (2008) 965–1007, [[hep-ph/0405132](#)].
- [73] G. Isidori, *Flavor Physics with light quarks and leptons*, *eConf* **C060409** (2006) 035, [[hep-ph/0606047](#)].
- [74] C. Smith, *Theory review on rare K decays: Standard model and beyond*, [hep-ph/0608343](#).
- [75] F. Mescia and C. Smith, *Improved estimates of rare K decay matrix-elements from $K_{\ell 3}$ decays*, *Phys. Rev.* **D76** (2007) 034017, [[arXiv:0705.2025](#)].
- [76] A. J. Buras, M. Gorbahn, U. Haisch, and U. Nierste, *The rare decay $K^+ \rightarrow \pi^+ \nu \bar{\nu}$ at the next-to-next-to-leading order in QCD*, *Phys. Rev. Lett.* **95** (2005) 261805, [[hep-ph/0508165](#)].
- [77] A. J. Buras, M. Gorbahn, U. Haisch, and U. Nierste, *Charm quark contribution to $K^+ \rightarrow \pi^+ \nu \bar{\nu}$ at next-to-next-to-leading order*, *JHEP* **11** (2006) 002, [[hep-ph/0603079](#)].
- [78] J. Brod and M. Gorbahn, *Electroweak Corrections to the Charm Quark Contribution to $K^+ \rightarrow \pi^+ \nu \bar{\nu}$* , *Phys. Rev.* **D78** (2008) 034006, [[arXiv:0805.4119](#)].
- [79] G. Isidori, F. Mescia, and C. Smith, *Light-quark loops in $K \rightarrow \pi \nu \bar{\nu}$* , *Nucl. Phys.* **B718** (2005) 319–338, [[hep-ph/0503107](#)].

- [80] **E949** Collaboration, A. V. Artamonov *et. al.*, *New measurement of the $K^+ \rightarrow \pi^+ \nu \bar{\nu}$ branching ratio*, *Phys. Rev. Lett.* **101** (2008) 191802, [[arXiv:0808.2459](#)].
- [81] **E391a** Collaboration, J. Ahn *et. al.*, *Experimental study of the decay $K_L^0 \rightarrow \pi^0 \nu \bar{\nu}$* , *Phys.Rev.* **D81** (2010) 072004, [[arXiv:0911.4789](#)].
- [82] J. Brod, M. Gorbahn, and E. Stamou, *Two-Loop Electroweak Corrections for the $K \rightarrow \pi \nu \bar{\nu}$ Decays*, *Phys.Rev.* **D83** (2011) 034030, [[arXiv:1009.0947](#)].
- [83] W. Altmannshofer, A. J. Buras, D. M. Straub, and M. Wick, *New strategies for New Physics search in $B \rightarrow K^* \nu \bar{\nu}$, $B \rightarrow K \nu \bar{\nu}$ and $B \rightarrow X_s \nu \bar{\nu}$ decays*, *JHEP* **04** (2009) 022, [[arXiv:0902.0160](#)].
- [84] J. F. Kamenik and C. Smith, *Tree-level contributions to the rare decays $B^+ \rightarrow \pi^+ \nu \bar{\nu}$, $B^+ \rightarrow K^+ \nu \bar{\nu}$, and $B^+ \rightarrow K^{*+} \nu \bar{\nu}$ in the Standard Model*, *Phys.Lett.* **B680** (2009) 471–475, [[arXiv:0908.1174](#)].
- [85] M. Bartsch, M. Beylich, G. Buchalla, and D.-N. Gao, *Precision Flavour Physics with $B \rightarrow K \nu \bar{\nu}$ and $B \rightarrow K l^+ l^-$* , *JHEP* **0911** (2009) 011, [[arXiv:0909.1512](#)].
- [86] **ALEPH** Collaboration, R. Barate *et. al.*, *Measurements of $BR(b \rightarrow \tau^- \bar{\nu}_\tau X)$ and $BR(b \rightarrow \tau^- \bar{\nu}_\tau D^{*\pm} X)$ and upper limits on $BR(B^- \rightarrow \tau^- \bar{\nu}_\tau)$ and $BR(b \rightarrow \nu \bar{\nu})$* , *Eur. Phys. J.* **C19** (2001) 213–227, [[hep-ex/0010022](#)].
- [87] **BELLE** Collaboration, K. F. Chen *et. al.*, *Search for $B \rightarrow h^{(*)} \nu \bar{\nu}$ Decays at Belle*, *Phys. Rev. Lett.* **99** (2007) 221802, [[arXiv:0707.0138](#)].
- [88] **BABAR** Collaboration, B. Aubert *et. al.*, *Search for $B \rightarrow K^* \nu \bar{\nu}$ decays*, *Phys. Rev.* **D78** (2008) 072007, [[arXiv:0808.1338](#)].
- [89] F. Mescia, C. Smith, and S. Trine, *$K_L \rightarrow \pi^0 e^+ e^-$ and $K_L \rightarrow \pi^0 \mu^+ \mu^-$: A binary star on the stage of flavor physics*, *JHEP* **08** (2006) 088, [[hep-ph/0606081](#)].
- [90] J. Prades, *ChPT Progress on Non-Leptonic and Radiative Kaon Decays*, *PoS KAON* (2008) 022, [[arXiv:0707.1789](#)].
- [91] G. Isidori, C. Smith, and R. Unterdorfer, *The rare decay $K_L \rightarrow \pi^0 \mu^+ \mu^-$ within the SM*, *Eur. Phys. J.* **C36** (2004) 57–66, [[hep-ph/0404127](#)].
- [92] S. Friot, D. Greynat, and E. De Rafael, *Rare kaon decays revisited*, *Phys. Lett.* **B595** (2004) 301–308, [[hep-ph/0404136](#)].
- [93] C. Bruno and J. Prades, *Rare Kaon Decays in the $1/N_c$ -Expansion*, *Z. Phys.* **C57** (1993) 585–594, [[hep-ph/9209231](#)].
- [94] **KTeV** Collaboration, A. Alavi-Harati *et. al.*, *Search for the Rare Decay $K_L \rightarrow \pi^0 e^+ e^-$* , *Phys. Rev. Lett.* **93** (2004) 021805, [[hep-ex/0309072](#)].

- [95] **KTEV** Collaboration, A. Alavi-Harati *et. al.*, *Search for the Decay $K_L \rightarrow \pi^0 \mu^+ \mu^-$* , *Phys. Rev. Lett.* **84** (2000) 5279–5282, [[hep-ex/0001006](#)].
- [96] M. Blanke, A. J. Buras, S. Recksiegel, and C. Tarantino, *The Littlest Higgs Model with T-Parity Facing CP-Violation in $B_s - \bar{B}_s$ Mixing*, [arXiv:0805.4393](#).
- [97] G. Buchalla, G. D’Ambrosio, and G. Isidori, *Extracting short-distance physics from $K_{L,S} \rightarrow \pi^0 e^+ e^-$ decays*, *Nucl. Phys.* **B672** (2003) 387–408, [[hep-ph/0308008](#)].
- [98] A. J. Buras, M. E. Lautenbacher, M. Misiak, and M. Munz, *Direct CP violation in $K_L \rightarrow \pi^0 e^+ e^-$ beyond leading logarithms*, *Nucl. Phys.* **B423** (1994) 349–383, [[hep-ph/9402347](#)].
- [99] M. Misiak, H. Asatrian, K. Bieri, M. Czakon, A. Czarnecki, *et. al.*, *Estimate of $\mathcal{B}(\bar{B} \rightarrow X(s)\gamma)$ at $\mathcal{O}(\alpha_s^2)$* , *Phys.Rev.Lett.* **98** (2007) 022002, [[hep-ph/0609232](#)].
- [100] P. L. Cho and M. Misiak, *$b \rightarrow s\gamma$ decay in $SU(2)_L \times SU(2)_R \times U(1)$ extensions of the Standard Model*, *Phys.Rev.* **D49** (1994) 5894–5903, [[hep-ph/9310332](#)].
- [101] G. Ricciardi, *Brief review on semileptonic B decays*, [arXiv:1209.1407](#).
- [102] **Belle Collaboration** Collaboration, I. Adachi *et. al.*, *Measurement of $b \rightarrow \tau\nu$ with a hadronic tagging method using the full data sample of belle*, [arXiv:1208.4678](#).
- [103] C. Tarantino, *Flavor Lattice QCD in the Precision Era*, [arXiv:1210.0474](#).
- [104] M. Antonelli, D. M. Asner, D. A. Bauer, T. G. Becher, M. Beneke, *et. al.*, *Flavor Physics in the Quark Sector*, *Phys.Rept.* **494** (2010) 197–414, [[arXiv:0907.5386](#)].
- [105] **LHCb collaboration** Collaboration, I. Bediaga *et. al.*, *Implications of LHCb measurements and future prospects*, [arXiv:1208.3355](#).
- [106] **Particle Data Group** Collaboration, K. Nakamura *et. al.*, *Review of particle physics*, *J.Phys.G* **G37** (2010) 075021.
- [107] J. Laiho, E. Lunghi, and R. S. Van de Water, *Lattice QCD inputs to the CKM unitarity triangle analysis*, *Phys. Rev.* **D81** (2010) 034503, [[arXiv:0910.2928](#)]. Updates available on <http://latticeaverages.org/>.
- [108] K. Chetyrkin, J. Kuhn, A. Maier, P. Maierhofer, P. Marquard, *et. al.*, *Charm and Bottom Quark Masses: An Update*, *Phys.Rev.* **D80** (2009) 074010, [[arXiv:0907.2110](#)].

- [109] **HPQCD Collaboration** Collaboration, I. Allison *et. al.*, *High-Precision Charm-Quark Mass from Current-Current Correlators in Lattice and Continuum QCD*, *Phys.Rev.* **D78** (2008) 054513, [arXiv:0805.2999].
- [110] **CDF Collaboration** Collaboration, A. Abulencia *et. al.*, *Observation of $B_s^0 - \bar{B}_s^0$ Oscillations*, *Phys.Rev.Lett.* **97** (2006) 242003, [hep-ex/0609040].
- [111] **LHCb Collaboration** Collaboration, R. Aaij *et. al.*, *Measurement of the $B_s^0 - \bar{B}_s^0$ oscillation frequency ΔM_s in $B_s^0 \rightarrow D_s^-(3)\pi$ decays*, *Phys.Lett.* **B709** (2012) 177–184, [arXiv:1112.4311].
- [112] P. Clarke, *Results on cp violation in b_s mixing*, .
<http://cdsweb.cern.ch/record/1429149/files/LHCb-TALK-2012-029.pdf>.
- [113] **CMS Collaboration** Collaboration, S. Chatrchyan *et. al.*, *Search for narrow resonances in dilepton mass spectra in pp collisions at $\sqrt{s} = 7$ TeV*, *Phys.Lett.* **B714** (2012) 158–179, [arXiv:1206.1849].
- [114] Y. Grossman and Y. Nir, *$K_L \rightarrow \pi^0 \nu \bar{\nu}$ beyond the standard model*, *Phys. Lett.* **B398** (1997) 163–168, [hep-ph/9701313].
- [115] A. J. Buras, K. Gemmler, and G. Isidori, *Quark flavour mixing with right-handed currents: an effective theory approach*, *Nucl.Phys.* **B843** (2011) 107–142, [arXiv:1007.1993].
- [116] A. J. Buras, *Relations between $\Delta M_{s,d}$ and $B_{s,d} \rightarrow \mu^+ \mu^-$ in models with minimal flavour violation*, *Phys. Lett.* **B566** (2003) 115–119, [hep-ph/0303060].
- [117] A. J. Buras, B. Duling, and S. Gori, *The Impact of Kaluza-Klein Fermions on Standard Model Fermion Couplings in a RS Model with Custodial Protection*, *JHEP* **0909** (2009) 076, [arXiv:0905.2318].
- [118] F. Botella, G. Branco, and M. Nebot, *The Hunt for New Physics in the Flavour Sector with up vector-like quarks*, arXiv:1207.4440.
- [119] T. Blum, P. Boyle, N. Christ, N. Garron, E. Goode, *et. al.*, *$K \rightarrow \pi\pi$ Decay amplitudes from Lattice QCD*, *Phys.Rev.* **D84** (2011) 114503, [arXiv:1106.2714].
- [120] T. Blum, P. Boyle, N. Christ, N. Garron, E. Goode, *et. al.*, *The $K \rightarrow (\pi\pi)_{I=2}$ Decay Amplitude from Lattice QCD*, *Phys.Rev.Lett.* **108** (2012) 141601, [arXiv:1111.1699].
- [121] T. Blum, P. Boyle, N. Christ, N. Garron, E. Goode, *et. al.*, *Lattice determination of the $K \rightarrow (\pi\pi)_{I=2}$ Decay Amplitude A_2* , arXiv:1206.5142.